ISSN 2227-1031 (Print)
ISSN 2414-0392 (Online)

НАУКА и ТЕХНИКА

Международный научно-технический журнал

Science and Technique

International Scientific and Technical Journal

V. 19, No 1 (2020)

Материалы 16-го Европейского автомобильного конгресса

Proceedings of the 16th European Automotive Congress

Издается с января 2002 года
Периодичность издания – один раз в два месяца

Published from January 2002
Publication frequency – bimonthly

Учредитель
Белорусский национальный технический университет

Founder
Belarusian National Technical University

Журнал включен в базы данных:
Web of Science (ESCI), EBSCO, DOAJ, WorldCat, OpenAIRE, Google Scholar, РИНЦ, ЭБС «Лань», НЭБ «КиберЛенинка», Соционет

The Journal is included in the following databases:
Web of Science (ESCI), EBSCO, DOAJ, WorldCat, OpenAIRE, Google Scholar, RISC, Lan, CyberLeninka, Socionet

CONTENTS

Proceedings of the 16th European Automotive Congress

Kreis A., Hirz M.
Optimized Data Exchange Process between Design and Production Engineering 5

Ufert M., Bäker B.
Battery Ageing as Part of the System Design of Battery Electric Urban Bus Fleets 12

Maddumage W. U., Abeyasighe K. Y., Perera M. S. M., Attalage R. A., Kelly P.
Comparing Fuel Consumption and Emission Levels of Hybrid Powertrain Configurations and a Conventional Powertrain in Varied Drive Cycles and Degree of Hybridization 20

Stężycki P., Kowalski M., Jankowski A., Sławinski Z.
Laser Research of the Fuel Atomization Process of Internal Combustion Engines 34

Gao H., Jézéquel L., Cabrol E., Vitry B.
Robust Design of Suspension System with Polynomial Chaos Expansion and Machine Learning 43

СОДЕРЖАНИЕ

Материалы 16-го Европейского автомобильного конгресса

Крайс А., Хирц М.
Оптимизированный процесс обмена данными в период между проектированием и производством 5

Уферт М., Бекер Б.
Старение аккумуляторов как часть системы проектирования парков городских аккумуляторных электрических автобусов 12

Маддумаге В. У., Абеясиге К. И., Перера М. С. М., Атталаге Р. А., Келли П.
Сравнение расхода топлива и уровня выбросов при обычной и гибридных конфигурациях трансмиссий с учетом циклов движения и степени гибридизации 20

Стенжицкий П., Ковальский М., Янковский А., Славиньский З.
Лазерное исследование процесса распыления топлива двигателей внутреннего сгорания 34

Гао Х., Йезеквель Л., Каброль Э., Витри Б.
Надежная конструкция подвески с полиномиальным хаотичным расширением и машинным обучением 43

Bogomolov V., Klimenko V., Leontiev D., Ryzhyh L., Smyrnov O., Kholodov M.
Improving the Brake Control Effectiveness of Vehicles Equipped with a Pneumatic Brake Actuator 55
Dorofeev R., Tumasov A., Sizov A., Kocherov A., Meshkov A., Porubov D.
Engineering of Light Electric Commercial Vehicle 63
Cheng W., Wang Y.
How to Make the Charging Simple, Convenient and Efficient 76
Cervera Á. S. J., Alonso F. J., García F. S., Alvarez Á. D.
Imitating a Safe Human Driver Behaviour in Roundabouts Through Deep Learning 85

Богомолов В., Клименко В., Леонтьев Д., Рыжих Л., Смирнов О., Холодов М.
К вопросу о повышении эффективности управления тормозами транспортных средств, оснащенных пневматическим тормозным приводом 55
Дорофеев Р., Тумасов А., Сизов А., Кочеров А., Мешков А., Порубов Д.
Разработка легкого коммерческого электромобиля 63
Ченг У., Ван И.
Как сделать зарядку электромобиля простой, удобной и эффективной 76
Сервера А. С. Х., Алонсо Ф. Х., Гарсиа Ф. С., Альварес А. Д.
Моделирование безопасного поведения водителя на перекрестках с помощью глубинного обучения 85

Ответственный секретарь редакции
В. Н. Гурьянчик

Executive Secretary of Editorial Staff
V. N. Guryanchyk

Адрес редакции
Белорусский национальный технический университет
пр. Независимости, 65, корп. 2, комн. 327
220013, г. Минск, Республика Беларусь

Тел. +375 17 292-65-14

E-mail: sat@bntu.by
http://sat.bntu.by

Address
Belarusian National Technical University
Nezavisimosty Avenue, 65, Building 2, Room 327
220013, Minsk, Republic of Belarus

Tel. +375 17 292-65-14

E-mail: sat@bntu.by
http://sat.bntu.by

Перерегистрировано в Министерстве информации Республики Беларусь 19 декабря 2011 г.
Регистрационный номер 285
С 2002 г. издание выходило под названием «Вестник БНТУ»

ISSN 2227-1031. Подписные индексы 00662, 006622

Подписано в печать 29.01.2020. Формат бумаги 60×84 1/8. Бумага мелованная. Печать цифровая.
Усл. печ. л. 11,5. Уч.-изд. л. . Тираж 100 экз. Дата выхода в свет . Заказ № .

Отпечатано в БНТУ. Лицензия ЛП № 02330/74 от 03.03.2014.
220013, г. Минск, пр. Независимости, 65.

https://doi.org/10.21122/2227-1031-2020-19-1-5-11

UDC 629

Optimized Data Exchange Process between Design and Production Engineering

A. Kreis[1)], M. Hirz[1)]

[1)]Institute of Automotive Engineering, Graz University of Technology (Graz, Republic of Austria)

Abstract. Growing vehicle variant diversity, legal requirements to reduce fleet CO_2 emissions and innovations in the area of drive train technologies, coupled with the increasing pressure to cut costs, pose new challenges for parties in the automotive sector. An implementation of optimized development and production processes supports the effective handling of these challenges. One important aspect includes engineering efficiency improvement by optimizing the entire automotive bodywork development process and the involved data management. Research activities focus on the data exchange processes between design, simulation and production engineering within various CA*x* environments. This concerns constantly changing boundary conditions and requirements in the area of automotive body development, including but not limited to the introduction of new materials and material combinations and new types of joining technologies. From the viewpoint of an automotive engineering supplier, additional challenges caused by different customer-related development environments have to be considered. To overcome these challenges, various data exchange strategies between OEMs (Original Equipment Manufacturer), automotive suppliers and the use of different data management tools need to be investigated. In this context, the paper presents an approach of an optimized data exchange process of CAD-based data between different CAD (Computer-Aided Design) and CAM (Computer-Aided Manufacturing) environments that supports the entire body development, including data provision for manufacturing engineering. In addition, an optimization of data exchange processes saves development costs and improves the product quality.

Keywords: CAD-CAM process optimization, data exchange, automotive bodywork development, joining technology

For citation: Kreis A., Hirz M. (2020) Optimized Data Exchange Process between Design and Production Engineering. *Science and Technique*. 19 (1), 5–11. https://doi.org/10.21122/2227-1031-2020-19-1-5-11

Оптимизированный процесс обмена данными в период между проектированием и производством

А. Крайс[1)], М. Хирц[1)]

[1)]Институт автомобилестроения, Грацкий технический университет (Грац, Австрийская Республика)

Реферат. Растущее разнообразие вариантов транспортных средств, законодательные требования по сокращению выбросов CO_2 ими, инновации в области технологий трансмиссии в сочетании с усиливающимся давлением, направленным на сокращение расходов, ставят новые задачи перед участниками автомобильного сектора. Внедрение оптимизированных процессов разработки и производства поддерживает эффективное решение этих проблем.

Адрес для переписки
Крайс Александр
Институт автомобилестроения,
Грацкий технический университет
ул. Инффельдгассе, 11/2,
8010, г. Грац, Австрийская Республика
Тел.: +43 677 623-195-44
alexander.kreis@tugraz.at

Address for correspondence
Kreis Alexander
Institute of Automotive Engineering,
Graz University of Technology
11/2 Inffeldgasse str.,
8010, Graz, Republic of Austria
Tel.: +43 677 623-195-44
alexander.kreis@tugraz.at

Одним из важных аспектов является повышение эффективности инженерных решений за счет оптимизации всего процесса разработки кузова и управления данными. Исследовательская деятельность сосредоточена на процессах обмена данными на этапах проектирования, моделирования и производства в различных средах CA*x*. Это касается постоянно меняющихся граничных условий и требований к разработке кузовов автомобилей, включая, помимо прочего, внедрение новых материалов и их комбинаций, а также новых технологий сборки. С точки зрения поставщика автомобильной техники, необходимо учитывать дополнительные факторы, вызванные различными средами проведения разработки, которые обусловлены потребностями пользователя. Чтобы решить эти проблемы, нужно изучить стратегии обмена данными между OEM-производителями (OEM – производитель оригинального оборудования) и поставщиками автомобилей с использованием различных инструментов. В статье представлен оптимизированный процесс обмена данными на основе CAD (компьютерное проектирование) между различными средами CAD и CAM (компьютерное производство), который поддерживает разработку всего кузова, включая предоставление необходимых показателей для производственного цикла. Кроме того, оптимизация процессов обмена данными позволяет уменьшить затраты на разработку и улучшить качество продукции.

Ключевые слова: оптимизация процесса компьютерного проектирования и производства, обмен данными, разработка автомобильного кузова, технология соединения

Для цитирования: Крайс, А. Оптимизированный процесс обмена данными в период между проектированием и производством / А. Крайс, М. Хирц // *Наука и техника*. 2020. Т. 19, № 1. С. 5–11. https://doi.org/10.21122/2227-1031-2020-19-1-5-11

Introduction

In order to be able to counteract the progressive requirements in the automotive industry, the development processes must be continuously adapted. An increasingly important aspect for automobile manufacturers and suppliers is the production of climate-friendly vehicles. Besides others, this adaptation affects vehicle body development and manufacturing processes, including all materials used. For some time now, the so-called "multi-material body design" has been used. Multi-material body design is considered in such a way that a combination of several materials is used to create the BIW (Body-in-White) with the target to reduce weight [1, 2].

In addition to these material-heterogeneous vehicle bodies, pure steel bodies (e. g. for low-budget cars) and pure aluminum bodies (e. g. Audi A8 [3]) are also used, which leads to a wide range of different body architectures and associated material combinations. The mentioned change in the area of materials simultaneously leads to a change in the area of the required joining technologies [4, 5]. While a pure steel body is mainly joined by spot welds and seam welds, other material combinations, in particular multi-material body design, use additional types of joining technologies [6].

Besides the application of different types of joining technologies, the various automobile manufacturers (OEMs – Original Equipment Manufacturer) also have their design-related preferences. Since a wide range of joining technologies is used, the automotive industry has to face new challenges in the areas of creating and managing joining technology data, as well as the exchange of these data and metadata between different disciplines and systems of computer-aided design and engineering disciplines (CA*x* – Computer-Aided *x*, where *x* serves as a placeholder).

This paper provides an approach of an optimized data exchange process of CAD-based (Computer-Aided Design) joining technology data between the engineering disciplines design and production (CAM – Computer-Aided Manufacturing). Furthermore, this article gives an overview of the state-of-the-art of body development processes and derives the increased requirements for the management of joining technology data.

Problem statement

Due to the mentioned changes in the field of automotive joining technology, there are no uniform processes for the exchange of joining technology data. In order to ensure an optimized data exchange process, the creation and administration of joining technology data (takes place in CAD environments), the data exchange process and the integration of data in target environments (e. g. CAE (Computer-Aided Engineering), CAM environment) must be considered.

Joining technology data contain all information required for the creation of joining technology elements in CAD environments. This includes all parameters and meta information that are required

in other CA*x* environments and are, therefore, relevant for the data exchange. Each joining technology element is assigned a position vector (*x*-, *y*-, *z*-coordinates), the type of joining technology (e. g. spot welds, bolts, rivets, adhesives…), the parts to be connected (e. g. part number, part thickness, material…) and additional parameters (e. g. diameter, normal direction…). The additional parameters are usually tailored to the joining technology element (e. g. a diameter of the spot weld, the thickness of the weld seam, the normal direction for rivets, thread dimensions for screws…) [7]. In addition, joining technology data must be distinguished from geometry data in CA*x* environments. Geometry data contain information that describe the components (e. g. metal sheets) of the vehicle body (e. g. geometric dimensions, material, center of gravity...).

Due to the lack of standards (data formats, data structure, tools for creation, administration and distribution) in the area of joining technology data exchange, there is a gap in the data management processes. The existing gap in the management of joining technology data occurs in both, internal and external data exchange processes.

Internal data exchange processes cover the entire spectrum of data exchange in different CA*x* environments of one company (e. g. OEM, supplier...). On the other hand, external data exchange processes have to integrate at least two separate data management environments. While OEMs mainly concentrate on the internal data exchange process, suppliers have to consider both internal and external processes.

For automotive suppliers, it is of great importance to record and implement the occurring boundary conditions for external data exchange processes effectively. In order to clarify the requirements in data exchange, possible variants of development projects are subdivided into two types in view of the exchange of joining technology data.

The first type includes projects where all processes are handled internally in one company. This means that the creation of the joining technology data and the associated meta information take place completely in the internally CAD environment. The data exchange process from CAD to the target environment is carried out by using internal tools and methods. This results in a homogeneous situation (i. e. path of the data exchange process is always the same) with regard to data exchange. Finally, the joining technology data are integrated into the CAM target environment, so that further steps of manufacturing engineering are supported with the required information.

The second project type contains projects where the creation and administration of joining technology data take place partially or completely in an internal CAD environment, while the target environment is placed at another company externally. For this reason, one or more CAD environments (at least one is externally placed) participate in the entire data creation process. Since joining technology data can be created in more than one CAD environment, a heterogeneous data exchange process may occur in this case. This has an impact on the used data exchange file formats and data exchange strategies between the involved companies. Finally, the externally created joining technology data must be integrated into the targeted CAM environment.

In order to close the mentioned gap in joining technology-based data exchange, this paper provides an approach for an optimized data exchange of joining technology data for the different introduced use cases.

Automotive body design

As prior stated, the development of automotive bodies (BIW), including but not limited to the topics body architectures, crash-, strengths- and durability, materials and joining technologies, has changed over the last decades [6, 8]. The change in this field is mainly driven by the issues of vehicle safety, weight management and cost reduction. Exemplary an aluminum vehicle body can save up to 40 % in weight compared to a steel body, taking into account similar stiffness and strength values [1, 3].

To enable balanced optimization, the “multi-material body design” approach has been around for some time now, as it enables weight savings, under consideration of material costs targets. The following Tab. 1 shows the distribution of materials used in exemplary modern car bodies (manufacturing year 2016) [9–11].

As can be seen in Tab. 1, modern vehicle bodies can be made of several materials. As a result,

the field of joining technology has become much more complex in terms of the use of new types of joining technology and the number of joining technology elements applied (Tab. 2) [12].

Table 1

List of BIW materials of exemplary selected cars

Material	Volvo V90 [9]	Peugeot 3008 [10]	Aston Martin DB11 [11]
Aluminum, %	6	5	53
Standard steel, %	27	27	5
High strength steel, %	67	62	–
Synthetics, %	–	65	42

Table 2

List of used joining elements of exemplary selected cars

Type of joining technology	Volvo V90 [9]	Peugeot 3008 [10]	Aston Martin DB11 [11]
Spot welds, pcs.	5250	4157	–
Rivets, pcs.	–	–	1278
Clinches, pcs.	–	14	–
Weld studs, pcs.	247	83	–
Screws, pcs.	–	–	52
Seam welds, m	9.3	150.29	–
Adhesive lines, m	79.4	20.22	152

Due to the increasing complexity in body design, material definition, manufacturing processes and joining technologies, the complexity and data volume in the development of automotive bodies is on the rise. In this context, effective data management processes must be introduced to ensure that all information between the different CA*x* environments is processed and transferred effectively and without unwanted losses. These exchange processes of CAD-based joining technology data include the usual suitable data formats and tools applied to support the exchange processes [13, 14].

With the main focus on joining technology data, information can be exchanged either as native CAD data (e. g. CATIA [15], NX [16]), or by using neutral data exchange formats (e. g. list-based, XML-based [17], JT (Jupiter Tessellation) [18], STEP (Standard for the Exchange of Product Model Data) [19], etc.). Above all, interfaces have to be created for external data exchange (e. g. between OEM and supplier), so that the involved data exchange file formats can be integrated successfully.

Approach

As previously mentioned, it must be ensured that both internally and externally created CAD-based joining technology data can be integrated into optimized data exchange processes (Fig. 1). Besides geometry-based data in native or neutral formats, joining technology data can also be available in neutral list-based formats (e. g. Excel file) or XML-based formats – depending on the agreed data exchange strategy of the involved companies. Because of the different input sources (file formats, file structure) available and the associated different data structuring, there is a high additional effort in the preparation of data for the CAM environment.

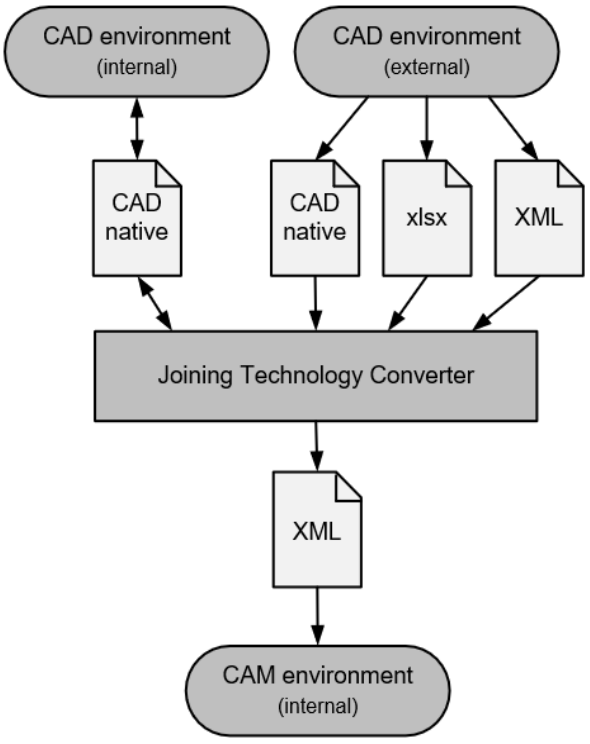

Fig. 1. Approach of the optimized data exchange process for joining technology data

This high expense results from the fact that the different input data must be prepared manually on a uniform data structure. Using a uniform data structure or a uniform data exchange format has the advantage that the data exchange process runs the same at all times. This can reduce

the preparation time in the target environment significantly. Expenses that increase the preparation time include, among others, restructuring of input joining technology data and clearing and adjusting unneeded information and parameters.

A simple example of a joining technology element, a spot weld, is used to illustrate these expenses. When creating a spot weld in CAD environments, information such as geometrical depiction, coordinates, diameter, height, weight, normal direction vector and parts to be connected is created. The target environment (e. g. CAM) only needs the coordinates, diameter, normal direction vector and part to be connected. Since further information is not needed or even undesired (leads to larger simulation models), the data must be prepared for each joining technology element.

In the present approach, the common data format XML (Extensible Markup Language) is used in the optimized data exchange process. XML combines the advantages of lean design, simple integrability in different tools and systems of the target environment as well as simple editability (if necessary). A leaner design of the data to be exchanged results from the fact that unneeded information and parameters are filtered and thus not transferred during the exchange, which reduces the amount and size of exchanged data.

The approach requires the implementation of an interface, which converts the data from the source formats into the used data exchange format (XML) of joining technology data. This interface is designed in such a way that it is a tailor-made tool, named “Joining Technology Converter”. This tool can collect, merge and convert both internally created data (CAD environment internal – CAD native) and externally created data (CAD environment external – CAD native, XML-based and list-based). Since neutral geometry-based exchange formats (e. g. JT, STEP...) are rarely used for joining technology data, they are not considered in the approach of the optimized data exchange process.

In case that some parts of the joining technology data are internally, and some parts are externally available (created), the tool “Joining Technology Converter” offers an additional function. In this function it is possible to integrate the originally externally created joining technology data (source file either CAD native, list-based or XML-based) into the internal CAD environment. Thus, the 3*D*-CAD model can be completed in addition to further processing of the joining technology data in an XML file. Due to the use of this function, the complete joining technology data are available both in the internal CAD and CAM environment.

Application of the approach

The application of the newly introduced approach of optimized data exchange for joining technology data is shown by means of an exemplary data exchange procedure, which can be assigned to real projects in the automotive industry. In this scenario, the CAD-based joining technology data are exchanged between an OEM and a Tier 1 supplier. Furthermore, parts of the joining technology data are created internally (CAD environment of the Tier 1 supplier). The production of the vehicle body takes place after the successful data exchange and after fulfilling all CAM-engineering – related tasks (e. g. space analyses, accessibility checks for tools to create joining elements, planning of optimized production processes, calculation of processing time for joining elements, creation of an optimized joining sequence...) at the supplier.

Fig. 2 shows the application of the approach of optimized data exchange process of joining technology data. As a leverage point it can be assumed that the entire geometry data (e. g. geometrical characteristics, dimensions of the sheets, center of gravity, material...) are provided in the internal CAD environment.

Parts of joining technology data have already been created by the OEM and are exchanged by using Excel files. By using the tool “Joining Technology Converter” the available data are further processed into two different data formats. Once the external joining technology data are converted into an XML file, it can be transferred to the CAM environment. A further conversion of the external joining technology data into a native CAD file is necessary so that the 3*D*-CAD model can be extended with the external joining technology data.

In the present exemplary project, the creation of the remaining CAD-based joining technology

data takes place in the internal CAD environment of the automotive supplier. As soon as the completion of these joining technology data is finished, the conversion of these native data into a neutral XML file takes place by use of the tool "Joining Technology Converter".

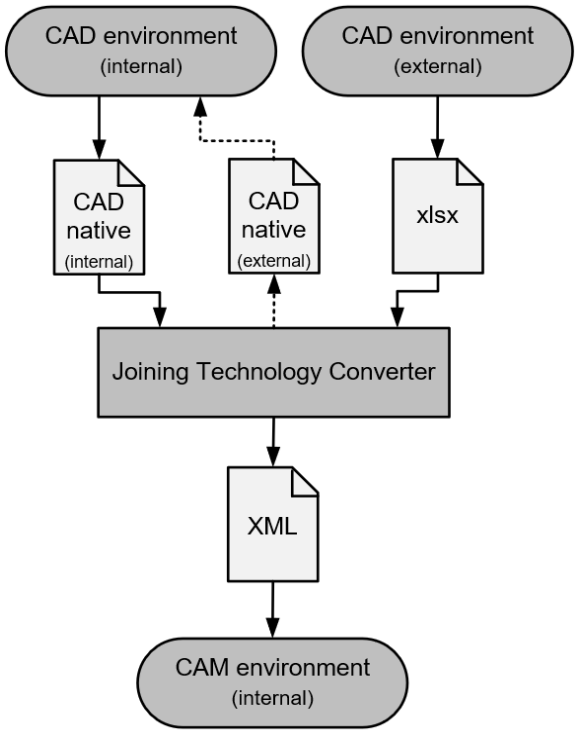

Fig. 2. Application of the approach of optimized data exchange for joining technology data in projects between different companies, e. g. OEM and supplier

Since the complete joining technology data are now available in XML file format, the data can be integrated into the CAM environment. As mentioned before, the joining technology data are prepared in such a way that they only need to be inserted into the corresponding processes. For this reason, no further data processing steps are necessary. Since the integration of geometry data takes place parallel to the integration of joining technology data, all necessary CAM – related engineering procedures can now be started effectively.

CONCLUSIONS

1. The current existing gaps in the data exchange of joining technology data is leading to increased efforts and expenses in the area of data management. These gaps are mainly caused by missing standards, as well as the high number of different exchange procedures applied. In this context, the present paper introduces an approach to close the gap in data exchange of joining technology data. Both internal and external data exchange possibilities as well as boundary conditions (e. g. data exchange file formats, data structure…) are considered.

2. In summary, it can be stated that the introduced approach of optimized data exchange processes of joining technology data can be applied to a large variety of projects. The optimized approach is flexibly designed so that it is possible to react quickly to new occurring requirements or boundary conditions (e. g. additional data exchange file formats, new types of joining technology, new parameters…).

3. Due to the implementation of process uniformity, the amount of information to be transferred is minimized. The reason for this is that the interface tool "Joining Technology Converter" only exchanges data required in the target environments. This leads to a shorter preparation time of data in the target environments and increases the efficiency in data management [20].

4. The presented optimized joining technology data exchange process provides a good starting point for a smart integration of knowledge-based design methods and design automation into car body development.

5. In practical investigations in automotive engineering projects, the application of the optimized data exchange process enabled a time reduction of up to 25 % per CAM simulation loop. The optimization was achieved is mainly due to the fact that data conversion is used (tool "Joining Technology Converter") to reduce data exactly to the required data level. Thus, the preparation time of the joining technology data in the individual CA*x* environments can be massively reduced.

6. Since in typical car body development processes several optimization loops are performed, optimized data management enables considerable time and cost savings, which also supports earlier market launches of newly developed vehicles and their derivatives.

REFERENCES

1. Niikura A. (2018) The Impact of the Application of Aluminum. *ATZ Extra Issue – Motor Fan Special Edition Illustrated* (Aluminum Technology 4).
2. Hirz M., Rossbacher P. (2016) Enhanced Knowledge-Based 3*D*-CAD Methods Supporting Automotive Body-in-White Production Engineering. *Management of Technology – Step to Sustainable Production, Porec, Croatia*.
3. Autoevolution, Homepage of Autoevolution. https://www.autoevolution.com/news/audi-a8-the-car-body-of-the-year-26659.html (Accessed 23 August 2019).
4. Pahl G., Beitz W., Feldhusen J., Grote K. H. (2007) Engineering Design: a Systematic Approach. *Springer, Berlin, Germany*.
5. Weber J. (2009) Automotive Development Processes – Processes for Successful Customer Oriented Vehicle Development. *Springer, Munich, Germany*. https://doi.org/10.1007/978-3-642-01253-2.
6. Malen D. E. (2011) Fundamentals of Automobile Body Structure Design. *SAE, Warrendale, PA, USA*.
7. Kreis A., Hirz M., Stadler S., Salchner M., Rossbacher P. (2018) Convenient Connection Technology Data Model Supporting Optimized Information Exchange between CA*x*-Systems. *Computer-Aided Design and Applications,* 15 (5), 771–778. https://doi.org/10.1080/16864360.2018.1441244.
8. Thum K., Hirz M., Mayr J. (2014) An Integrated Approach Supporting Design, Simulation, and Production Engineering of Connection Techniques in Automotive Body-in-White Development. *Computer-Aided Design and Applications,* 11 (4), 411–416. http://dx.doi.org/10.1080/16864360.2014.881183.
9. Nedic S., D'Elia A., Palmquist N. (2016) The All-New Volvo V90 Car Body. *EuroCarBody2016, Bad Nauheim, Germany*.
10. Robert H., Scherrer J. M. (2016) New Peugeot 3008. *EuroCarBody2016, Bad Nauheim, Germany*.
11. Pugh-Jones Y., Richardson P., Walker F. (2016) Aston Martin DB11. *EuroCarBody2016, Bad Nauheim, Germany*.
12. Hachino M. (2018) Evolving Joining Technologies for Aluminum. *ATZ Extra Issue – Motor Fan Special Edition Illustrated* (Aluminum Technology 4).
13. Hirz M., Dietrich W., Gfrerrer A., Lang J. (2013) Integrated Computer-Aided Design in Automotive Development. *Springer, Berlin, Germany.* https://doi.org/10.1007/978-3-642-11940-8.
14. Kovacs G. L., Kochan D. (2013) Digital Product and Process Development Systems, IFIP TC 5 International Conference. *Springer, Dresden, Germany,* ISBN 978-3-642-41328-5. https://doi.org/10.1007/978-3-642-41329-2.
15. Dassault Systems CATIA. *Homepage of Dassault Systems.* https://www.3ds.com/de/produkte-und-services/catia/ (Accessed 23 August 2019).
16. Siemens NX. *Homepage of Siemens.* https://www.plm.automation.siemens.com/global/de/products/nx/ (Accessed 23 August 2019).
17. Norm ISO 8879, Information Processing – Text and Office Systems – Standard Generalized Markup Language, 1986.
18. Norm ISO 14306, Industrial Automation Systems and Integration – JT File Format Specification for 3*D* Visualization, 2017.
19. Norm ISO 10303, Industrial Automation Systems and Integration – Product Data Representation and Exchange, 2014.
20. Hirz M., Rossbacher P., Gavačová J. (2016) Future Trends in CAD – from the Perspective of Automotive Industry. *Computer-Aided Design and Applications,* 14 (6), 734–741. https://doi.org/10.1080/16864360.2017.1287675.

Received: 08.10.2019
Accepted: 10.12.2019
Published online: 31.01.2020

https://doi.org/10.21122/2227-1031-2020-19-1-12-19

UDC 629

Battery Ageing as Part of the System Design of Battery Electric Urban Bus Fleets

M. Ufert[1)], B. Bäker[1)]

[1)]Dresden University of Technology, Dresden Institute of Automobile Engineering (Dresden, Federal Republic of Germany)

Abstract. The lifetime of traction battery systems is an essential feature of the economy of battery electric urban bus fleets. This paper presents a model for the analysis and prediction of the lifetime of urban electric bus batteries. The parameterization of the model is based on laboratory measurements. The empirical ageing model is an integral part of a three-stage battery model, which in turn is an important component of the methodology for the overall system design, evaluation and optimisation of battery electric urban bus fleets. In an equidistant closed simulation loop, the electrical and thermal loads of the traction battery are determined, which are then used in the ageing model to calculate the SOH (state of health) of the battery. The closed simulation loop also considers the effects of a constantly changing SOH on the driving dynamics of the vehicles. The model for lifetime analysis and prognosis is presented in the paper, placed in the context of the overall system design and demonstrated by means of a practice-oriented example. The results show that the optimal system design depends, among other things, on whether an ageing simulation was used. Taking battery aging into account, system costs in the example presented can be reduced by up to 17 %.

Keywords: electric buses, battery modelling, battery aging, charging infrastructure, optimisation

For citation: Ufert M., Bäker B. (2020) Battery Ageing as Part of the System Design of Battery Electric Urban Bus Fleets. *Science and Technique.* 19 (1), 12–19. https://doi.org/10.21122/2227-1031-2020-19-1-12-19

Старение аккумуляторов как часть системы проектирования парков городских аккумуляторных электрических автобусов

М. Уферт[1)], Б. Бекер[1)]

[1)]Дрезденский технический университет, Дрезденский институт автомобилестроения (Дрезден, Федеративная Республика Германия)

Реферат. Срок службы систем тяговых аккумуляторов играет существенную роль в вопросе экономии для парка электрических городских автобусов. В статье представлена модель для анализа и прогнозирования срока службы аккумуляторных батарей электрических городских автобусов. Параметризация модели основана на лабораторных измерениях. Эмпирическая модель старения – неотъемлемая часть трехступенчатой модели аккумуляторов, которая, в свою очередь, является важным компонентом методологии для общего проектирования системы, оценки и оптимизации парка аккумуляторных электрических городских автобусов. В эквидистантном замкнутом контуре моделирования определяются электрические и тепловые нагрузки тягового аккумулятора, используемые в модели старения для расчета SOH (состояния работоспособности) аккумулятора. Замкнутый цикл моделирования также учитывает влияние постоянно меняющегося SOH на динамику вождения транспортных средств. Предлагаемая модель используется в контексте общего проектирования системы; показан пример практического применения. Согласно результатам исследования, оптимальное проектирование системы зависит, помимо прочего, от того, используется или нет моделирование процесса старения. Принимая во внимание старение аккумулятора, системные затраты в рассматриваемом примере могут быть уменьшены до 17 %.

Ключевые слова: электрические автобусы, моделирование аккумулятора, старение аккумулятора, инфраструктура процесса зарядки, оптимизация

Для цитирования: Уферт, М. Старение аккумуляторов как часть системы проектирования парков городских аккумуляторных электрических автобусов / М. Уферт, Б. Бекер // *Наука и техника*. 2020. Т. 19, № 1. С. 12–19. https://doi.org/10. 21122/2227-1031-2020-19-1-12-19

Адрес для переписки
Уферт Мартин
Дрезденский технический университет,
Дрезденский институт автомобилестроения
ул. Дезернат, 8,
01062, г. Дрезден, Федеративная Республика Германия
Тел.: +49 351 463-39-563
martin.ufert@tu-dresden.de

Address for correspondence
Ufert Martin
Dresden University of Technology,
Dresden Institute of Automobile Engineering
8 Dezernat str.,
01062, Dresden, Federal Republic of Germany
Tel.: +49 351 463-39-563
martin.ufert@tu-dresden.de

Introduction

Driven by the ongoing discussion about clean air in German cities, many municipal transport companies are pushing ahead with the conversion of their bus fleets from diesel buses to electric buses. In many cities, this is an elementary step in the pack-age of measures to reduce emissions and comply with legal limits.

In recent years, various pilot projects have been launched and completed in various calls for proposals (e. g. Berlin, Hamburg, Dresden) [1]. In Dresden, for example, a 12 m electric bus with a conductive high power charging system was extensively tested as part of the "Electric Bus Line 79" project [2]. The aim of all of these projects was to test the different systems available on the market with regard to readiness for use and to gain initial experience in handling electric buses and their use in regular passenger service. An overview of the pilot projects in Germany is given in [1]. In many of these projects mainly vehicles were put into operation, which are then used on specially selected routes – often with low daily mile-age in order to avoid the range problem. Only in a few projects was the number of vehicles procured sufficient to operate an entire line with electric buses.

In the coming years, the next step towards switching bus fleets to electric mobility is to be taken. Many public transport companies are planning to procure a larger number of vehicles with which entire lines can then be operated completely with electric buses. In order to maximise public awareness, there is often a desire to choose so-called volume lines. These are lines that have a high passenger volume and often a high daily mileage and require a corresponding range.

The vehicles currently available on the market have very different ranges. The manufacturer's specifications range: from approx. 150 km for a 12 m vehicle [3] to over 300 km for an 18 m vehicle [4]. However, depending on the choice of line, this range may be too short to ensure safe operation under all circumstances. In such cases, charging the energy storage device during operation is required in order to be able to perform the daily driving performance. This charging can be carried out in different ways. The main degrees of freedom are the location, duration and power of the charging.

Switching from diesel buses to electric buses does not only mean simply replacing the vehicles, but is to be understood as a way of designing the system. Today, this design is often based on empirical values. For example, specific mean values (in kW·h/km) are used to estimate the required energy content of the traction battery for a certain distance. For charging, known combinations of charging location and charging power are then used, which are often known from the pilot projects. However, in many cases such a system design has a rather heuristic character and often only a few design scenarios are compared with each other. This procedure is shown exemplarily in [5, 6]. An optimal design, for example with regard to the required investment and operating costs, cannot be determined thereby.

This paper presents a methodology which automatically calculates and evaluates a multitude of technically possible configurations for a given route under given boundary conditions. The core of the methodology is a detailed, multi-stage battery model, since the traction battery is currently the most expensive single component of an electric vehicle [7] and its consideration therefore has a particularly high priority in system design.

Probably the most important differences between electric buses and diesel buses in daily operation are the limited range and the much more complex charging process (charging energy storage vs. refuelling in conventional diesel buses). Analogous to the refuelling process, charging the vehicles in the depot during the night break is the state of the art. The required charging infrastructure confronts transport companies with great challenges, especially if a large number of vehicles are to be charged simultaneously in the depot. However, the charging process in the depot and the required hardware will not be examined in detail in this paper.

The focus of the methodology presented here is on the choice of a suitable energy storage device as well as a possibly necessary charging infrastructure along the route being considered. The following questions are to be answered:

- What is the power requirement of a vehicle to cover the considered distance?
- What is the required energy content of the traction battery?

• How many charging points are required along the line and where are they positioned?

• What charging power must be installed at the charging points?

• Is the stop time planned according to the timetable at the charging points sufficient?

• How does the intended operation affect the lifetime of the traction battery?

Simulation framework

The developed framework was especially designed to answer these questions. The aim is to carry out a system simulation with subsequent parameter variation within the framework. Thus, a large number of technical configurations can be calculated for a specific system and be evaluated in a post-process. The following variation parameters are defined for this purpose:

• energy content of the traction battery;

• number and position of charging points in the network;

• power to be installed at the charging points.

The route to be investigated is first examined with regard to the possible charging point locations. All locations that could be used as potential charging points are marked. Criteria for this can be, for example, the amount of space required, the available network connection or a pause in operation. A Tab. 1 with all possible combinations is then created. For an example route with two potential locations, this results in 4 combinations.

Table 1

Combination of charging points

ID	Depot charging	Charging point 1	Charging point 2
(0/0)	1	0	0
(1/0)	1	1	0
(0/1)	1	0	1
(1/1)	1	1	1

It is assumed that depot charging always takes place so that it is not part of the parameter variation. Only the combination possibilities of charging point 1 and charging point 2 are varied at this point. The variation parameters of charging power and battery energy content are varied within (user-defined) limits in discrete increments.

All possible combinations of variation parameters are now calculated within the framework. The subsequent evaluation of the results is initially carried out with regard to technical feasibility. Often not all theoretically possible combinations are technically feasible. In the second step, the technically feasible configurations are economically evaluated and compared with each other. In the following chapters, the individual models of the system simulation are presented.

System modelling

The system simulation consists of two main modules: module 1 determines the power requirement of the vehicle during operation on a given route. The structure and functionality of this module are explained in [8] and will not be discussed in detail here.

In module 2 the dimensioning of the energy storage as well as the required charging infrastructure is carried out. The core of this module is a detailed, three-stage battery model. The system simulation is completed by an electrical model of the charging infrastructure as well as a cost model for the evaluation of the determined configurations. The individual models are explained below.

Battery model. The battery model consists of 3 sub-models (Fig. 1): electric, thermal and aging model. The sub-models are called serially.

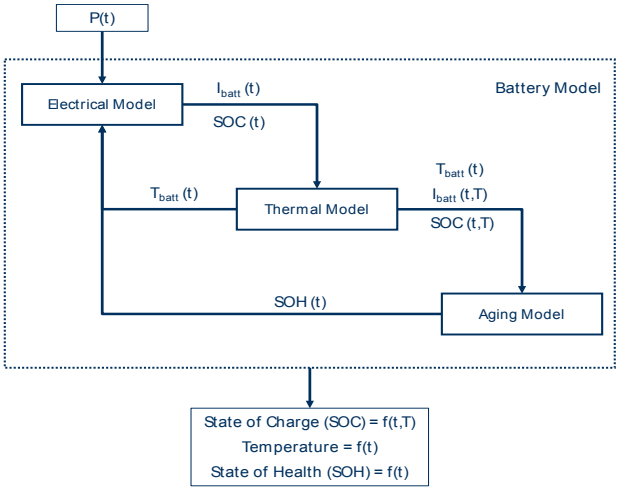

Fig. 1. Three-stage battery model

The power curve $P(t)$, which is calculated in module 1 for the considered vehicle serves as input to the battery model. In the electrical model, the battery current resulting from the power require-

ment and the State of Charge (SOC) are calculated. Both values are transferred to the thermal model. Now the battery temperature is determined. Then the battery current, the SOC and the battery temperature are transferred to the aging model, in which the aging of the battery resulting from the specific load is calculated.

Both the results of the thermal model and the aging model are fed back into the electrical model. On the one hand, the battery temperature determines the maximum permissible current, so that current limitation (and thus power limitation) may be necessary. On the other hand, due to battery aging, the parameterization of the electrical model must be adapted before a new calculation of the power curve can be performed.

Electrical model. An equivalent circuit diagram model is used to model the electrical behaviour of the battery. Different depths of modelling are known from the literature [9]. Common to all is the approach consisting of an open-circuit voltage source and an ohmic internal resistance. Then, depending on the desired accuracy, one or more *RC* elements are connected. As the number of *RC* elements increases, the accuracy of the results generally increases, but the computational and parameterization effort increases as well. As a compromise, an equivalent circuit diagram containing one *RC* element was chosen (Fig. 2).

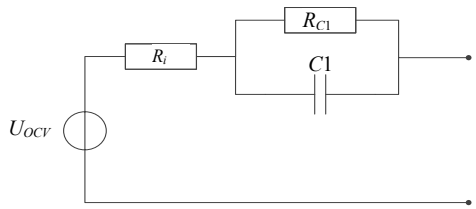

Fig. 2. Equivalent circuit diagram of a single battery cell

The equivalent circuit diagram is first parameterized for a single cell. Subsequently, an equivalent circuit diagram for the entire battery storage is drawn up using the known connections to the series and parallel connection. The following information is essential for the parameterization of the cell model:

- open circuit voltage (*OCV*);
- ohmic internal resistance R_i;
- capacity *C* and resistance value *R* of the *RC* element.

All mentioned components are not constant quantities and have non-linear progressions, so that corresponding characteristic diagrams have to be defined in the simulation.

- *OCV*. The open circuit voltage depends on the SOC of the individual cell. In addition, a capacity is assigned, since a battery cell can only absorb and release a limited amount of charge. The capacity of the cell depends on the temperature.
- *Ohmic internal resistance.* The ohmic internal resistance depends on both temperature and SOC.
- *RC element.* Both components of the *RC* element are temperature and SOC dependent.

Some of the required parameters can be taken from cell data sheets. Especially the values of the RC element are rarely given, so that these values have to be measured in the laboratory. A procedure for this is explained in [10].

In addition to the parameterization of the individual equivalent circuit components, limit values for battery operation can be stored in the electrical model. In real operation, these limits are usually specified in the battery management system (BMS) and are intended to ensure safe and reliable operation of the battery. A simple and effective way of such a BMS parameterization are current characteristic diagrams depending on the battery temperature and the SOC (Fig. 3).

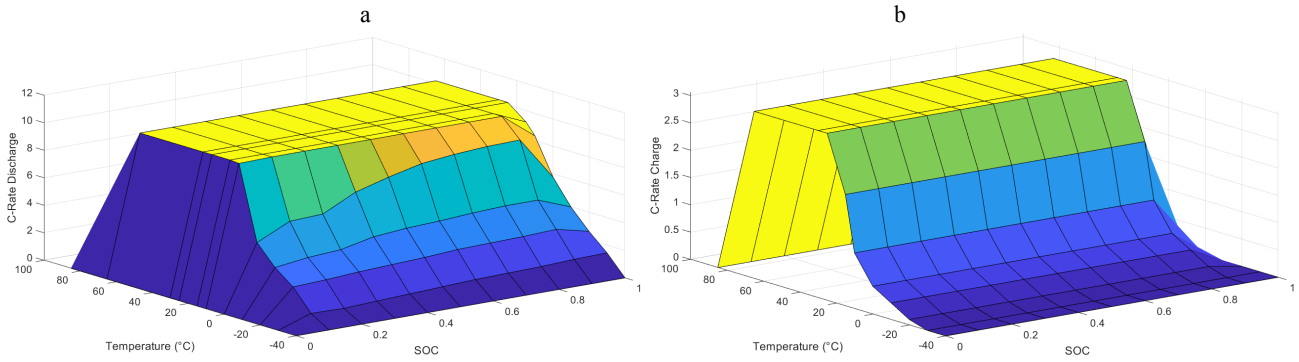

Fig. 3. Permissible battery current: a – discharge; b – charge

Thermal model. In the thermal model, the temperature of the entire battery storage device is deter-mined. From the literature different modelling depths for single cells are known. In [11] the principal representation of 0*D*-, 1*D*-, 2*D*- and 3*D*-models is shown. The relationship between parameterization effort, model complexity, result accuracy and calculation time is also shown.

For this methodology, a 0*D*-model is chosen due to the low parameterization effort and the short computation times. Analogous to the electrical model, a model at cell level is first created here as well. However, the interconnection to the full storage is not trivial. Often individual cells are grouped into modules, which in turn are connected in series and parallel to the full storage device. In order to determine the battery temperature, the consideration of such a module is essential.

In the 0*D*-model, a heat flow is injected in the middle of a rectangular body (Fig. 4a). Part of the heat is then released across all 6 body surfaces according to the thermal cell properties. If several cells are connected together to form a module, the cell does not release the corresponding proportion of heat from the contact surface into the environment, but transfers it to adjacent cells.

Thus, the interconnection of 0*D* cell models results in a 1*D*-module model (Fig. 4b), since the inner cells have a higher temperature due to the heat transfer from the outer cells and thus a temperature curve in the *x*-direction of the module results. The model used is only valid for rectangular bodies. Accordingly, only prismatic cells and pouch cells can be simulated. For round cells a differentiated analysis is required.

Aging model. The aging model was developed on the basis of the institute's own measurements. A detailed description of the model structure as well as the parameterisation and the required workflow for the determination of a concrete aging can be found in [12].

As state of the art, four essential influencing factors on the aging process of Li-ion batteries are known:

- battery temperature;
- SOC swing or ΔSOC;
- battery current (*C* rate);
- SOC.

All influencing factors mentioned lead to the aging of the battery with different quantities. This has the following effects: on the one hand the usable capacity (reduced range) of the battery decreases, on the other hand the internal resistance increases (lower performance, e. g. regarding acceleration, max. speed or charging time). By definition, a Li-ion battery reaches its End of Life (EoL) if at least one of the following two criteria is met:

- doubling of the internal cell resistance (to 200 %);
- reduction of usable capacity to 80 % of the nominal capacity.

In [12] it was shown by aging measurements that both the decrease of the capacity and the increase of the internal resistance can be approximated by linear functions. On the basis of these measurements, damage factors *S* were determined, which describe the respective share of an influencing factor on the total aging. This results in the following model equations for the determination of aging:

$$C_1 = m_{ref,C} S_{Temp,C} S_{\Delta SOC,C} S_{SOC,C} S_{C-Rate,C} Q + C_0;$$

$$R_{i1} = m_{ref,R} S_{Temp,R} S_{\Delta SOC,R} S_{SOC,R} S_{C-Rate,R} Q + R_{i0},$$

were C_0 – initial capacity; Q – charge throughput; C_1 – resulting (reduced) capacity; S – specific damage factor.

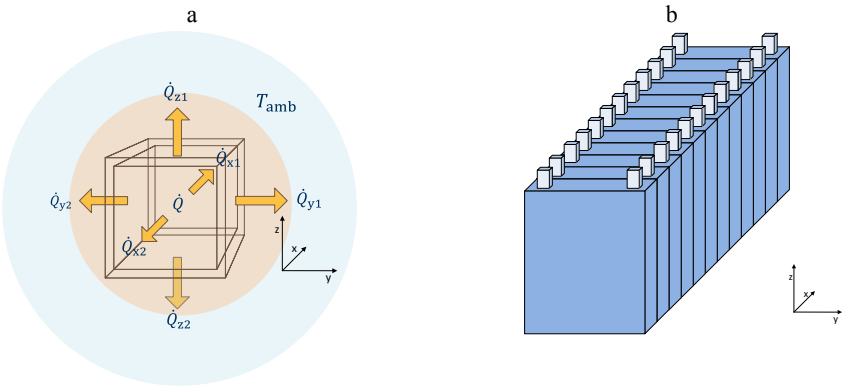

Fig. 4. Thermal model: a – single cell model; b – module model

The denominations apply analogously to the equation of internal resistance.

Model of charging points. A simple approach is used to model the charging points. They provide a constant power, which is composed of the charge voltage and the charge current. A constant efficiency can optionally be used to take conversion and transmission losses into account. A retroactive effect on the feeding grid is not considered. The selected constant charging power represents the maximum value. Depending on the operating point of the battery, a derating can be activated. In this case, the available charging current at the charging point is higher than the permissible battery charging current must be limited accordingly.

Cost model. A cost model is to be used to evaluate the technical configurations determined. The model does not aim at providing a classical TCO calculation, as it is done in [13]. Rather, at this point only the individual technical configurations are to be com-pared with each other. Therefore, a simple cost model is used here, which only contains the main cost components of an electric bus system, in which the considered configurations differ. Therefore, the term system costs is used here. The individual components of the model are shown in Fig. 5. The model is parameterized exemplarily for demonstration purposes (Chapter 4).

Conventional diesel buses are usually in service for 12–15 years. A similar period is also assumed for electric buses. It is expected that the traction battery will reach the EoL criteria at least once during this period and will have to be replaced. The number of battery replacements thus has a significant influence on the lifecycle costs of an electric bus, which is why the cost share for this is correspondingly two-stage (Fig. 5).

System simulation

In this chapter the functionality of the system simulation with parameter variation will be demonstrated by means of an example. The following scenario is given in Tab. 2.

Table 2

Operational data and parameter boundaries

Type of vehicle	18 m articulated bus
Type of battery	Lithium-Iron-Phosphate
Length of line	38 km
Number of rounds	6
Daily mileage	6 · 38 km = 228 km
Cycle time	20 min
Vehicle life cycle	12 years
Max. ΔSOC	0.9–0.1
Ambient temperature	15 °C
Battery voltage	420–710 V
Max. charging time CP 1	15 min
Max. charging time CP 2	10 min

The power requirement of the selected vehicle to cover the considered distance is determined by means of the approach described in [8] and is available as a function of time $P(t)$. The following limits are defined for the variation parameters defined in Chapter 2 (Tab. 3).

Table 3

Boundaries of variation parameter

Number of charging points	0–2
Position of charging points	At turning points of the line
Charging power	50–400 kW
Energy content of battery	68–377 kW·h

In the system simulation, all possible combinations of the variation parameters within the defined boundaries are calculated. In this example, the step size of the charging power is 10 kW. The step size of the energy content of the battery is 13 kW·h and results from the fact that the calculation is based on real cells available on the market.

In a first step, all technically possible configurations within the defined boundaries are determined. At this point, the evaluation criteria is the daily SOC curve, at which the lower limit SOC_{min} must not be violated.

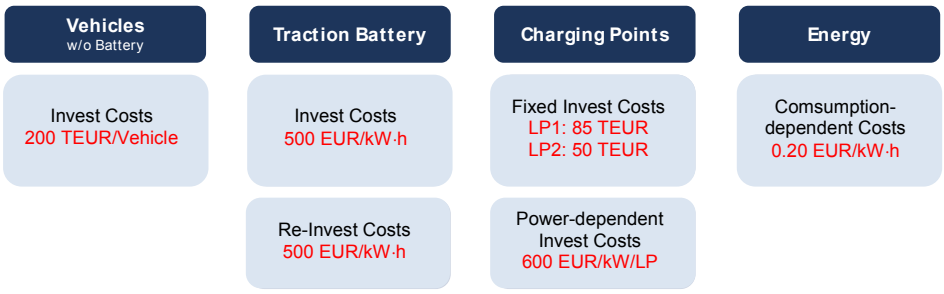

Fig. 5. Cost model including example parameters

Fig. 6 shows the minimum possible energy content of the battery, which can be achieved with the respective combination of number of charging points and charging power. It can be seen that no feasible configurations exist for variants of the charging point combination (0/0). Therefore, the considered route cannot be operated as a depot charger. The maximum energy content of 377 kW·h in connection with the defined SOC boundaries is not sufficient to cover the daily energy demand of the vehicle. Due to the lower available charging time (10 min), the charging point combination (0/1) has fewer feasible configurations than the combination (1/0) with 15 min charging time. The largest number of feasible configurations results consequently from the charging point combination (1/1).

The next step is to evaluate all calculated variants using the cost model (Fig. 5). The expected life time of the traction battery is calculated and on this basis the required battery replacement during the defined vehicle life of 12 years is calculated. In order to avoid a distortion of the results due to integer rounding, decimal numbers for the necessary number of battery changes are permitted. Fig. 7 shows the resulting system costs for all calculated configurations. It can be seen that the lowest system costs are for load point combination (1/1).

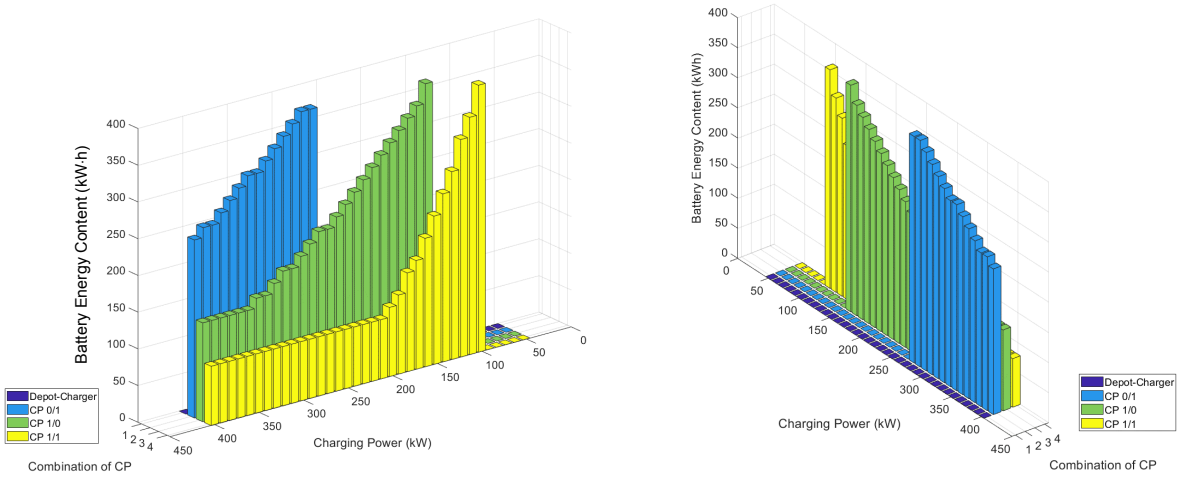

Fig. 6. Minimum energy content of the battery as a function of the charging point combination and the charging power

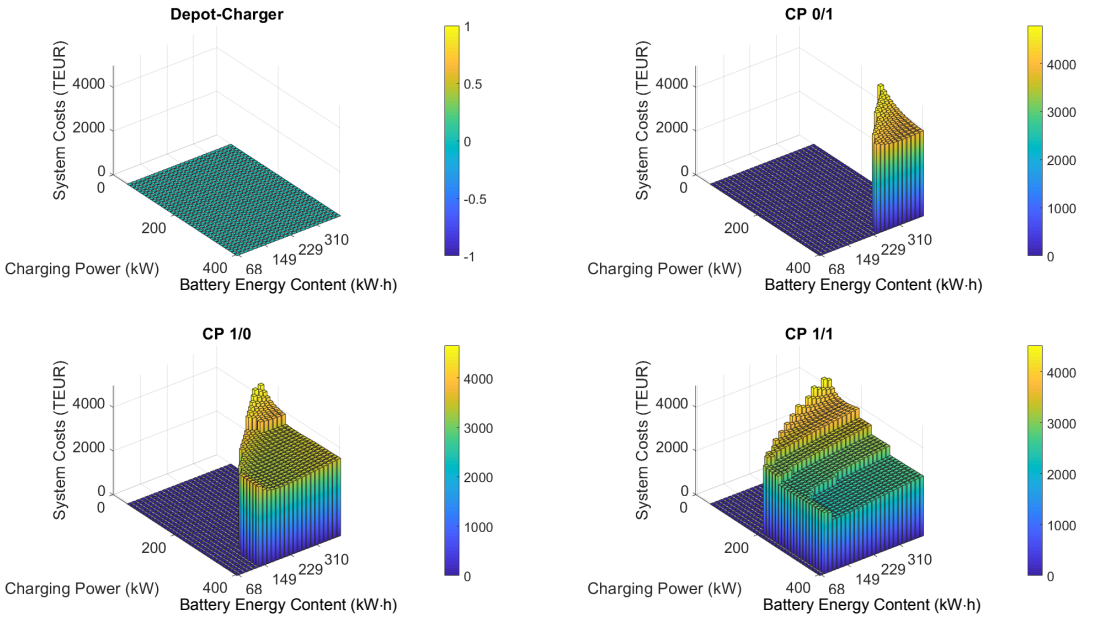

Fig. 7. System costs of all technical feasible configurations

The absolute minimum is not directly recognizable due to the very low variance of the results. The optimum cost can be determined using a minimum search function:

- charging point combination (1/1);
- energy content of the battery: 122 kW·h;
- charging power: 320 kW.

In order to classify the found optimum, this is to be compared with the minimum technically feasible configuration with the same charging capacity and CP. The minimum possible energy content of the battery is 81 kW·h (Fig. 6).

In Tab. 4, both configurations are compared with each other.

Table 4

Predicted lifetime of the traction battery at EoL-criteria

Min. feasible energy content of the battery acc. to Fig. 6	Energy content of the battery at cost minimum acc. to Fig. 7
81 kW·h 100 %	122 kW·h 150 %
1072 days of operation (2.9 years) 100 %	1822 days of operation (5.0 years) 170 %
2761 TEUR 100 %	2300 TEUR 83 %

The results show that choosing a 50 % larger battery results in a 70 % increase of battery life. Ac-cording to the cost model (Fig. 5), the cost of a single battery set also increases by 50 %. However, the system costs over the vehicle life cycle can be reduced by 17 % due to the extended lifetime.

CONCLUSIONS

1. In this paper a methodology was presented which enables the dimensioning of energy storage and charging infrastructure of electric bus lines. Therefore, a framework was developed which varies the parameters battery energy content, charging power as well as location and number of charging points within definable limits. Within this framework, individual lines can be analysed by means of system simulation. The core of the system simulation is a three-stage battery model consisting of electrical, thermal and aging model.

2. The functionality of the methodology was demonstrated by an example. In this example, all technically feasible configurations within the set variation limits were first determined. A cost model was used to evaluate these configurations. It could be shown that an economically optimal combination does not necessarily correspond to the combination with minimum technical effort. This is mainly due to the aging of the energy storage device. In this example, a battery with a larger energy content leads to a longer service life of the storage device and thus to a reduction in system costs over the vehicle life cycle.

REFERENCES

1. Union Internationale des Transports Publics (2017) *ZeEUS eBus Report #2: an Updated Overview of Electric Buses in Europe*, 2017. Available at: https://alatransit.kz/sites/ default/files/zeeus-ebus-report-internet.pdf.
2. Bunzel A., Petersohn R., Bäker B. (2016) Dresden's Bus Route 79 Turned into Full Electric – Opportunity and Challenge. Hoff C., Sirch O. (eds.) *Elektrik, Elektronik in Hybrid- und Elektrofahrzeugen und Elektrisches Energiemanagement VII. Renningen.* Expert-Verlag, Fachbuch / Haus der Technik, Band 142 (in German).
3. Werwitzke C. (2018) *Mercedes-Benz rückt Serien-eCitaro ins Rampenlicht*. Available at: https://www.electrive.net/2018/ 07/10/mercedes-benz-rueckt-den-ecitaro-ins-rampenlicht (Accessed 17 January 2019).
4. *Technische Daten: Sileo S18*. Available at: https://www. sileo-ebus.com/fileadmin/user_upload/service/download/ datenblaetter/Sileo_Datenblatt_S18_DE_Ansicht_11-10-2018.pdf (Accessed 17 January 2019).
5. Ufert M. (2018) *Systemauslegung Batterie-Elektrischer Stadtbuslinien Unter Berücksichtigung des Alterungsverhaltens der Hochvolt-Traktionsenergiespeicher* [System Design of Battery-Electric Urban Bus Lines Considering the Ageing Behaviour of the High-Voltage Traction Energy Storage Devices]. *6th International E-Bus Conference*. Solingen, Germany (in German).
6. Ufert M. (2018) Dimensionierung von Energiespeicher und Ladeinfrastruktur am Beispiel von Elektrobussen. *Symposium "Elektrische Fahr-Zeugantriebe und – Ausrüstungen". Dresden, 30.11.2018.* Available at: https://www.researchgate.net/ publication/329309560_Dimensionierung_von_Energies pei cher_und_Ladeinfrastruktur_am_Beispiel_von_Elektrobussen (in German).
7. Kampker A., Vallée D., Schnettler A. (eds.) (2018) *Elektromobilität: Grundlagen einer Zukunftstechnologie*. Berlin, Springer-Verlag (in German). https://doi.org/10.1007/ 978-3-662-53137-2.
8. Bunzel A., Baker B. (2018) Energy Consumption of Electric City Buses: Determination as a Part of a Technological and Economic Evaluation of Bus Lines with Regards to their Electrifiability. *2018 IEEE International Conference on Electrical Systems for Aircraft, Railway, Ship Propulsion and Road Vehicles & International Transportation Electrification Conference (ESARS-ITEC).* https://doi.org/ 10.1109/esars-itec.2018.8607520.
9. Einhorn M., Conte V., Kral C., Fleig J. (2011) Comparison of Electrical Battery Models Using a Numerically Optimized Parameterization Method. *IEEE Vehicle Power and Propulsion Conference.* https://doi.org/10.1109/vppc.2011.6043060.
10. Morawietz L., Kutter S., Falsett R., Bäker B. (2008) Thermoelektrische Modellierung Eines Lithium-Ionen-Energiespeichers Fuer den Fahrzeugeinsatz. *Innovative Fahrzeugantriebe 2008*: Tagung Dresden, 6. und 7. November 2008. Düsseldorf, VDI-Verlag, 299–318 (in German).
11. Fleckenstein M. (2013) *Modellbasiertes Thermomanagement für Li-Ionen-Zellen in Elektrischen Fahrzeuganwendungen*. München, Verlag Dr. Hut. Zugl.: Technische Universität Dresden, Diss. (in German).
12. Ufert M., Batzdorf A., Morawietz M. (2018) Prädiktion der Lebensdauer von Traktionsbatteriesystemen für Reale Nutzungsszenarien. *VDI-Fachtagung Innovative Antriebe 2018: Der Ausblick auf die Fahrzeugantriebe für die Kommenden Dekaden,* 33–48 (in German).
13. Kunith A. W. (2017) *Elektrifizierung des Urbanen Öffentlichen Busverkehrs: Technologiebewertung für den Kosteneffizienten Betrieb Emis-Sionsfreier Bussysteme.* Springer Vieweg, Wiesbaden (in German). http://dx.doi.org/10. 1007/978-3-658-19347-8.

Received: 08.10.2019
Accepted: 10.12.2019
Published online: 31.01.2020

https://doi.org/10.21122/2227-1031-2020-19-1-20-33

UDC 629

Comparing Fuel Consumption and Emission Levels of Hybrid Powertrain Configurations and a Conventional Powertrain in Varied Drive Cycles and Degree of Hybridization

W. U. Maddumage[1)], K. Y. Abeyasighe[1)], M. S. M. Perera[1)], R. A. Attalage[1)], P. Kelly[2)]

[1)]Sri Lanka Institute of Information Technology (Malabe, Sri Lanka),
[2)]Loughborough University (Loughborough, United Kingdom)

Abstract. Hybrid electric powertrains in automotive applications aim to improve emissions and fuel economy with respect to conventional internal combustion engine vehicles. Variety of design scenarios need to be addressed in designing a hybrid electric vehicle to achieve desired design objectives such as fuel consumption and exhaust gas emissions. The work in this paper presents an analysis of the design objectives for an automobile powertrain with respect to different design scenarios, i. e. target drive cycle and degree of hybridization. Toward these ends, four powertrain configuration models (i. e. internal combustion engine, series, parallel and complex hybrid powertrain configurations) of a small vehicle (motorized three-wheeler) are developed using Model Advisor software and simulated with varied drive cycles and degrees of hybridization. Firstly, the impact of vehicle power control strategy and operational characteristics of the different powertrain configurations are investigated with respect to exhaust gas emissions and fuel consumption. Secondly, the drive cycles are scaled according to kinetic intensity and the relationship between fuel consumption and drive cycles is assessed. Thirdly, three fuel consumption models are developed so that fuel consumption values for a real-world drive cycle may be predicted in regard to each powertrain configuration. The results show that when compared with a conventional powertrain fuel consumption is lower in hybrid vehicles. This work led to the surprisingly result showing higher CO emission levels with hybrid vehicles. Furthermore, fuel consumption of all four powertrains showed a strong correlation with kinetic intensity values of selected drive cycles. It was found that with varied drive cycles the average fuel advantage for each was: series 23 %, parallel 21 %, and complex hybrids 33 %, compared to an IC engine powertrain. The study reveals that performance of hybrid configurations vary significantly with drive cycle and degree of hybridization. The paper also suggests future areas of study.

Keywords: hybrid electric vehicle, vehicle performance, emissions, fuel economy, driving cycle, degree of hybridization, powertrain simulation, conventional vehicle, three wheeler

For citation: Maddumage W. U., Abeyasighe K. Y., Perera M. S. M., Attalage R. A., Kelly P. (2020) Comparing Fuel Consumption and Emission Levels of Hybrid Powertrain Configurations and a Conventional Powertrain in Varied Drive Cycles and Degree of Hybridization. *Science and Technique*. 19 (1), 20–33. https://doi.org/10.21122/2227-1031-2020-19-1-20-33

Сравнение расхода топлива и уровня выбросов при обычной и гибридных конфигурациях трансмиссий с учетом циклов движения и степени гибридизации

В. У. Маддумаге[1)], К. И. Абеясиге[1)], М. С. М. Перера[1)], Р. А. Атталаге[1)], П. Келли[2)]

[1)]Институт информационных технологий Шри-Ланки (Малаб, Шри-Ланка),
[2)]Университет Лафборо (Лафборо, Великобритания)

Реферат. Применение гибридных электрических трансмиссий в автомобильной промышленности – это решение проблемы выбросов и экономии топлива в сравнении с обычными автомобилями с двигателем внутреннего сгорания. Для достижения желаемых результатов при проектировании гибридного электромобиля необходимо рассматривать

Адрес для переписки
Маддумаге Варуна
Институт информационных технологий Шри-Ланки
Нью Кэнди роуд,
10115, г. Малаб, Шри-Ланка
Тел.: +9471 815-03-28
waruna.m@sliit.lk

Address for correspondence
Maddumage Waruna
Sri Lanka Institute of Information Technology
New Kandy Road,
10115, Malabe, Sri Lanka
Tel.: +9471 815-03-28
waruna.m@sliit.lk

различные варианты, учитывая при этом расход топлива и выбросы выхлопных газов. В статье представлен анализ проектирования автомобильной трансмиссии, рассмотрены различные варианты и ситуации, например целевой цикл движения и степень гибридизации. Разработаны четыре модели конфигурации трансмиссии (двигатель внутреннего сгорания, серийная, параллельная и комплексная конфигурации гибридной трансмиссии) для небольшого транспортного средства (моторизованный трехколесный автомобиль) с использованием программного обеспечения Model Advisor. Перечисленные конфигурации трансмиссии моделировались с различными циклами движения и разной степенью гибридизации. Во-первых, влияние стратегии управления мощностью транспортного средства и эксплуатационных характеристик всевозможных конфигураций трансмиссии исследуется на основе анализа выбросов выхлопных газов и расходов топлива. Во-вторых, циклы движения масштабируются в соответствии с кинетической интенсивностью и оценивается взаимосвязь между расходом топлива и циклами движения. В-третьих, разработаны три модели расхода топлива, так что расход топлива для реального цикла движения может быть спрогнозирован в отношении каждой конфигурации трансмиссии. Исследования показали, что по сравнению с обычной трансмиссией потребление топлива меньше у гибридных транспортных средств. Испытания дали неожиданный результат: более высокие уровни выбросов CO у гибридных транспортных средств. Кроме того, расход топлива всех четырех трансмиссий указывает на сильную корреляцию со значениями кинетической интенсивности выбранных циклов движения. Выявлено, что при различных циклах вождения в среднем предпочтение по топливу для каждого цикла составило: 23 % – для последовательных, 21 % – для параллельных и 33 % – для комплексных гибридов в сравнении с трансмиссией двигателя внутреннего сгорания. Эксперименты показали, что производительность гибридных конфигураций варьируется в зависимости от цикла вождения и степени гибридизации. В статье определены перспективные направления исследований.

Ключевые слова: гибридный электромобиль, работа транспортного средства, выбросы, экономия топлива, цикл вождения, степень гибридизации, моделирование трансмиссии, обычное транспортное средство, трехколесное транспортное средство

Для цитирования: Сравнение расхода топлива и уровня выбросов при обычной и гибридных конфигурациях трансмиссий с учетом циклов движения и степени гибридизации / В. У. Маддумаге [и др.] // *Наука и техника*. 2020. Т. 19, № 1. С. 20–33. https://doi.org/10.21122/2227-1031-2020-19-1-20-33

Introduction

Hybrid electric technology is of great interest to users and manufacturers alike due to the technologies ability to reduce fleet fuel consumption and emissions [1]. When designing a hybrid powertrain system particular set of scenarios need to be considered, and each of these scenarios directly affects the performance or design objectives of the final vehicle design, e. g. fuel consumption, emissions [2]. Solving the design problem of a hybrid vehicle implies, identifying the suitable design parameters, that maximize the design objectives of the vehicles for a given set of design scenarios. Design parameters in a hybrid vehicle may be categorized into three layers as topology, component size and control strategy [3]. The present study examines how the topology parameters in a hybrid design affect the performance or design objectives of a hybrid vehicle for varied design scenarios.

Design scenarios are the main set of decisions considered by a design engineer or a researcher when developing a hybrid powertrain, such as vehicle type, vehicle application, drive cycle, degree of hybridization and duty cycle. Design scenarios set the roadmap for the development of the hybrid vehicle.

Present study examines design objectives under three design scenarios: vehicle type, drive cycle and degree of hybridization. Firstly, the vehicle type, a motorized three-wheeler is used as the developing hybrid vehicle. Three-wheelers are a type of vehicle that has three wheels in a Delta configuration (1 front, 2 rear), powered by an internal combustion engine. The current numbers of three-wheelers globally are approximately 4.5 million. According to WHO 2017 report, these vehicles contribute to ground level ozone, particles in the air and other types of pollution that impact human health and welfare [4]. Secondly, the drive cycle, range of drive cycles are used, representing highway, country and urban cycle characteristics. Thirdly, degree of hybridization, three parallel hybrid powertrains with varied hybridization values are developed.

Design objectives for a hybrid vehicle design are derived from the vehicle type (e. g. three-wheeler, car, bus) and application (e. g. heavy-duty, comfort, operation cost). In solving the design problem of a hybrid vehicle, the goal is to maximize the design objectives by varying design parameters [5]. This paper considers four design objectives, i. e. fuel consumption, CO, HC and NO_x gas emissions.

Nomenclature

Acronym	
WHO	World Health Organization
IC	Internal Combustion
CG	Center of Gravity
HWFET	Highway Fuel Economy Test
CSHVC	City Suburban Heavy Vehicle Cycle
CBD	Central Business District
OCC	Orange County Cycle
GPS	Global Positioning System
SOC	State Of Charge
DC	Drive Cycle
US	United States
WLTP	Worldwide harmonized Light vehicles Test Procedure

Variable

t	Time
h	Height
g	Gravity
HA	Hybrid Advantage
FC	Fuel Consumption
EL	Emission Level
H	Degree of Hybridization
P_{EM}	Power of electric motor
P_{ICE}	Power of engine
KI	Kinetic Intensity
v	Speed
$\tilde{a}$	Characteristic acceleration
v_{aero}^2	Square of aerodynamic speed
D	Distance

Topology design parameters determine the components and energy flow of the hybrid powertrain. The top layer of the topology parameters is the powertrain configuration. Three types of hybrid powertrain configurations may be identified as series, parallel and complex hybrid configurations. Series hybrid configuration is an extension of the electric powertrain by introducing an IC engine in series to the vehicle powertrain. In the parallel hybrid configuration, both engine and motor are connected parallelly to the transmission. The complex hybrid utilizes the best of both series and parallel configurations. By integrating an additional linkage and a generator between the IC engine and battery allows the complex hybrid to operate as both a series and a parallel hybrid. All three configurations harness from down-slope driving and braking to recharge the battery [6].

Many studies have been carried on fuel consumption and emissions of hybrid vehicles with varied design scenarios [7–9]. Y. Huang et al. [1] study fuel consumption and emissions of a conventional and hybrid vehicle under real driving. A. Ahmed in [10] examine emissions and fuel economy of a parallel hybrid and a conventional vehicle for varied drive cycles. M. Karaoglan in [11] investigated the effect gear ratios (design scenario) on emission and fuel consumption for a parallel hybrid. However, a comprehensive study investigating the effect on design objectives of hybrid vehicles with varied design scenarios is yet to be concluded. Hence, present work investigates how different hybrid configurations performs compared to its counterpart conventional powertrain configuration (IC engine powertrain) with varied drive cycles and hybridization values.

Contribution of this paper can be elucidated as follows. First, the fuel consumption and emission values are examined for series and parallel configurations. Relationship between these factors is examined with hybridization and drive cycle. Next, fuel consumption of series hybrid, parallel hybrid, complex hybrid and conventional configurations under various drive cycles are examined. Thereafter, three fuel consumption models to predict fuel economy of the hybrid configurations are proposed. Models are tested with a real-life drive cycle and accuracy of the models are examined. Finally, Hybrid advantage of the three hybrid configurations under varied drive cycles is discussed.

Methodology

Simulation of the four powertrains (i. e. series, parallel, complex hybrid and conventional powertrains) with different drive cycle and hybridization values are done using the MatLab/Simulink based ADVISOR software environment. Advance Vehicle Simulator (ADVISOR) was first developed in September 1994 by the US department of energy's National Renewable Energy Laboratory (NREL) [12]. The software was created in support of the hybrid vehicle subcontracts with the auto industry and the Department of Energy [13]. The number of public users of the software

tool has grown since, with academics and industry users alike [14].

Software is open-source and used offline. A lot of users have contributed to libraries of ADVISOR through new components and data. The robustness of the model and relevance of the model with other simulators are crucial for determining the authenticity of the software. NREL has been making agreements with universities to encompass more accurate data for models [15].

The model used in the simulation is backwards-looking. The drive cycle speed is traced by controlling the vehicle speed using a driver model. Torque, speed and power are propagated backwards from the wheels to the engine and battery. All four configurations share a common driveline (final drive, wheels and chassis).

Vehicle model

Vehicle model for the simulation of the present study is defined with the characteristics of a motorized three-wheeler, based on the BAJAJ RE 205cc three-wheeler (Fig. 1) [16].

Fig. 1. BAJAJ RE 205cc motorized three-wheeler [17]

The main assumptions in modelling the four powertrain models are as follows, the road-load equations considered are for the longitudinal movement of the vehicle; it is assumed that the vehicle model is always capable to meet the power demands of the drive-cycles; tire model assumes a constant rolling resistance coefficient and a constant tire radius; and the system vibrations are neglected.

Road-load acting on the vehicle is modelled as a representation of the force balance at the tire patch. The classical equations of longitudinal vehicle dynamics are considered, i. e. force equals mass into acceleration, where among the forces are rolling resistance, aerodynamic drag, and the force of gravity [16].

A common set of powertrain components were chosen and scaled to meet the vehicle requirements. Engine, Motor and Battery of the powertrains were modelled as quasi-static models (Fig. 2). Data of powertrain components such as efficiency maps, torque maps and model specifications are from the ADVISOR software libraries (Tab. 1) [18].

Table 1

Specifications of the vehicle model

Coefficient of drag [16]	0.44
Frontal area	1.86 m^2
CG height from ground	0.4 m
Wheelbase	2 m
Rear track	1.3 m
Wheel radius	0.2 m
Glider mass (without propulsion)	280 kg
Final drive ratio [16]	0.24
Primary ratio [16]	0.88
Rolling resistance coefficient [16]	0.015

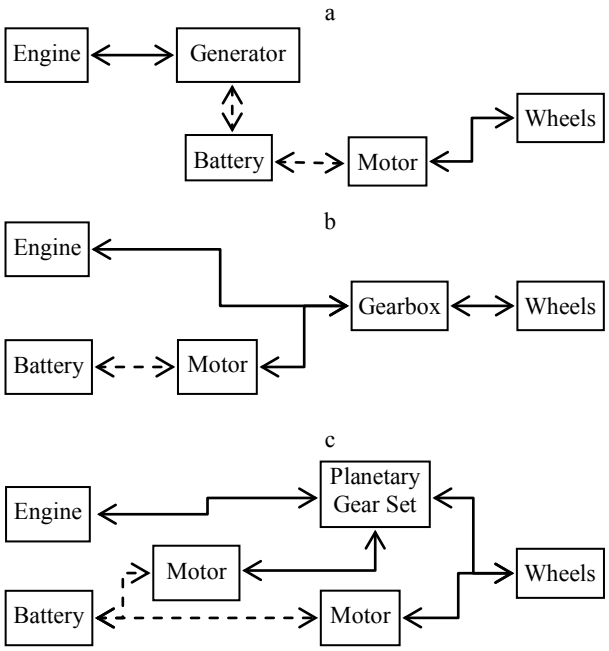

Fig. 2. Hybrid configurations: a – series; b – parallel; c – complex configurations

Battery model used is based on the test data of the 12 V/6 Ah Saft Lithium-Ion battery. Number of batteries were varied to match necessary vehicle characteristics in each powertrain.

Main characteristics of the mechanical components are summarized in Tab. 2.

Table 2

Motor and engine characteristics

Component	Peak efficiency, %	Remark
Engine	30	Gasoline, spark-ignited, Geo Metro 1.0 L SI engine
Traction motor	94	Permanent magnet, top speed 7500 RPM, max torque 112 Nm
Generator	84	Permanent magnet, top speed 5500 RPM, max torque 55 Nm

The transmission used in the conventional powertrain is a 4-speed manual with gear ratios 7.4, 4.1, 2.7 and 1.8 (final and primary ratio included). The gearbox of the parallel transmission is modelled as a 4-speed automatic with the same gear ratios. In series and complex hybrids same final drive ratio was considered, primary drive ratio (between the engine and generator) is considered as two. The planetary gearbox of the complex hybrid powertrain is modelled similar to a Toyota Camry/Prius power split device with 30 teeth in sun gear and 78 in ring gear [8].

Additional electric load of 300 W was considered in the four vehicle models for the load exerted by the accessories.

Control strategies of the four powertrain configurations were taken from ADVISOR libraries, hybrid control strategies are optimized for a small car considering a single objective, i. e. fuel consumption. Control strategy for the parallel hybrid was implemented using the basic power assist control strategy of the ADVISOR software, series hybrid using the power follower control strategy and complex hybrid with the Toyota Prius hybrid 1999 control strategy.

Vehicle sizing

For the four vehicle models to be comparable, a set of requirements are pre-defined. Powertrain components of the four vehicles are sized to meet the said requirements. The vehicle requirements are chosen based on the characteristics of a typical motorized three-wheeler [16, 17, 19]. Vehicle requirements are as follows [8].

- Perform the real world Malabe drive cycle derived for a three-wheeler indefinitely (indefinitely here means using fuel as the energy source and, if applicable, operating any electric machine at or below its maximum continuous torque).
- Reach 0–20 km/h in 6 s and 20–40 km/h in 10 s.
- Reach a top speed greater than 65 km/h.
- Sustain 5 % grade at 35 km/h indefinitely.

Powertrain components for each powertrain configuration differ due to the different power source combinations.

To calculate the component sizes of the four hybrid power trains. a sizing routing is carried out through the automated sizing option available in the ADVISOR software. All the powertrain components are sized, the characteristic maps of the powertrain components are linearly scaled to match required power levels to achieve the defined vehicle requirements. Firstly, Battery and electric motors are sized for the acceleration and maximum speed characteristics, i. e. 0–20 km/h in 6 s/(20–40) km/h in 10 s and top speed greater than 65 km/h. Then the engine is sized to meet the grade requirements. Then the vehicle is tested for the Malabe drive cycle. If the vehicle failed to trace the drive cycle, engine size is increased. This routine is done for several iterations until results converge. The characteristics of the sized vehicles are summarized in Tab. 3. Each powertrain is developed with the same glider mass (Vehicle mass without the propulsion system). However, the overall weight of each configuration varies in comparison to the conventional powertrain due to the different powertrain component combinations equipped in different configurations.

Table 3

Specifications of the four vehicle models

Component	Conventional configuration	Series configuration	Parallel configuration (degree of hybridization)			Complex configuration
			0.2	0.3	0.4	
Engine max power, kW	8	4	7	6	5	5
Traction motor max power, kW	–	5	2	3	4	3
Generator max power, kW	–	4	–	–	–	2
Battery, No of modules	–	15	5	6	7	12
Total weight, kg	438	465	452	448	448	458

Hybrid advantage

The degree of hybridization explains how much the electric machine is involved in vehicle propulsion and it is defined as the ratio of the electric motor power over the total power of the IC engine and the electric motor, as shown in the following equation

$$H = \frac{P_{EM}}{P_{EM} + P_{ICE}}. \quad (1)$$

Two examples in the extreme are the conventional vehicle with the hybridization value of 0 and a full electric vehicle with a hybridization value of 1.

Drive cycles

Several standard drive cycles are chosen for the simulation with a range of kinetic intensity values, representing urban, country and highway driving characteristics. Due to the low-performance characteristics of the motorized three-wheeler, standard drive cycles are modified by linearly scaling down. Five standard drive cycles are used, i. e. Cons (Constant drive cycle), HWFET (EPA Highway Fuel Economy Test), CSHVC (City Suburban Heavy Vehicle Cycle), CBD (Central Business District Segment) and OCC (Orange County Transit Bus Cycle) [20]. Cons, HWFET to represent highway conditions, CSHVC to represent suburban country conditions and OBD, OCC to represent urban driving conditions.

The real-world "Malabe" drive cycle represents an unknown drive cycle. Drive cycle data was found by driving a real-world motorized three-wheeler in local roads. The exact route followed is represented in Fig. 3. The speed and time data represented in Fig. 4 were recorded using the GPS Module NEO-6M. It should be noted that this drive cycle only represents the driving characteristics of the route represented. Tab. 4 summaries the characteristics of the used drive cycles.

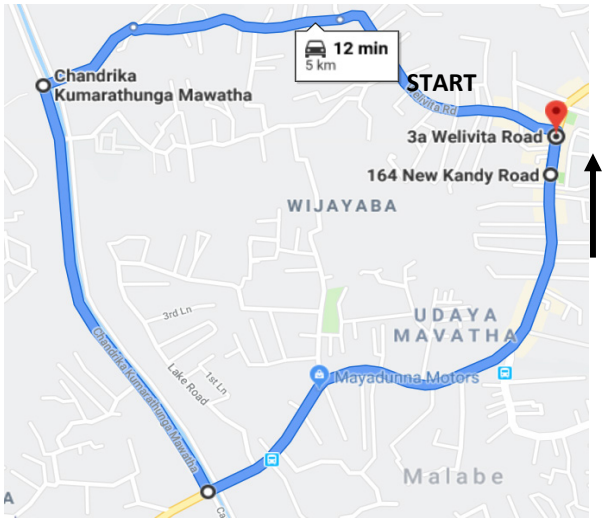

Fig. 3. Malabe drive cycle route (New Kandy road – Waliwita road – Chandrika Kumaratunga road)

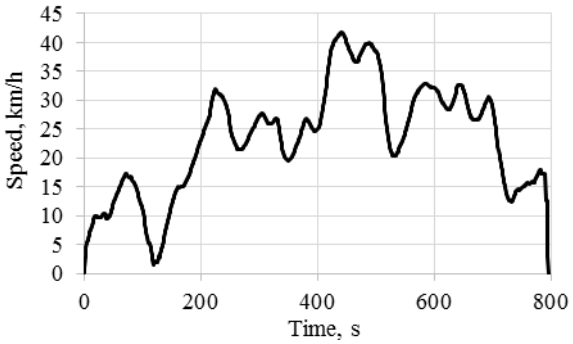

Fig. 4. Malabe drive cycle speed profile (from a real-world driven motorized three-wheeler)

Table 4

Characteristics of the drive cycles

	Cons (modified)	HWFET (modified)	Malabe (real world)	CSHVC (modified)	CBD (modified)	OCC (modified)
Kinetic intensity, 1/km	0.065	0.275	1.33	1.8	2.52	4.45
Duration, s	360	765	800	1700	850	1900
Distance, km	4	8	5.13	6.5	4	5
Max speed, km/h	40	50	40	40	30	30
Average speed, km/h	40	39	25	14	15	10
Max acceleration, m/s^2	0	0.71	0.51	0.7	0.36	0.91
Max deceleration, m/s^2	0	–0.73	–1.4	–1.06	–0.63	–1.15
Average acceleration, m/s^2	0	0.1	0.07	0.24	0.29	0.23
Average deceleration, m/s^2	0	–0.11	–0.09	–0.29	–0.56	–0.32
Idle time, s	0	6	1	397	159	407

Kinetic intensity

Kinetic intensity metrics introduced by O'Keefe et al. is used to analytically characterize drive cycles [7]. Kinetic intensity relates well with the inherent qualities of a hybrid vehicle such as energy harvesting from brake energy. An apparent relationship between fuel usage of a hybrid as well as a conventional vehicle exists for cases where idle fuel usage and vocational loads are small compared to the fuel usage consumed to meet the road load. Kinetic intensity is derived from characteristic acceleration and aerodynamic speed, based on basic road load equations [21]

$$KI = \frac{\text{Characteristic acceleration}}{\text{Aerodynamic speed}^2}. \quad (2)$$

Characteristic acceleration ($\tilde{a}$) and the square of aerodynamic speed (v_{aero}^2) can be calculated for an entire drive cycle as follows:

$$\tilde{a} = \frac{\sum_{j=1}^{N-1} positive\left(\frac{1}{2}\left(v_{j+1}^2 - v_j^2\right) + g\left(h_{j+1} - h_j\right)\right)}{D}; \quad (3)$$

$$v_{aero}^2 = \frac{\sum_{j=1}^{N-1} \overline{v_{j,j+1}^3} \cdot \Delta t_{j,j+1}}{D}; \quad (4)$$

$$KI = \frac{\sum_{j=1}^{N-1} positive\left(\frac{1}{2}\left(v_{j+1}^2 - v_j^2\right) + g\left(h_{j+1} - h_j\right)\right)}{\sum_{j=1}^{N-1} \overline{v_{j,j+1}^3} \cdot \Delta t_{j,j+1}}. \quad (5)$$

Present study uses the kinetic intensity metrics to characterize the drive cycles assuming that idle and vocational load fuel consumption is negligible compared to the fuel consumed for the road load.

Simulation results and discussion

A two-fold approach is followed to assess the effect of design scenarios on traditional hybrid configurations in terms of design objectives. Firstly, the impact of drive cycles and hybridization is assessed in regard to fuel consumption and vehicle emissions for three different powertrain configurations. Secondly, the fuel consumption of four different powertrain configurations is investigated with five drive cycles.

Powertrain models are developed with similar characteristics, thus operational behaviour may be compared. Four powertrain configurations (i. e. series, parallel, complex and conventional) are modelled with the same vehicle characteristics, powertrain components and drive cycle, eliminating the effect of vehicle configuration, driving behaviour and initial conditions from the performance comparison. In general, motorized three-wheelers in the consumer market are not equipped with any emission control technology. Hence, powertrains were modelled without an emission control technology such as a catalytic converter to represent the actual characteristics of a motorized three-wheeler.

Vehicle emissions and fuel consumption

Generally, a hybrid vehicle is designed with the design objective as either fuel consumption or vehicle emission levels. In some cases, both factors are considered, approaching the design problem with multiple objectives. Solving the design of a hybrid is complex, with two objectives. Understanding the behaviour of emissions and fuel rate with operational characteristics of the engine simplifies the design problem. In general, literature considers the fuel consumption as the sole design objective, assuming fuel consumption level as an adequate comparator for emission levels.

Present work assesses the fuel consumption rate and emission gases: CO, NO_x and HC rates with series hybrid, parallel hybrid and conventional powertrains. Moreover, Parallel configuration is further investigated with three different degrees of hybridization. The effect of drive cycle and hybridization on fuel consumption and emissions under different powertrain configurations is examined.

Fig. 5, 6 compare the fuel consumption values and emission values of series and parallel configurations against a conventional powertrain. The three powertrain configurations are simulated on the modified HWFET drive cycle.

Fig. 5 compares the fuel consumption, CO, HC and NO_x emissions for the three vehicle configurations. Fig. 6 compares the hybrid advantage in each hybrid vehicle design compared to the conventional powertrain using the following relationship

$$HA = \frac{FC \text{ or } EL._{Hybrid} - FC \text{ or } EL._{Conv}}{FC \text{ or } EL._{Conv}} \cdot 100\,\%. \quad (6)$$

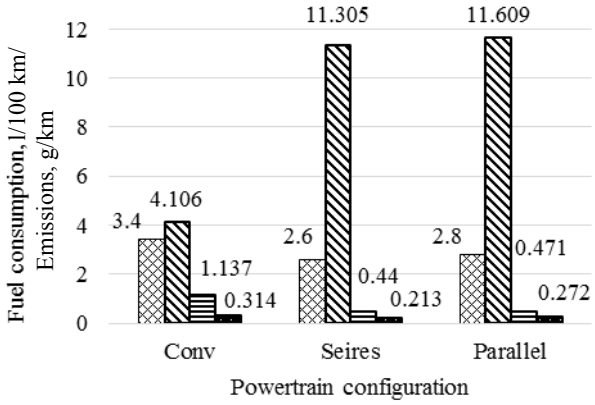

Fig. 5. Fuel consumption and emission values for series, parallel and conventional vehicles: ▒ – fuel consumption; ▒ – CO; ▒ – No_x; ▒ – HC

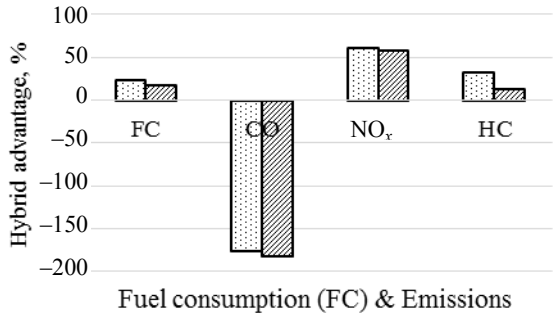

Fig. 6. Hybrid advantage (HA) of series and parallel powertrains for fuel consumption (FC), CO, NO_x and HC emissions: ▒ – HA (series); ▒ – HA (parallel)

Fig. 5, 6 indicate even though a reduction in fuel consumption may be expected in a hybrid vehicle, a reduction of emissions cannot be expected conclusively. Series and parallel configurations show a clear advantage in fuel consumption compared to conventional powertrain with 24 % fuel saving with series and 18 % fuel saving with the parallel configurations. Though, in terms of emission levels only HC and NO_x levels has a hybrid advantage. Both configurations show surprisingly higher CO emission levels with a 175 % increase with series configuration and a 183 % increase with parallel configuration compared to the conventional powertrain. However, results reinforce the findings from [1], Yuhan Huang et al. investigates the emission levels with a real-world hybrid car and a conventional car using a portable emissions measurement system. Similar to the present study, consistently higher CO emissions were observed with the hybrid vehicle.

Higher emission levels may be caused by the following two reasons. Firstly, the engine operating conditions. Engine operation conditions are different with a hybrid vehicle compared to a conventional vehicle. The higher amount of engine on and off frequency and higher engine power fluctuations may be a contribution for the increased emissions. Secondly, more power is required of a hybrid configuration due to the higher weight of the vehicle from the relatively smaller IC engine, with the engine of series 50 % and parallel 25 % smaller than the size of the convention vehicle. In order to understand the effect of engine operation and power requirement with the drive cycle and the effect on fuel consumption and emission levels, through Fig. 5–7 fuel rate and emission rate is investigated.

Fig. 7 compares the fuel consumption rate of the IC engine against CO emission rates, Fig. 8 against HC and Fig. 9 against NO_x emission rates for series, parallel and conventional powertrains under 100–425 s of the modified HWFET drive cycle. To understand the effect of engine operation in response to the drive cycle, the fuel rate and emission rates are plotted against the drive cycle (as km/h) after scaling, so that drive cycle characteristics can be shown against other parameters. Energy management strategy dictates the operation characteristics of the engine. Battery State of Charge minimum (SOC min.) point indicated is the minimum SOC level allowed. After this point, the power management strategy increases the power of IC engine to accelerate recharging of the battery.

Results from Fig. 7 indicate the fuel rate of series and parallel powertrains are relatively low compared to a conventional powertrain. With the series configuration, before SOC min. point indicated CO levels are lower, however after the SOC min. point power of the engine will be increased considerably by the power management strategy. Thus, increasing the CO emission rate. With the parallel configuration, the fuel rate indicates a higher fluctuation of the engine operation points than the conventional powertrain and a resulting increase in CO emissions. Similar to the series powertrain, after the SOC min point engine power is increased in the parallel hybrid resulting an increase in CO emission levels.

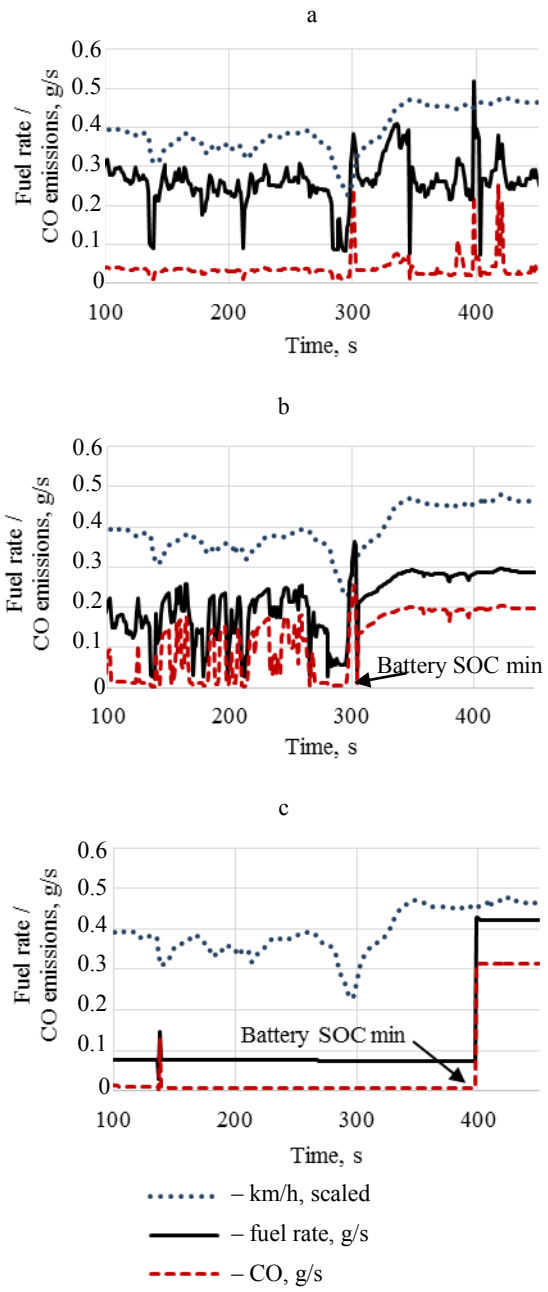

Fig. 7. Fuel rate against CO emissions:
a – conventional; b – parallel; c – series

Even though CO emissions are increased, NO_x and HC emissions are lower compared to the conventional powertrain. HC and NO_x levels for the drive cycle are respectively 32 % and 61 % lower with series hybrid and 13 % and 59 % lower with the parallel hybrid. Both hybrids significantly reduced NO_x emission levels. With HC emissions, the series hybrid has the highest advantage, which may be caused due to the stable operation of the series IC engine compared to the parallel hybrid. Fuel rate of the parallel hybrid indicates that with fluctuating engine operation, higher HC emissions are resulted compared to a series hybrid.

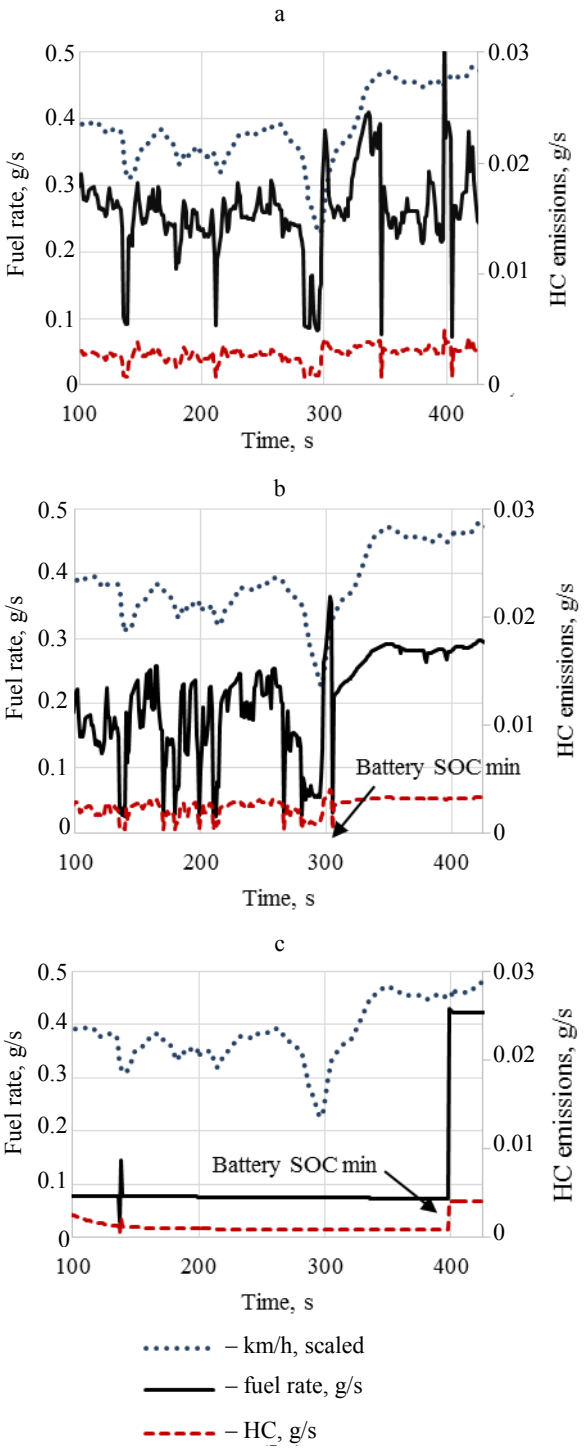

Fig. 8. Fuel rate against HC emissions:
a – conventional; b – parallel; c – series

Similar to powertrain configuration, hybridization affects the fuel consumption and emission levels for a hybrid vehicle. Fig. 10 indicate the fuel

consumption and emission levels of CO, NO_x and HC for three parallel hybrid powertrains with varying degrees of hybridization against a conventional powertrain. Four powertrains, i. e. conventional, parallel (0.2), parallel (0.3) and parallel (0.4) are simulated on the modified HWFET drive cycle.

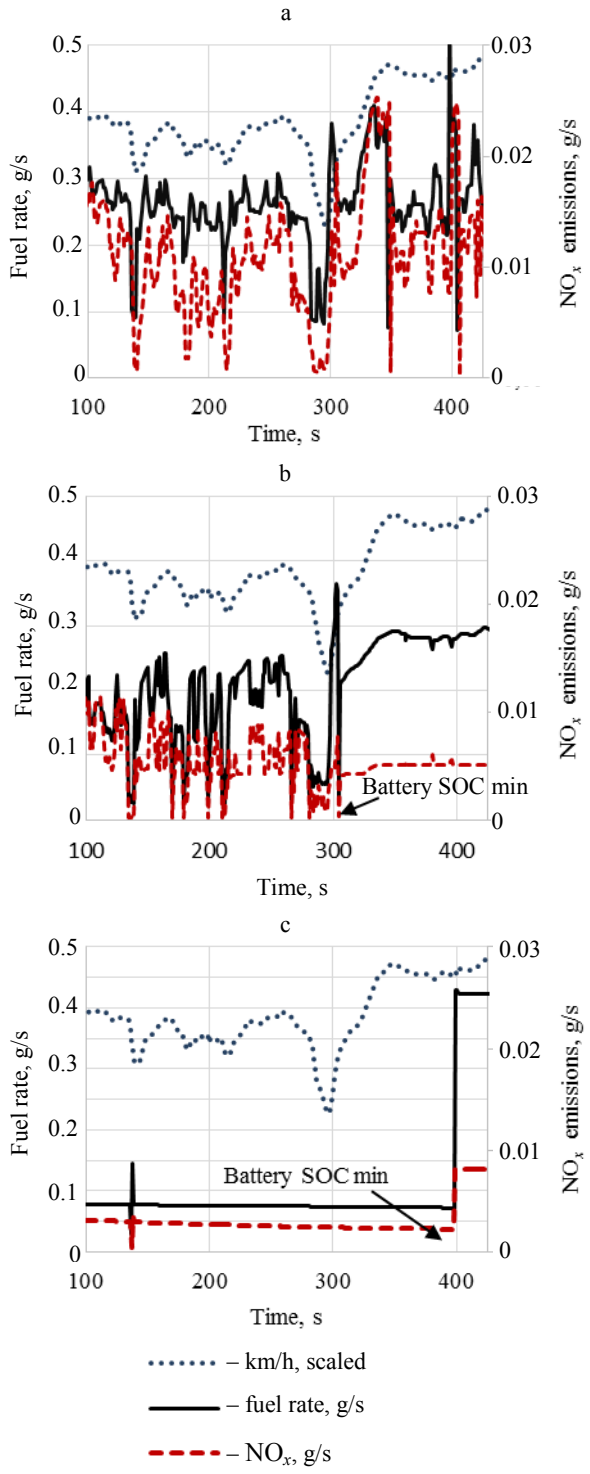

Fig. 9. Fuel rate against NO_x emissions: a – conventional; b – parallel; c – series

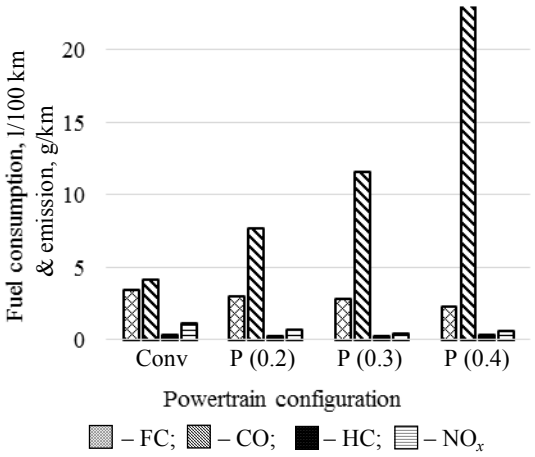

Fig. 10. Fuel consumption and emission values of conventional and parallel (with different hybridization values) powertrains

Results indicate, although fuel consumption is decreased with hybridization, CO emissions have increased significantly. Note that a catalytic converter is not modelled in the simulation. All three parallel configurations showed a significant hybrid advantage in fuel consumption with P (0.4) with 32 %, P (0.3) with 18 % and P (0.2) with 12 %. However, CO emissions increased by 88, 183 and 479 % in P (0.2), P (0.3) and P (0.4) respectively. This may be due to the power demand from the engine. Higher the hybridization, smaller the IC engine in a parallel hybrid. The power demand of the vehicle is approximately constant while the IC engine is sized smaller. Thus, increasing the power demand from the engine. Results reinforce the previous hypothesis; CO emissions increase may be caused by the higher power demand requested from a relative smaller engine.

Effect of drive cycle, hybridization and powertrain configuration on fuel consumption and emission levels is a complex relationship. Amount of data is inadequate to conclusively state that, CO emissions increases in a hybrid vehicle compared to its counterpart conventional vehicle due to the engine operation strategy and power demand. However, present study clearly shows that a reduction in fuel rate cannot be taken as an indicator for a reduction in emission levels for a hybrid vehicle.

Fuel consumption and drive cycle

A drive cycle provides a concise, repeatable sequence of vehicle operation over a time period [7]. A general drive cycle consists of second

by second values of speed, some literature includes elevation and time-based information of the vehicle as well [7]. Drive cycles are valuable for the design process, as cycle data may be used to understand the vehicle behaviour in a target application. Depending on the target application (drive conditions) fuel characteristics of different hybrid powertrain configurations may vary considerably [3]. Present study examines the effect of drive cycle characteristics on the fuel consumption for different hybrids (i. e. series, parallel and complex hybrids) against its conventional counterpart.

The wide range of drive cycles makes the analysis a challenge. Most well-known characterization of drive cycle is by urban, country and highway. However, this assessment is highly objective as the route and the drive conditions are highly varying with vehicle uses and their lifestyle. Hence in order to understand the effect of the drive cycle on the energy usage of a hybrid, an analytical characterization of drive cycle is necessary. To better assess the drive cycles, the kinetic intensity may be defined using two-cycle metrics based on the road load equation: aerodynamic speed and characteristic acceleration [7]. Present study uses kinetic intensity to characterize drive cycles, and the fuel consumption is assessed against the kinetic intensity of the drive cycles.

Fig. 11 represent fuel consumption against kinetic intensity for the developed four powertrains, i. e. series, parallel, complex hybrid and conventional powertrains. Five standard drive cycled are analyzed for kinetic intensity. Fuel consumption values for the five drive cycles are plotted against kinetic intensity values of the drive cycles. Results show that with varied drive cycles; series, parallel and complex hybrids have an average fuel advantage of 23, 21 and 33 % compared to an IC engine powertrain. Moreover, the trendline for the five drive cycles are plotted, and linear regression value is calculated for the trendlines.

Strong linearity is present with all four powertrains in terms of fuel consumption and kinetic intensity values of the drive cycle. Thus, linear trendline may be used to analyze overall fuel consumption behaviour in different hybrid configurations and predict fuel consumption values for unknown drive cycles. A uniformly strong linear correlation (R^2 values <0.9) is evident between cycle kinetic intensity values and the simulated fuel consumption values. However, it must be noted that data is insufficient to accurately examine and predict fuel consumption in hybrid vehicles.

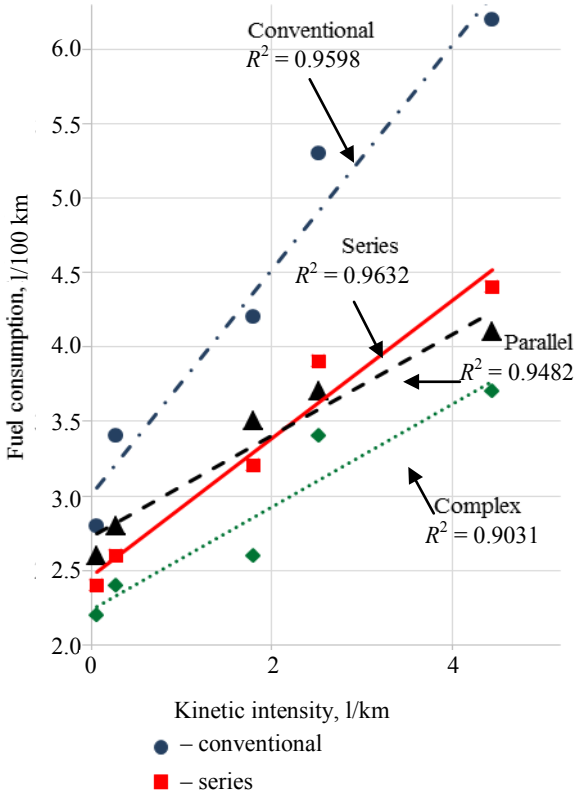

Fig. 11. Fuel consumption against drive cycles (scaled by KI factor) for conventional and hybrid powertrains

A methodology to predict hybrid fuel saving in an application is highly informative. However, finding fuel consumption values through simulation or by experimentation is a complex and tedious task that requires expert knowledge. The present study proposes the best fit linear curves of the three hybrids be adopted as fuel consumption models to approximately predict fuel consumption for an unknown drive cycle.

Proposed fuel consumption models are tested with a real-world drive cycle in Fig. 12. Three powertrains are simulated with the “Malabe” drive cycle. The “Malabe DC” points represent fuel consumption values from the simulation for the three hybrids. These points are compared with the predicted fuel consumption from the three hybrid fuel consumption models. Models predicted the fuel consumption values for the series, parallel and complex hybrids with 7, 12 and 7 % error percentages respectively. Tab. 5 summaries the predicted fuel consumption

values by the best fit curve of Fig. 10 and actual fuel consumption values from the developed powertrain models in MatLab/Simulink ADVISOR.

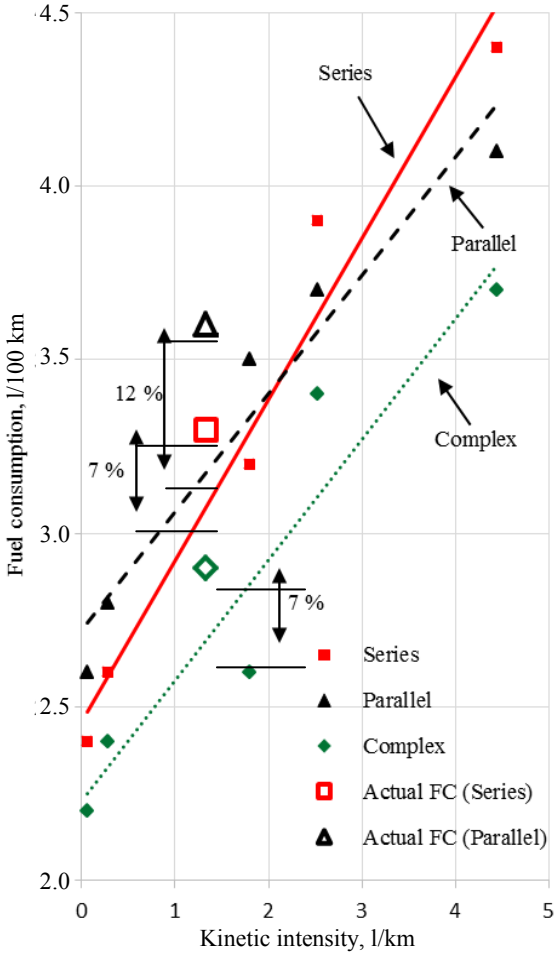

Fig. 12. Actual (simulation results from ADVISOR) and predicted (linear best fit curves) fuel consumption (FC) for the Malabe drive cycle of the three hybrid configurations

Table 5

Predicted and actual fuel consumption for the Malabe drive cycle

	Predicted FC (l/100 km)	Actual FC (l/100 km)	Error percentage, %
Series hybrid	3.0	3.3	7
Parallel hybrid	3.1	3.6	12
Complex hybrid	2.6	2.9	7

Results from Fig. 12 indicate that the approximate fuel consumption values can be predicted with reasonable accuracy (error percentages <12 %) using the proposed models. Only the parallel hybrid fuel consumption model shows a higher percentage level than 10 %. Both series and parallel hybrid models are able to predict within a 7 % error percentage.

The study proposes that fuel consumption levels with kinetic intensity metric can be used to predict approximately how a series, parallel and complex hybrid perform in an unknown drive cycle in terms of fuel consumption. However, further real-world drive cycle data is necessary to conclusively state hybrid models are capable of predicting fuel consumption values for any unknown drive cycle.

Fig. 13 represent the hybrid advantage of the three hybrid configurations against kinetic intensity. The hybrid advantage is the percentage reduction in fuel consumption of a hybrid vehicle over a conventional vehicle, calculated by equation (6). Hybrid advantage of each hybrid for different drive cycles are a good metrics to determine the performance characteristics of each vehicle. Hybrid advantage and kinetic intensity values were found for the same five standard drive cycles. The best fit line for the three data sets are plotted and linear regression values are calculated for each data set.

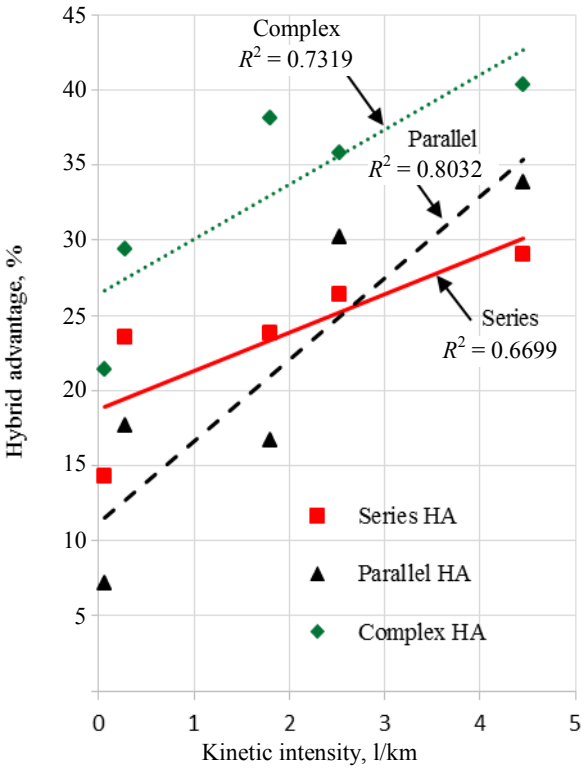

Fig. 13. Hybrid advantage of hybrid configurations against the kinetic intensity

While the linear correlation between the hybrid advantage and kinetic intensity of the drive cycles are weaker compared to fuel consumption and kinetic intensity, a linear correlation exists with R^2 values less than 0.65. Both complex and parallel hybrid has a linear regression value higher than 0.7. Trendline of all three hybrids is with a positive gradient as expected. Parallel hybrid has the highest gradient with a value of 0.054. Both series and complex have a gradient of 0.0254 and 0.0365. The kinetic intensity is a good representation of brake energy in a drive cycle, the study proposes that gradients of the three graphs may be used as an indication of the ratio between the brake energy harnessed out of the available energy of a hybrid.

CONCLUSIONS

1. Simulation of four powertrains (i. e. series, parallel, complex hybrid and conventional powertrain configurations) was carried out in MatLab/ Simulink ADVISOR environment. This paper assesses the emissions and fuel consumption of hybrid configurations under varied hybridization values and drive cycles.

2. The analysis of emissions independent of the fuel consumption showed that even though both series and parallel hybrids showed a decrease of fuel consumption by 24 and 18 % respectively, CO emissions increased significantly in both hybrid vehicles (series 175 % and parallel 183 %). Similarly, with higher hybridization values fuel consumption have decreased and CO emission has increased. Note that a catalytic converter is not modelled in the simulation. Results of the study elucidate that a decrease in fuel economy is not an accurate comparator to predict the emission levels. In some instances, while fuel consumption is decreased, emission levels can be higher than a conventional powertrain.

3. When fuel consumption is assessed with kinetic intensity, a strong correlation was seen for both hybrid and conventional powertrains. Moreover, the proposed fuel consumption models were able to predict the fuel economy of an unknown drive cycle within an error percentage of 12 %. Results show that models can be used to predict the fuel consumption of an unknown drive cycle to an approximate value.

4. Present work reveals, for a particular light vehicle, the fuel and emission performance of hybrid configurations significantly vary with different drive cycles and degrees of hybridization. The study considered many variables and the following points were not included, but could be addressed in future research papers. First, the control strategy used for the complex hybrid powertrain was taken from the Toyota Prius 1999 and efforts to obtain a later version need to be investigated to assess any improvements. Secondly, the control strategies of the three hybrid configurations are optimized for a small car considering a single objective, i. e. fuel consumption. Other objectives or vehicle types could be considered to assess their impact. Thirdly, the study focusses on CO, HC, and NO_x emissions. The globally important CO_2 emission levels should be planned for the next evaluation. Finally, the WLTP (Worldwide harmonized Light vehicles Test Procedure) could be realized in a future drive cycle assessment.

ACKNOWLEDGMENT

This research was supported by Sri Lanka Institute of Information Technology and we thank our colleagues of the said institution, namely Mr. Sampath Liyanarachchi and Mr. Miran Dabare. Although any errors are of our own and should not tarnish the reputation of those esteemed persons.

REFERENCES

1. Huang Y., Surawski N. C., Organ B., Zhou J. L., Tang O. H. H., Chan E. F. C. (2019) Fuel Consumption and Emissions Performance Under Real Driving: Comparison between Hybrid and Conventional Vehicles. *Science of the Total Environment,* 659, 275–282. https://doi.org/10.1016/j.scitotenv.2018.12.349.
2. Silvaş E., Hofman T., Steinbuch M. (2012) Review of Optimal Design Strategies for Hybrid Electric Vehicles. *IFAC Proceedings*, 45 (30) 57–64. https://doi.org/10.3182/20121023-3-FR-4025.00054.
3. Silvas E. (2015) Integrated Optimal Design for Hybrid Electric Vehicles. *Eindhoven: Technische Universiteit Eindhoven*. Available at: https://research.tue.nl/en/publications/integrated-optimal-design-for-hybrid-electric-vehicles.
4. World Health Organization (2017). Powered Two and Three Wheeler Safety: a Road Safety Manual for Decisionmakers and Practitioners. *World Health Organization*. Available at: https://www.who.int/violence_injury_prevention/publications/road_traffic/ptw_manual/en/.

5. Christensen J., Bastien C. (2016) Introduction to General Optimization Principles and Methods. *Nonlinear Optimization of Vehicle Safety Structures.* Elsevier Inc., 107–168. https://doi.org/10.1016/B978-0-12-417297-5.00003-1.
6. Çağatay Bayindir K., Gözüküçük M. A., Teke A. (2011) A Comprehensive Overview of Hybrid Electric Vehicle: Powertrain Configurations, Powertrain Control Techniques and Electronic Control Units. *Energy Conversion and Management,* 52 (2), 1305–1313. https://doi.org/10.1016/j.enconman.2010.09.028.
7. O'Keefe M. P., Simpson A., Kelly K. J., Pedersen D. S. (2007) Duty Cycle Characterization and Evaluation Towards Heavy Hybrid Vehicle Applications. *SAE Technical Paper Series*, 2007-01-0302. https://doi.org/10.4271/2007-01-0302.
8. Karbowski D., Pagerit S., Kwon J., Rousseau A., von Pechmann K.-F. F. (2009) "Fair" Comparison of Powertrain Configurations for Plug-In Hybrid Operation Using Global Optimization. *SAE Technical Paper Series*, 2009-01-1334. https://doi.org/10.4271/2009-01-1334.
9. Taymaz I., Benli M. (2014) Emissions and Fuel Economy for a Hybrid Vehicle. *Fuel*, 115, 812–817. http://dx.doi.org/10.1016/j.fuel.2013.04.045.
10. Al-Samari A. (2017) Study of Emissions and Fuel Economy for Parallel Hybrid Versus Conventional Vehicles on Real World and Standard Driving Cycles. *Alexandria Engineering Journal,* 56 (4), 721–726. https://doi.org/10.1016/j.aej.2017.04.010.
11. Karaoğlan M. U., Kuralay N. S., Colpan C. O. (2019) The Effect of Gear Ratios on the Exhaust Emissions and Fuel Consumptıon of a Parallel Hybrid Vehicle Powertrain. *Journal of Cleaner Production*, 210, 1033–1041. https://doi.org/10. 1016/j.jclepro.2018.11.065.
12. Wipke K. B., Cuddy M. R. (1996) Using an Advanced Vehicle Simulator (ADVISOR) to Guide Hybrid Vehicle Propulsion System Development. *NESEA Sustainable Transportation and S/EV Symposium*, *New York City, 16–18 Sep. 1996,* 120–126. Available at: https://www.nrel.gov/docs/legosti/fy96/21615.pdf.
13. Same A., Stipe A., Grossman D., Park J. W. (2010) A Study on Optimization of Hybrid Drive Train Using Advanced Vehicle Simulator (ADVISOR). *Journal of Power Sources*, 195 (19), 6954–6963. http://dx.doi.org/10.1016/j.jpowsour.2010.03.057.
14. Markel T., Brooker A., Hendricks T., Johnson V., Kelly K., Kramer B., O'Keefe M., Sprik S., Wipke K. (2012) ADVISOR: a Systems Analysis Tool for Advanced Vehicle Modeling. *Journal of Power Sources,* 110 (2), 255–266. https://doi.org/10.1016/S0378-7753(02)00189-1.
15. Turkmen A. C., Solmaz S., Celik C. (2017) Analysis of Fuel Cell Vehicles with Advisor Software. *Renewable and Sustainable Energy Reviews,* 70, 1066–1071. https://doi.org/10.1016/j.rser.2016.12.011.
16. Hofman T., van der Tas S. G., Ooms W., van Meijl E.W.P., Laugeman B. M. (2009) Development of a Micro-Hybrid System for a Three-Wheeled Motor Taxi. *World Electric Vehicle Journal,* 3 (3), 572–580. https://doi.org/10.3390/wevj3030572.
17. BAJAJ. BAJAJ RE 4s Specifications. *GlobalBajaj.com*. Available at: https://www.globalbajaj.com/global/english/brands/intracity/re/re-4s/specifications/.
18. Wipke K., Cuddy M., Bharathan D., Burch S., Johnson V., Markel A., Sprik S. (1999) *Advisor 2.0: a Second-Generation Advanced Vehicle Simulator for Systems Analysis*. Golden, Colorado. https://doi.org/10.2172/5023.
19. Bokare P. S., Maurya A. K. (2016) Study of Acceleration Behaviour of Motorized Three Wheeler in India. *Transportation Research Procedia*, 17, 244–252. http://dx.doi.org/10.1016/j.trpro.2016.11.088.
20. National Renewable Energy Laboratory (2019) *NREL DriveCAT – Chassis Dynamometer Drive Cycles*. Available at: https://www.nrel.gov/transportation/drive-cycle-tool.
21. Robinson B., Eastlake A. (2014) *Development of Test Cycles and Measurement Protocols for a Low Carbon Truck Technology Accreditation Scheme.*

Received: 08.10.2019
Accepted: 10.12.2019
Published online: 31.01.2020

https://doi.org/10.21122/2227-1031-2020-19-1-34-42

UDC 621

Laser Research of the Fuel Atomization Process of Internal Combustion Engines

P. Stężycki[1)], M. Kowalski[2)], A. Jankowski[2)], Z. Sławinski[3)]

[1)]Łukasiewicz Research Network – Institute of Aviation (Warsaw, Republic of Poland),
[2)]Air Force Institute of Technology (Warsaw, Republic of Poland),
[3)]Lublin University of Technology (Lublin, Republic of Poland)

Abstract. The paper presents test methods (mechanical, electrical and optical) for the fuel spray research in combustion engines. Optical methods, imaging and non-imaging can be used in laboratory and engine tests. Imaging methods include flash photography and holography. Their use is limited to testing droplet dimensions larger than 5 μm. Imaging methods have an advantage over non-imaging ones because they allow the droplet to be seen at the point and time where its measurement is required. Non-imaging methods can be divided into two groups: the first, which counts and measures, individual droplets one at a time, and the second, which measures a large number of droplets simultaneously. Exemplary results of research of droplet size distribution in fuel sprays are shown. In tests of atomized fuel spray, in conditions reflecting the conditions of the internal combustion engine, the size of droplets, their distribution in the spray and the velocity of individual droplets are presented. To determine the quality of the fuel spray, two substitute diameters Sauter (D_{32}) and Herdan (D_{43}) were selected, the first of which refers to heat transfer and the second to combustion processes. Laser research equipment including Particle Image Velocimetry laser equipment (PIV), Laser Doppler Velocimeter (LDV) and Phase Doppler Particle Analyzer (PDPA) were applied for testing fuel spray distribution for two kind of fuel. The atomization process from the point of view of combustion and ignition processes, as well as emission levels, is characterized by the best substitute diameter D_{43}, which value is close to the median volume. The most harmful droplets of fuel in the spray are large droplets. Even a few such droplets significantly change the combustion process and emission of toxic exhaust components, mainly NO_x.

Keywords: combustion engine, fuel injection equipment, fuel atomization, laser method, engine emission

For citation: Stężycki P., Kowalski M., Jankowski A., Sławinski Z. (2020) Laser Research of the Fuel Atomization Process of Internal Combustion Engines. *Science and Technique.* 19 (1), 34–42. https://doi.org/10.21122/2227-1031-2020-19-1-34-42

Лазерное исследование процесса распыления топлива двигателей внутреннего сгорания

П. Стенжицкий[1)], М. Ковальский[2)], А. Янковский[2)], З. Славиньский[3)]

[1)]Научно-исследовательская сеть Лукасевича – Институт авиации (Варшава, Республика Польша),
[2)]Технологический институт ВВС (Варшава, Республика Польша),
[3)]Люблинский технический университет (Люблин, Республика Польша)

Реферат. В статье представлены методы испытаний (механические, электрические и оптические) для исследования распыления топлива в двигателях внутреннего сгорания. Оптические методы, техническая визуализация, системы без отображения цели могут быть использованы в лабораторных работах и испытаниях двигателя. Методы визуализации включают в себя съемку со вспышкой и голографию. Их применение ограничено размерами капель для тестирования, которые должны быть более 5 мкм. Методы визуализации имеют преимущество перед методами без отображения цели,

Адрес для переписки
Янковский Антоний
Технологический институт ВВС
ул. Принца Болеслава, 6,
01-494, г. Варшава, Республика Польша
Тел.: +4826 185-13-10
antoni.jankowski@itwl.pl

Address for correspondence
Jankowski Antoni
Air Force Institute of Technology
6 Ks. Boleslawa str.,
01-494, Warsaw, Republic of Poland
Tel.: +4826 185-13-10
antoni.jankowski@itwl.pl

потому что они позволяют видеть каплю в той точке и в то время, когда требуется произвести ее измерение. Методы без отображения цели можно разделить на две группы: первая, которая за один раз подсчитывает и измеряет отдельные капли, и вторая, когда одновременно производится измерение большого количества капель. В статье показаны типовые результаты исследований распределения капель по размерам в распылителях топлива. При проведении испытаний по распылению топлива в условиях работы двигателя внутреннего сгорания учитывались размеры капель, их распределение в распылителе, а также принималась во внимание скорость отдельных капель. Для определения качества распыления топлива были выбраны два подсменных диаметра Suter (D_{32}) и Herdan (D_{43}), первый из которых относится к процессу теплообмена, а второй – к процессу сгорания. Лазерный научно-исследовательский комплекс, включающий в себя лазерное оборудование для измерения скорости частиц (PIV), лазерный доплеровский измеритель скорости (LDV) и фазовый доплеровский анализатор частиц (PDPA), использовался для проведения испытаний по распределению распыления двух типов топлива. Распыление, с точки зрения процессов горения и воспламенения, а также уровней выбросов, характеризуется лучшим сменным диаметром D_{43}, значение которого очень близко к средней величине. Наиболее вредными каплями топлива в аэрозоле являются капли крупного размера. Даже несколько таких капель значительно влияют на процесс горения и выброс токсичных компонентов, главным образом NO_x.

Ключевые слова: двигатель внутреннего сгорания, устройство для вдувания топлива, распыление топлива, лазерный метод, выбросы двигателя

Для цитирования: Лазерное исследование процесса распыления топлива двигателей внутреннего сгорания / П. Стенжицкий [и др.] // *Наука и техника*. 2020. Т. 19, № 1. С. 34–42. https://doi.org/10.21122/2227-1031-2020-19-1-34-42

Introduction

The fuel injection system is one of the key elements that are the subject of numerous experimental and theoretical works necessary for the development of modern combustion systems in both spark-ignition and Diesel engines. The direct fuel injection system into the engine's combustion chamber is one of the most advanced solutions and has to implement at least two or even more different engine modes. Parameters not related to the atomization process itself with regard to fuel supply systems include, among others, opening time, closing time, needle stroke, durability, stream range, noise level, power consumption, leaks and operating pressure range.

Fuel injection systems are dominant in spark-ignition and Diesel engines [1, 2]. These systems allow for accurate metering of fuel and feeding it to the combustion chamber [3]. They also allow for the appropriate shaping of the injection process for the shape of the spray, the dimensions of droplets, and the dosing of the amount of fuel. The use of optical methods using lasers to measure droplets' diameters and speed allow for significant progress in this field of research. In tests of atomized fuel spray, in conditions reflecting the conditions of the internal combustion engine, the size of droplets, their distribution in the spray and the velocity of individual droplets are possible to determine [3]. Droplets in the spray have different diameters, depending on the discharge conditions and fuel properties. From the point of view of the economics of the combustion engine operation and the emission of toxic exhaust components, differences in the size of droplets should be within a narrow range [4, 5]. To determine the quality of the fuel spray, two substitute diameters Sauter (D_{32}) and Herdan (D_{43}) were selected, the first of which refers to heat transfer and the second − to combustion processes. The stream parameters include the average diameters of the fuel droplets of the main stream and the surrounding spray, as well as the associated statistical parameters that result from the droplet size distribution. Important stream parameters include stream cone angles, both start and end angles, stream skew, penetration speed of the stream end and maximum speed, dripping after injection and fuel distribution within the stream. Additional stream parameters are related to the variability between individual fuel injections. The conducted research tests allow assessing the occurrence of dripping after the injection and its influence on the characteristics of the fuel atomization process. Dripping is particularly disadvantageous for fuel jets with small droplet sizes.

The common rail injection system allows full monitoring and computer injection control by the time and pulse length, as well as by adding additional fuel pulses or multiple injections for one engine cycle [6]. The average injection pressure increases steadily up to 10 MPa, and in some applications up to 12 and even 20 MPa. There is insufficient data yet to assess the impact of such pressure increases on wear processes and average

durability of supply systems. Such data could ultimately reduce the tendency to increase fuel injection pressure for spark-ignition engines.

Work on back-up injectors, which at very low injection pressure (0.6–1.0 MPa) offer comparable levels of fuel atomization with multi-hole vortex injectors, which are characterized by over 10 times higher injection pressures. This type of injectors, however, requires the use of two separate injection control systems; moreover, it requires individual two controllers for one injector with different characteristics regarding pulse duration. It also requires the supply of compressed gas and air, which somewhat complicates the solution of the power supply system, e. g. a compressor is required. This system uses one system to control the fuel supply to the combustion chamber and another system synchronously to introduce the appropriate amount of compressed air [7].

Test methods for the fuel spray process in combustion engines

Various methods are used to test fuel atomization processes, which can be classified into three basic groups: mechanical, electrical and optical methods.

Mechanical methods for example include collecting droplets on a glass surface with a suitable coating to stop settling droplets, collecting fuel droplets for dishes with a liquid that does not dissolve fuel droplets, using molten wax.

The electric methods include the method of electrically charged wire, which removes the charges depending on the droplet dimensions, and the hot wire method, which consists in the fact that fuel droplets settling on the pipe evaporate and cool it. When there are no droplets on the wire, its electrical resistance is large and uniform along the length. When the droplets settle on the duct, its resistance decreases locally, in proportion to the droplet dimensions. The latter method is however an invasive method.

Optical methods can be used in both laboratory and motor tests. These imaging methods include flash photography and holography. Their use is limited in practice to testing droplet dimensions larger than 5 μm. Imaging methods have an advantage over non-imaging ones because they allow the droplet to be seen at the point and time where its measurement is required.

Non-imaging methods can then be divided into two groups, the first, which counts and measures individual droplets one at a time, and the second, which measures a large number of droplets simultaneously. It is important to know both the drop size and the speed for an accurate result. Some devices for the non-imaging methods can provide both information regarding dimensions and velocity.

Many optical research methods can be used to analyze the process of fuel atomization. However, they all have an important attribute, because they allow measurements without disturbing the stream of sprayed fuel. Optical research methods include: high speed photography, video stream analyzer, holographic analyzer, single particle counters, scattered light interferometry, non-axial scattered light detection, Particle Image Velocimetry (PIV) [8], Phase Doppler Particle Analyzer (PDPA), Laser Doppler Analyzer Speed (LDA).

Laser research equipment. Particle image velocimetry laser equipment

Laser PIV equipment allows determining the distribution of the velocity of fuel droplets. PIV equipment allows simultaneous measurements of 12000 points, has a very high resolution, and guarantees high accuracy of measurements, enables visualization of flows, including turbulent flow structures. An important advantage is the ability to determine turbulence and Reynolds stresses. In addition, it ensures fast operation in an automatic cycle. Fig. 1 shows a diagram of PIV equipment, and Fig. 2 shows a view of PIV equipment.

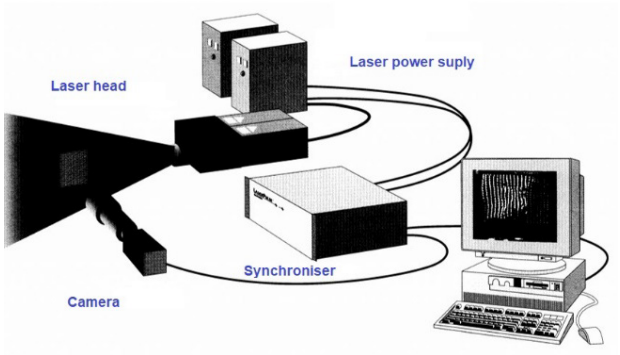

Fig. 1. Scheme of the PIV optical system

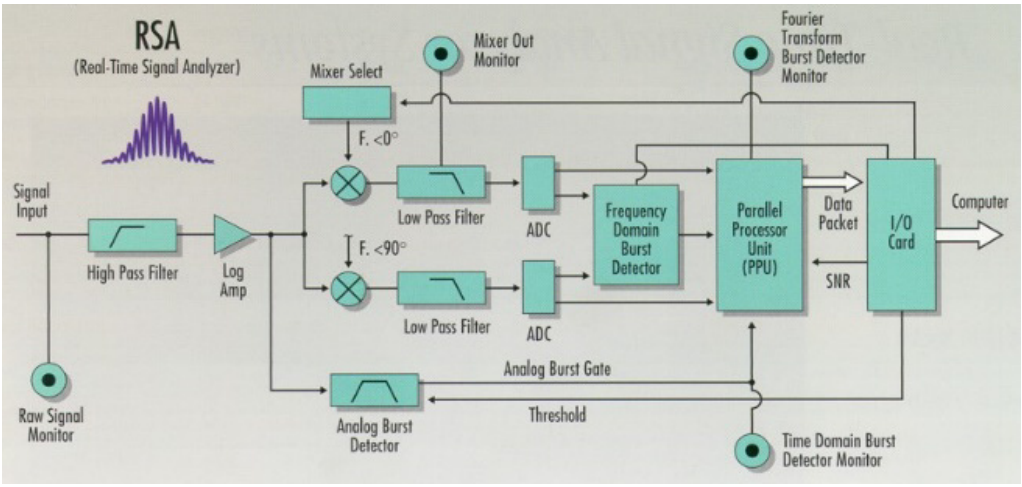

Fig. 2. Block scheme of the laser measuring system

PDPA and LDV laser research equipment

In tests of the atomized fuel stream, in conditions reflecting engine conditions, it is also important to know the size and distribution of droplets in the fuel stream. In engine conditions, the droplets have different diameters, depending on the discharge conditions and fuel properties. For the purposes of analyzing the stream creation process, it is better to use not a set of droplets of different diameters, but a droplet with a constant diameter, characteristic of given flow conditions. Several such conventional diameter droplets are specified in the literature. These include, among others, the average diameter of Sauter (D_{32}), arithmetic (D_{10}), surface (D_{20}), volumetric (D_{30}) and Herdan (D_{34}).

The tests were carried out using the LDV (Laser Doppler Velocimeter) and PDPA laser equipment, with a 5 W laser cooled with water. The block diagram of the laser measuring system is shown in Fig. 2. The measurements are carried out in the measuring space, which is determined by the intersecting two laser rays, zero and Doppler from each transmitter. This space occurs in the optical focus area of the laser transmitter and has the shape of a rhomboidal body whose maximum dimensions in the tuned optical system were 1.76×1.4×1.4 mm. The diameter of the laser beam was 1.4 mm; the distance between zero and Doppler rays was 39.74 mm, the focal length was 250 mm. The dimensions of the measuring space can be changed by means of the optical system of the transmitter (focal length), which should be selected for the expected range of droplet diameters occurring in the sprayed fuel stream. Droplet dimensions that can be measured are in the range from 0.5 to 2.0 mm, and when changing the parameters of the optical system, even up to 3.822 mm, except that the best results are obtained when choosing the optical system adapted to the sprayed fuel, in whose maximum droplet size is about 300 times larger than the minimum. The measuring range depends on the optical system and the type of the RSA (Real Time Signal Analyzer) processor, whereby laser phase shifts from 30 to 3500 can be recorded. In any case, the optical system should be arranged in such a way that the maximum droplet size is smaller from the smaller diagonal of the diamond section perpendicular to the fuel jet velocity component, while the minimum droplet size that can be recorded is 0.5 μm or is the one whose phase shift of the laser beam is 30 or greater. The PDPA system for measuring droplet dimensions is calibrated, while the LDV system for measuring speed does not require calibration. The measuring system of the apparatus allows the measurement of velocity in three directions (3*D*), and the principle of measuring the velocity component is to register a change in the frequency of the laser beam, which is proportional to the velocity of the fuel droplet. The velocity component may be determined from the following relationship

$$v_i = \frac{f_D}{f_0 2\sin\Phi}, \qquad (1)$$

where v_i − droplet velocity component; f_D − modulated frequency of the laser Doppler beam; f_0 − zero beam frequency; Φ − intersection angle of zero and Doppler beams.

The measuring system allows the use of three different laser rays: green with a wavelength of 514.5 nm, blue with a wavelength of 488 nm and purple with a wavelength of 476.5 nm. Measurement of droplets consists in registering the deviation of the laser beam when passing through the droplet, which is proportional to its size. A droplet of fuel is observed from 2 detectors with two different distances AB 10.79 mm and AC 32.15 mm. In relation to the PDPA system, five diameters were selected to determine the stream parameters: D_{10}, D_{20}, D_{30}, D_{32}, D_{43}. The differences in the dimensions of individual droplet diameters are a measure of the uniformity of dimensions of the fuel stream. The droplet size is determined based on the relative modulation of the laser signal by the droplets flowing through the measurement area. The droplet size is determined from the following relationship:

$$M = \frac{I_{\max} - I_{\min}}{I_{\max} + I_{\min}}, \qquad (2)$$

where M – intensity parameter; $I_{\max}$, $I_{\min}$ – maximum and minimum intensities.

The relationship between the value determining the intensity of the M laser beam measured by the measuring system and the droplet size is determined by equation

$$M = \frac{2J_1(\pi D/\delta)}{\pi D/\delta}, \qquad (3)$$

where J_1 – first type first order Bessel function; D – droplet size; δ – distance between interference fringes.

Placing optical systems to measure velocity components in the combustion chamber is not possible in an orthogonal system. An oblique coordinate system is used, which requires the use of transformation to transition to the orthogonal system. The best results are obtained when the laser scattered light receiver is placed at an angle of 30° to the direction of the beam of the transmitter.

Fig. 3 shows the 3*D*-measuring laser and the Bragg cell. Fig. 4 shows the system of signal analysis, acquisition and presentation of results. Fig. 5 shows a constant volume test chamber for research the atomization and combustion process.

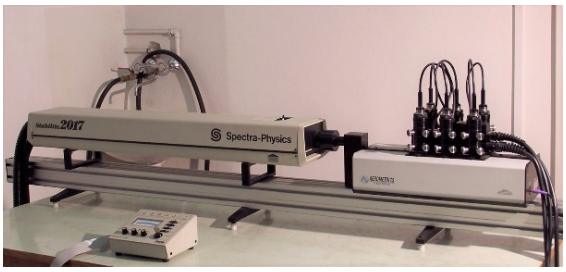

Fig. 3. 3*D*-measuring laser and Bragg cell

Fig. 4. View of the signal analysis system, acquisition and presentation of results

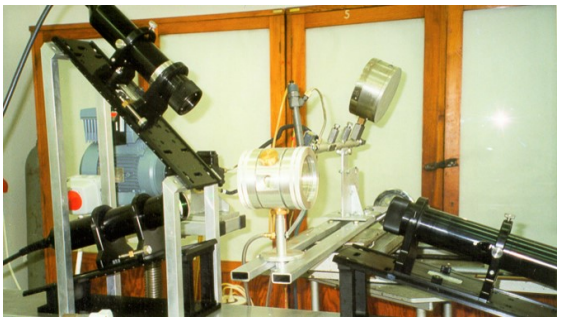

Fig. 5. Test chamber for testing the atomization and combustion process

Test results

Tests with the use of PIV apparatus [9] were carried out on the stand enabling the implementation of a single injection for different injection pressure values for two fuels (Fig. 6–8) with the properties presented in Tab. 1.

Table 1

Values of tested fuels

	Dynamic viscosity, mm^2/s	Density, kg/m^3	Surface tension, J/m^2
Fuel No 1	4.7	803.53	$35.9 \cdot 10^{-3}$
Fuel No 2	1.7	826.04	$36.8 \cdot 10^{-3}$

Tests using PIV apparatus allow determining the structure and distribution of velocity in the stream. The tests revealed velocity discontinuities and change of directions in individual areas of the stream, with the stream image significantly different for fuels with different viscosities. It should be

noted that PIV velocity field measurements provide excellent illustrative material illustrating the velocity field. In most cases, the test results are rather qualitative.

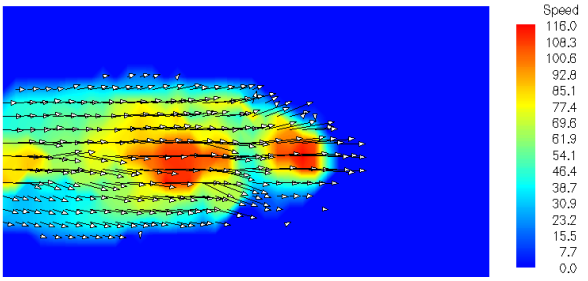

Fig. 6. Vector distribution and velocity fields for fuel No 1 for an injection pressure of 50 MPa

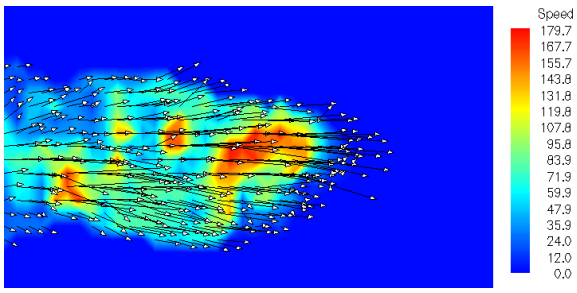

Fig. 7. Vector distribution and velocity fields for fuel No 1 for 100 MPa injection pressure

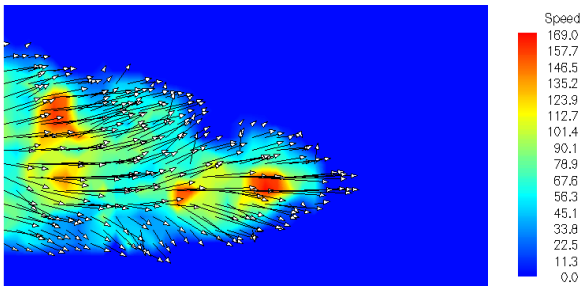

Fig. 8. Vector distribution and velocity fields for fuel No 2 for 100 MPa injection pressure

The laser equipment (PIV–PDPA) allows measurements of droplets in the range from 0.5 μm to 2.0 mm, and for the change of optical system (500 mm focal length) parameters even up to 3.822 mm.

Tests were carried out on the special stand shown in Fig. 5. The results of the droplet velocity tests that were made using the LDV laser apparatus are shown in Tab. 2. Examples of measurements were made in the injector axis at a distance of 65 mm from its hole in the fuel injection into the atmosphere. The results of testing the dimensions of fuel droplets using PDPA laser equipment are presented in Tab. 3.

Table 2

Results of velocity tests at measuring point 1 (LDV)

Injection pressure, MPa	v_1, m/s	v_2, m/s	v_{av}, m/s	v_{RMS}, m/s	Fuel
100	0.66	0.36	0.663	1.628	No 1
70	1.23	0.73	1.235	3.681	
100	0.50	0.39	0.501	1.266	No 2
70	1.31	0.39	1.312	2.847	

Table 3

Test results for the diameter of the droplets at measuring point 1 (PDPA)

Injection pressure, MPa	D_{10}, μm	D_{20}, μm	D_{30}, μm	D_{32}, μm	D_{43}, μm	Fuel
100	4.426	5.117	5.918	7.915	10.07	No 1
70	5.109	6.086	7.183	9.990	12.97	
100	4.451	5.241	6.171	8.554	11.04	No 2
70	6.388	7.441	8.807	11.52	14.72	

Test results of the sprayed fuel stream regarding the droplet diameters for small droplet sizes – D_{32} = 13.8 μm, D_{43} = 15.38 μm are shown in Fig. 9, 10. Fig. 11 shows the combustion process in a constant volume chamber for a fuel stream with the properties presented in Fig. 9, 10 (λ = 1).

Exemplary results of studies of droplet size distribution in a homogeneous spray are shown in Fig. 12, and in a spray with a dispersion of droplets − in Fig. 13. Fig. 12, 13 indicate that the Sauter diameter is 18.41 μm/20.99 μm, respectively and the Herdan diameter − 20.4 μm/25.94 μm.

The differences between the Herdan and Sauter diameters are respectively 1.99 μm/4.95 μm, which are 9.7 %/19.1 %. The smaller the average diameters between diameters, the greater the homogeneity of the fuel stream. An important role in assessing the fuel injection stream has a volume median of droplets, which is 20.14 μm/24.94 μm respectively, which is 99 %/94 % of the Herdan diameter, respectively.

The most harmful droplets of fuel in the spray are large droplets. Even a few such droplets significantly change the combustion process and emission of toxic exhaust components, mainly (NO_x) [9–11]. The atomization process from the point of view of combustion and ignition processes, as well as emission levels, is characterized by the best substitute diameter D_{43}, which value is close to the median volume.

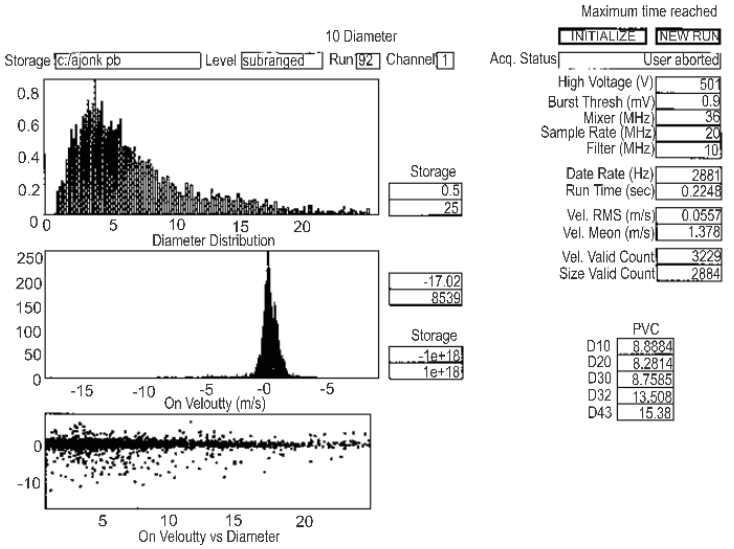

Fig. 9. Test results of the sprayed fuel stream regarding droplet diameters for small droplet sizes – D_{32} = 13.8 μm, D_{43} = 15.38 μm

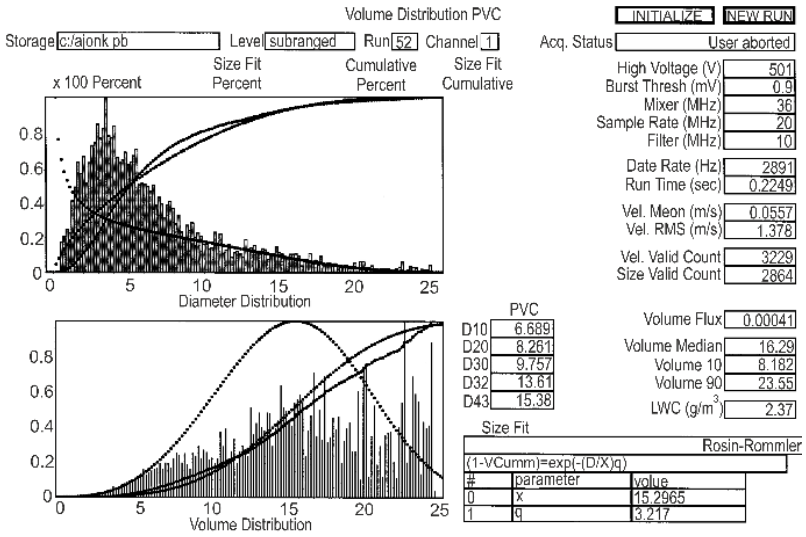

Fig. 10. Test results of the sprayed fuel stream regarding droplet diameters for small droplet sizes – D_{32} = 13.8 μm, D_{43} = 15.38 μm

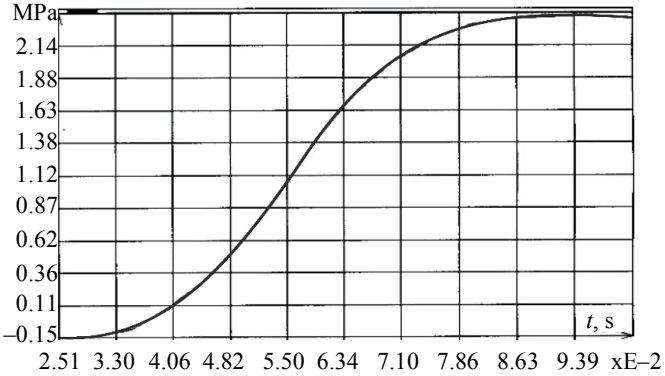

Fig. 11. The course of the combustion process in a constant volume chamber for the fuel stream with the properties presented in Fig. 9, 10 (λ = 1)

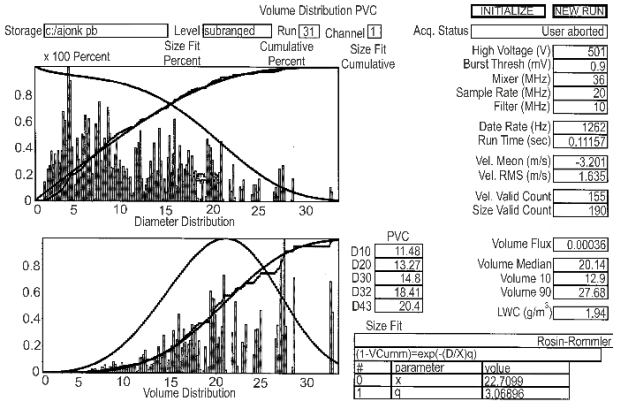

Fig. 12. Diameter distribution in fuel homogeneous spray

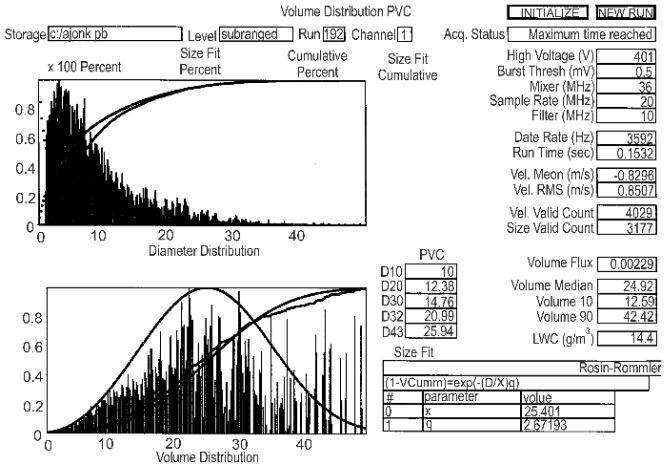

Fig. 13. Diameter distribution in fuel spray with dispersion

The main reasons for excessive fuel consumption and the emission of toxic exhaust components are inaccurate metering of fuel and improper preparation of the mixture. For proper fuel, metering as well as fuel preparation the fuel atomization process has the main influence. For the evaluation of the fuel apparatus, measurement of the Herdan diameter (D_{43}) should take place along the length of the stream at a distance of 2/3 of the spray range from the injector and 2/3 of the stream radius value from the spray axis.

CONCLUSIONS

1. The PIV test method allows the structure and distribution of velocity to be determined in a stream. It allows for qualitative rather than quantitative assessment.

2. PDPA and LDV laser methods allow determining droplet diameters, their velocity and dispersion.

3. The atomization process from the point of view of combustion and ignition processes, as well as the level of emissions is best characterized by a substitute diameter D_{43}, whose value is close to the median volume.

4. Directions of development of mix formation processes are aimed at obtaining streams with small droplet sizes. This applies not only to the homogeneous combustion process strategy, but above all to the cold start strategy, where it is necessary to use small-sized droplets.

5. Fuel viscosity, density and surface tension, depending on fractional composition, crude oil processing and additives, have the greatest impact on the physical stream formation processes.

6. Droplets in the large stream of fuel are the most harmful. Even a few such droplets definitely change the combustion process and the emission of toxic exhaust components, mainly (NO_x).

7. With increasing injection pressure, the diameter of the droplets decreased; the Sauter diameter of the droplets with pressure increase from 70

to 130 MPa decreased by 47 % for fuel No 1 and by 41 % for fuel No 2.

8. During tests of the ignition and combustion process for elevated pressures in a constant volume chamber (up to 1 MPa) at large droplet sizes, when D_{43} is greater than 30 μm, ignition is not possible, even with a significant increase in pressure in the combustion chamber. Fuel dispersion has a significant impact on ignition in cold combustion chamber conditions.

REFERENCES

1. Arndt P., Putz W. (1997) Der neue Vierzylinder Dieselmotor OM 611 mit Common-Rail Einspritzsystem ein Neues Kapitel der Dieseleinspitztechnik. *MTZ – Motortechnische Zeitschrift*, 58 (11), 652–659 (in Russian).
2. Corcione F. E. (2001) (KA-4) Optical Diagnostics in Engines. *The Proceedings of the International Symposium on Diagnostics and Modeling of Combustion in Internal Combustion Engines (COMODIA 2001),* 01.204. https://doi.org/10.1299/jmsesdm.01.204.4.
3. Doerr T. (2012) The Significance of Fuel Preparation for Low Emissions Aero-Engine Combustion Technology. *ICLASS 2012, 12th Triennial International Conference on Liquid Atomization and Spray Systems, Heidelberg, Germany, September 2–6*.
4. Jankowski A., Kowalski M. (2018) Alternative Fuel in the Combustion Process of Combustion Engines. *Journal of KONBIN*, 48 (4), 55–68. https://doi.org/10.2478/jok-2018-0047.
5. Kowalski M., Jankowski A. (2018) Engine Test Results of Fuel-Water Microemulsion. *Proceedings of 31st Congress of the International Council of the Aeronautical Sciences, ICAS 2018 − Belo Horizonte, Brazil.* Available at: www.icas.org/ICAS_ARCHIVE/ICAS2018/data/preview/ICAS2018_0769.htm. Code 143115.
6. Kozakiewicz A., Kowalski M. (2013) Unstable Operation of the Turbine Aircraft Engine. *Journal of Theoretical and Applied Mechanics*, 51 (3), 719–727.
7. Żurek J., Kowalski M., Jankowski A. (2015) Modelling of Combustion Process of Liquid Fuels under Turbulent Conditions. *Journal of KONES,* 22 (4), 355–363. https://doi.org/10. 5604/12314005.1193063.
8. Raffel M., Willert C. E., Kompenhans J. (1998) *Particle Image Velocimentry*. Springe Verlog. https://doi.org/10.1007/978-3-662-03637-2.
9. Jankowski A., Kowalski M., Slawinski Z. (2016) Research of Alternative Fuel Water-Fuel Micro Emulsion from Point of View Reduction of Emissions. *Proceedings of 30th Congress of the International Council of the Aeronautical Sciences, ICAS 2016,* Code 126186. Available at: www.icas.org/ ICAS_ARCHIVE/ICAS2016/ data/preview/2016_0667.htm.
10. Jankowski A., Kowalski M. (2015) Influence of the Quality of Fuel Atomization on the Emission of Exhaust Gases Toxic Components of Combustion Engines. *Journal of KONBIN*, 36 (1), 43–50. https://doi.org/10.1515/jok-2015-0055.
11. Jankowski A., Kowalski M. (2015) Creating Mechanisms of Toxic Substances Emission of Combustion Engines. *Journal of KONBIN*, 36 (1), 33–42. https://doi.org/10.1515/jok-2015-0054.

Received: 08.10.2019
Accepted: 10.12.2019
Published online: 31.01.2020

https://doi.org/10.21122/2227-1031-2020-19-1-43-54

UDC 629

Robust Design of Suspension System with Polynomial Chaos Expansion and Machine Learning

H. Gao[1, 2], L. Jézéquel[1], E. Cabrol[2], B. Vitry[2]

[1]Ecole Centrale de Lyon (Ecully, French Republic),
[2]Renault SAS (Guyancourt, French Republic)

Abstract. During the early development of a new vehicle project, the uncertainty of parameters should be taken into consideration because the design may be perturbed due to real components' complexity and manufacturing tolerances. Thus, the numerical validation of critical suspension specifications, such as durability and ride comfort should be carried out with random factors. In this article a multi-objective optimization methodology is proposed which involves the specification's robustness as one of the optimization objectives. To predict the output variation from a given set of uncertain-but-bounded parameters proposed by optimization iterations, an adaptive chaos polynomial expansion (PCE) is applied to combine a local design of experiments with global response surfaces. Furthermore, in order to reduce the additional tests required for PCE construction, a machine learning algorithm based on inter-design correlation matrix firstly classifies the current design points through data mining and clustering. Then it learns how to predict the robustness of future optimized solutions with no extra simulations. At the end of the optimization, a Pareto front between specifications and their robustness can be obtained which represents the best compromises among objectives. The optimum set on the front is classified and can serve as a reference for future design. An example of a quarter car model has been tested for which the target is to optimize the global durability based on real road excitations. The statistical distribution of the parameters such as the trajectories and speeds is also taken into account. The result shows the natural incompatibility between the durability of the chassis and the robustness of this durability. Here the term robustness does not mean "strength", but means that the performance is less sensitive to perturbations. In addition, a stochastic sampling verifies the good robustness prediction of PCE method and machine learning, based on a greatly reduced number of tests. This example demonstrates the effectiveness of the approach, in particular its ability to save computational costs for full vehicle simulation.

Keywords: chassis durability, data mining, machine learning, multi-objective optimization, polynomial chaos expansion, robust design

For citation: Gao H., Jézéquel L., Cabrol E., Vitry B. (2020) Robust Design of Suspension System with Polynomial Chaos Expansion and Machine Learning. *Science and Technique.* 19 (1), 43–54. https://doi.org/10.21122/2227-1031-2020-19-1-43-54

Надежная конструкция подвески с полиномиальным хаотичным расширением и машинным обучением

Х. Гао[1, 2], Л. Йезеквель[1], Э. Каброль[2], Б. Витри[2]

[1]Центральная школа Лиона (Экюли, Французская Республика),
[2]Компания «Рено САС» (Гюйанкур, Французская Республика)

Реферат. На начальном этапе разработки нового транспортного средства необходимо учитывать момент неопределенности параметров, поскольку конструкционные работы предполагают отклонения, вызванные сложностью изготовления ряда элементов с соблюдением производственных допусков. Поэтому числовая оценка критических

Адрес для переписки
Гао Ханвэй
Центральная школа Лиона
просп. Ги де Коллонг, 36,
69134, г. Экюли Седекс, Французская Республика
Тел.: +33176 85-67-51
hanwei.gao@ec-lyon.fr

Address for correspondence
Gao Hanwei
Ecole Centrale de Lyon
36 Guy de Collongue Ave.,
69134, Ecully Cedex, French Republic
Tel.: +33176 85-67-51
hanwei.gao@ec-lyon.fr

характеристик подвески, таких как долговечность и комфортные условия во время движения, должна проводиться с учетом факторов случайности. В статье предлагается применять многоцелевую методологию оптимизации, которая рассматривает надежность спецификации в качестве одной из задач. С целью прогнозирования конечного результата на основании заданного набора неопределенных, но ограниченных параметров, предлагаемых в процессе оптимизационных итераций, используется адаптивное полиномиальное хаотичное расширение для объединения локального проектирования экспериментов и глобальных поверхностей отклика. Кроме того, чтобы уменьшить количество дополнительных тестов, которые необходимы для построения полиномиального хаотичного расширения, используется алгоритм машинного обучения, основанный на межпроектной корреляционной матрице, для проведения классификации текущих проектных точек с помощью интеллектуального анализа данных и кластеризации. Таким образом, появляется возможность прогнозировать надежность разрабатываемых оптимизированных решений без использования дополнительных моделей. По завершении процесса оптимизации может быть получен фронт Парето между спецификациями и их надежностью, который представляет наилучшее компромиссное решение с поставленными целями. Оптимальный набор на данном фронте классифицируется и может являться ориентиром для проектирования. Примером этого может служить тестирование модели автомобиля с целью оптимизации его глобальной долговечности на основе дорожных ситуаций. При этом статистическое распределение параметров, таких как траектории и скорости, тоже принимается во внимание. Результаты исследований показывают несовместимость между долговечностью шасси и надежностью этого параметра. В данном случае термин «надежность» не означает «прочность». В статье этот термин предполагает, что функционирование является менее чувствительным к каким-либо отклонениям. Кроме того, стохастическая выборка подтверждает правильность прогноза надежности методом применения полиномиального хаотичного расширения и машинного обучения, в основе которого лежит значительное уменьшение количества тестов. Показана эффективность предлагаемого подхода, в частности отмечается возможность экономии расчетных затрат на разработку моделей транспортного средства.

Ключевые слова: долговечность шасси, анализ данных, машинное обучение, многоцелевая оптимизация, полиномиальное хаотичное расширение, надежная конструкция

Для цитирования: Надежная конструкция подвески с полиномиальным хаотичным расширением и машинным обучением / Х. Гао [и др.] // *Наука и техника*. 2020. Т. 19, № 1. С. 43–54. https://doi.org/10.21122/2227-1031-2020-19-1-43-54

Introduction

The robustness of vehicle specifications is given more and more attention in Renault because original designs during the development can be perturbed by many uncertain sources: actual road charges, manufacturing tolerances, aging of materials, etc. As a result, sometimes the validation of important specifications such as chassis' durability may take a lot of time and resources to ensure the design is robust enough and can be satisfied all through the vehicle's life cycle [1].

In this paper, the term of robustness is defined as system's ability of tolerating outside perturbations. The robustness is an opposite notion of sensitivity where the least variation of vehicle performance is searched within the random input parameters. Instead of analyzing the impact of each parameter on the final output, the robust optimization focuses on minimizing the overall variations while the statistic characters of input are predefined. Meanwhile, these two notions can easily be transformed after the result of a design of experiments is obtained.

There are several numerical methods to calculate the robustness of one given set of parameters under perturbation.

- Monte-Carlo analysis is to generate random samples in uncertain spaces according to their distributions. The method is easy to integrate and reliable but it requires a huge number of samples to eliminate the random effects of sampling. Other similar methods such as Latin Hypercubic Sampling (LHS) or orthogonal design of experiments are proposed to reduce the total number of tests but are still expensive when the simulation itself is very heavy.
- Min-Max analysis is to run simulations with the combination of upper and lower bounds of uncertain parameter intervals to estimate the worst case under perturbation [1]. It needs less tests compared to random sampling and the result is reasonable as long as the effects of parameters are linear or quasi-linear. However, the statistic characters of the systems cannot be obtained when only the bounds of interval are considered and the robustness estimation may put too much emphasis on the case of which the possibility can be neglect able.
- Analytical methods such as Taylor expansion or direct interval analysis [2] are very efficient because only partial differential equations of the systems are needed instead of a large amount of

simulations. However, the mathematical expressions in the industrial problems are difficult to obtain while simplifying a complex system into an academic model may raise the problem of representativity.

One of the targets during project development is to integrate the robustness into the optimization procedure where the optimum of vehicle specifications and their robustness are searched at the same time. It becomes even more important to reduce the additional simulation number. In this article, an approach based on polynomial chaos expansion (PCE) is applied where only a limited local design of experiments is need for each design point.

The Hermite polynomial chaos was first introduced by Wiener [3] to model stochastic response of a system under Gaussian distributed parameters. Then it has been extended into other type of orthogonal polynomial bases according to different probability distributions [4, 5]. In this study Chebyshev polynomials of the second kind have been applied, which fits better real industrial uncertainties.

The target of polynomial chaos expansion is to establish a relationship between a system output and parameter inputs based on a given series of polynomials. Once the coefficient in front of each polynomial is calculated, system can be described and the robustness can be calculated. For a black box system additional tests are needed in order to decide the maximum order and important interactive terms of polynomials included in this expansion.

This paper proposes a multi-objective optimization plan with the integration of adaptive-sparse polynomial chaos expansions. The polynomial chaos expansion is calculated by a projection method which reuses response surfaces constructed in the optimization process. To further reduce the additional tests, a machine learning algorithm based on data mining is applied to justify by advance the quality of response surface before running the local design of experiments.

Section II of this paper introduces the construction of polynomial chaos expansion as well as its integration into the optimization strategy. In section III a data mining and machine learning algorithm is presented which aims to further reduce sample numbers but keep the accuracy of robustness prediction. Section IV demonstrates the optimization of a quarter-car example with the proposed approach.

Robust optimization with PCE

Introduction of polynomial chaos expansion and Chebyshev polynomials of the second kind. An N-dimensional random variable vector $\boldsymbol{x} = (x_1, x_2, \ldots, x_n)$ is considered. For each input variable $x_i \in \Gamma_i$, where Γ_i is a one-dimension random space, its probability density function (PDF) can be defined by $p_i(x_i)$. Assuming that all the random variables are independent, the overall PDF $P(x)$ can be defined as

$$P(\boldsymbol{x}) = p_1(x_1)\, p_2(x_2) \ldots p_N(x_n) \quad \text{in } \Gamma = \Gamma_1 \Gamma_2 \ldots \Gamma_n. \tag{1}$$

The system at one set of parameters $\boldsymbol{x}$ an be written as a converged series of polynomial basis

$$f(\boldsymbol{x}) = \sum_{i=0}^{\infty} s_i \phi_i\left(\xi(\boldsymbol{x})\right) = s_0\phi_0 + \sum_{j_1=1}^{\infty}\sum_{i_1=1}^{n} s_{i_1}^{j_1}\phi_1^{j_1}\left(\xi_{i_1}(\boldsymbol{x})\right) + \sum_{j_2=1}^{\infty}\sum_{i_1=1}^{n}\sum_{i_2=1}^{i_1} s_{i_1,i_2}^{j_2}\phi_2^{j_2}\left(\xi_{i_1}(\boldsymbol{x}), \xi_{i_2}(\boldsymbol{x})\right) + \tag{2}$$

$$+ \sum_{j_3=1}^{\infty}\sum_{i_1=1}^{n}\sum_{i_2=1}^{i_1}\sum_{i_3=1}^{i_2} s_{i_1,i_2,i_3}^{j_3}\phi_3^{j_3}\left(\xi_{i_1}(\boldsymbol{x}), \xi_{i_2}(\boldsymbol{x}), \xi_{i_3}(\boldsymbol{x})\right) + \ldots,$$

where $\xi(\boldsymbol{x}) = \{\xi_1(\boldsymbol{x}), \xi_2(\boldsymbol{x}), \ldots, \xi_n(\boldsymbol{x})\}$ – set of ran-dom variables obtained by normalization of x according to known mean values and the standard deviations; $\phi_n^j\left(\xi(\boldsymbol{x})\right)$ – n-dimension chaos of order j in terms of $\xi(\boldsymbol{x})$.

The inner product of two orthogonal polynomial basis can be expressed as

$$\left\langle \phi_i, \phi_j \right\rangle = \delta_{ij} \left\langle \phi_i^2 \right\rangle, \tag{3}$$

where δ_{ij} – Kronecker delta, $\delta_{ij} = 1$ when $i = j$ and $\delta_{ij} = 0$ when $i \neq j$.

To simplify the expression, the equation (2) is truncated to maximum order M and it includes only univariate and bivariate terms, which can be rewritten as

$$f(\boldsymbol{x}) = \sum_{i=0}^{M} s_i \phi_i\left(\xi(\boldsymbol{x})\right) = s_0\phi_0 + \sum_{j_1=1}^{M}\sum_{i_1=1}^{n} s_{i_1}^{j_1}\phi_1^{j_1}\left(\xi_{i_1}(\boldsymbol{x})\right) + \\ + \sum_{j_2=1}^{M}\sum_{i_1=1}^{n}\sum_{i_2=1}^{i_1} s_{i_1,i_2}^{j_2}\phi_2^{j_2}\left(\xi_{i_1}(\boldsymbol{x}), \xi_{i_2}(\boldsymbol{x})\right). \quad (4)$$

The form of the polynomial basis ϕ_i is defined by the distribution types of random parameters. Chebyshev polynomial of the second kind is applied in this study. As its probability density function corresponded is Wagner semicircle distribution defined in (Fig. 1) $[-1.1]$. The semicircle law is more suitable to industry problems where the parameters have more weights around the design values and will never go to infinity. The polynomials can be defined by a recurrence method:

$$U_{n+1}(\xi_i) = 2xU_n(\xi_i) - U_{n-1}(\xi_i), \\ \text{for } n \geq 1 \\ \text{with } U_0(\xi_i) = 1;\ U_1(\xi_i) = 2\xi_i \quad (5) \\ \text{and } \xi_i \in [-1.1],$$

where ξ_i – respects a Wagner semicircle distribution.

The distribution function is normalized to make sure the integration in [–1.1] equals to 1, so in fact it becomes a semi ellipse

$$w(\xi_i) = \frac{2}{\pi}\sqrt{1-\xi_i^2}. \quad (6)$$

The equation (3) can be expressed as for two one-dimension polynomials

$$\langle U_m U_n \rangle = \int_{-1}^{1} U_m(\xi_i) U_n(\xi_i) w(\xi_i)\, dx = \\ = \begin{cases} 0, & \text{if } i \neq j; \\ 1, & \text{if } i = j. \end{cases} \quad (7)$$

In equation (4) coefficients s_i are unknown and need to be calculated. For a black-box system, two non-intrusive methods exist to calculate s_i.

- Regression method: the order and the terms of the expansion are assumed a priori. The coefficients are then calculated by linear regression method based on the samples around the reference point. By iterations the algorithm will decide whether to add or remove terms from the expansion until all the important terms are included [6].
- Projection method: an analytical expression has been pre-defined used to represent the black-box system. Then based on this expression, each coefficient is calculated one by one according to orthogonal projection. Additional samples are also necessary to justify if the expansion order has been converged [7].

In the optimization process expressed in Section III, the analytical expressions for the result outputs have already been calculated. The projection method will be introduced in detail and applied. Another advantage for the projection method is that the accuracy of robustness estimation depends more on the quality of analytical expressions but is less sensitive to the number of samples compared to the regression method.

Assuming $f(\boldsymbol{x})$ is a performance function defined in the design space, one can obtain by multiplying $\phi_j(\xi)$ to both sides of (4):

$$\left\langle f(\boldsymbol{x})\phi_j(\xi)\right\rangle = \left\langle \sum_{i=0}^{M} s_i \phi_i(\xi)\phi_j(\xi)\right\rangle; \quad (8)$$

$$s_j = \frac{\left\langle f(\boldsymbol{x})\phi_j(\xi)\right\rangle}{\left\langle \phi_j(\xi)^2\right\rangle}, \quad (9)$$

where $\left\langle \phi_j(\xi)^2\right\rangle$ – constant; $\left\langle f(\boldsymbol{x})\phi_j(\xi)\right\rangle$ – calculated by multi integration.

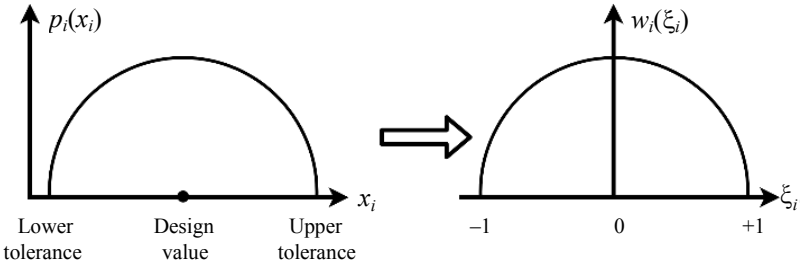

Fig. 1. Transformation of a real design parameter to a normalized random variable of Wagner semicircle distribution

The reference [8] has proposed a decomposition method of $f(x)$ and the numerator of equation (9) can be expanded into univariate and bivariate terms

$$s_j^k = \frac{\left\langle f(\boldsymbol{x})\phi_j(\xi_k)\right\rangle}{\left\langle \phi_j(\xi_k)^2\right\rangle} =$$

$$= \frac{\left(\left\langle \sum_{i=1}^{n} f(x_i,\mu_i)\phi_j(\xi_k)\right\rangle -}{\left\langle \phi_j(\xi_k)^2\right\rangle} \rightarrow$$

$$\rightarrow \frac{-(n-1)f(\mu)\left\langle \phi_j(\xi_k)\right\rangle\left\langle f(x_k,\mu_k)\phi_j(\xi_k)\right\rangle}{\left\langle \phi_j(\xi_k)^2\right\rangle}; \quad (10)$$

$$s_{j_1 j}^{k,l} = \frac{\left\langle f(\boldsymbol{x})\phi_{j_1 j}(\xi_k,\xi_l)\right\rangle}{\left\langle \phi_{j_1 j}(\xi_k,\xi_l)^2\right\rangle} =$$

$$= \frac{\left\langle\left(\sum_{j_2=1}^{n}\sum_{i_1=1}^{j_2} f(x_{i_1},x_{i_2},\mu_{i_1,i_2}\right) -}{\left\langle \phi_{j_1 j}(\xi_k,\xi_l)^2\right\rangle} \rightarrow$$

$$\rightarrow \frac{-(n-2)\sum_{i=1}^{n} f(x_i,\mu_i)\Big)\phi_{j_1 j}(\xi_k,\xi_l)\Big\rangle}{\left\langle \phi_{j_1 j}(\xi_k,\xi_l)^2\right\rangle} +$$

$$+ \frac{\frac{(n-1)(n-2)}{2} f(\boldsymbol{\mu})\left\langle \phi_{j_1 j}(\xi_k,\xi_l)\right\rangle}{\left\langle \phi_{j_1 j}(\xi_k,\xi_l)^2\right\rangle} =$$

$$= \frac{\left\langle f(x_k,x_l,\mu_{k,l})\phi_{j_1 j}(\xi_k,\xi_l)\right\rangle}{\left\langle \phi_{j_1 j}(\xi_k,\xi_l)^2\right\rangle}, \quad (11)$$

where s_j^k – coefficient for the j^{th} order univariate polynomial term of $\xi(x_k)$; $s_{j_1 j}^{k,l}$ – coefficient for the j^{th} order bivariate polynomial term of $\xi(x_k)$ and $\xi(x_l)$ (j_1^{th} order for $\xi(x_k)$ and $(j-j_1)^{\text{th}}$ order for $\xi(x_l)$); (x_i,μ_i) – vector that replaces all the random variables by its reference value except x_i; $\left(x_{i_1},x_{i_2},\mu_{i_1,i_2}\right)$ – vector of reference values excluding x_{i_1},x_{i_2}; $f(\boldsymbol{\mu})$ – function value when all the variables are equal to the reference ones.

It can be noticed that equations (10) and (11) require only one- or two-dimensional integrations. The higher order interaction terms are neglected because of the weak non-linearity in mechanical systems, which saves greatly the computational resources.

One determination coefficient R^2 is calculated to justify the correlation between the PCE and test results

$$R^2(J) = 1 - \frac{\frac{1}{N}\sum_{I=1}^{N}\left(f_{test}\left(\boldsymbol{x}^I\right) - f^J\left(\boldsymbol{x}^I\right)\right)^2}{\frac{1}{N}\sum_{I=1}^{N}\left(f_{test}\left(\boldsymbol{x}^I\right) - \frac{1}{N}\sum_{J=1}^{1} f_{test}\left(\boldsymbol{x}^I\right)\right)^2}, \quad (12)$$

where J – order of the PCE; $\boldsymbol{x}^I$ – I^{th} sample of local experiment design; $f_{test}\left(\boldsymbol{x}^I\right)$ – test result of this sample.

It can be seen that the quality of prediction is improved with $R^2(J)$ approaching to 1.

When the PCE order is increased by iterations, the PCE is converged if the difference of R^2 between two orders is smaller than a threshold ε_1 which means including new terms has nearly zero impact on the expansion

$$R^2(J) - R^2(J-1) < \varepsilon_1. \quad (13)$$

Furthermore, as 2*D*-integration is usually more expensive to calculate, another indicator is defined to justify if the bivariate terms of $\xi(x_k)$ and $\xi(x_l)$ for PCE have converged before the total expansion

$$\frac{1}{N}\frac{\sum_{i=1}^{N}\left(\sum_{j_1=1}^{1} s_{j_1 j}^{k,l}\phi_{j_1 j}\left(\xi\left(x_k^i,x_j^i\right)\right)\right)^2}{e_{TSS}} < \varepsilon_2. \quad (14)$$

If the equation (14) is satisfied it means the contribution of j^{th} order bivariate terms of $\xi(x_k)$ and $\xi(x_l)$ is negligible with respect to the expansion and for the next order this term will not be calculated. A summary of the procedure of calculation of PCE around one reference solution can be seen in Fig. 2.

Once the PCE is constructed, the mean value and standard deviation of $f(x)$ can be estimated by:

$$\overline{f}(\boldsymbol{x}) = \left\langle f(\boldsymbol{x})\right\rangle = \left\langle \sum_{i=0}^{M} s_i\phi_i \right\rangle = s_0; \quad (15)$$

$$\sigma\left(f\left(\boldsymbol{x}\right)\right)=\left\langle\left(\sum_{i=1}^{M}s_i\phi_i\right)^2\right\rangle=\sum_{i=1}^{M}s_i^2. \qquad (16)$$

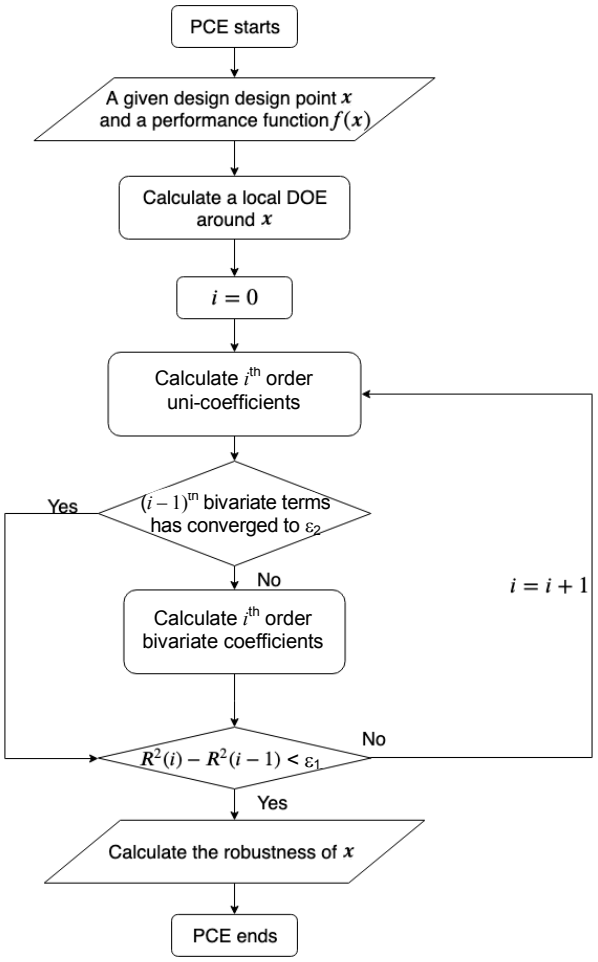

Fig. 2. Summary of PCE calculation by PCE method for one reference solution

Multi-objective optimization. Chassis systems has multiple demands on durability, ride comfort and handling, etc. while each of them is often incompatible with the others. Therefore, during the design phase, the optimization of chassis system is naturally multi-objective where the best compromises are searched.

The robustness of objectives included in the optimization plan are also integrated and listed as the objectives for optimizing. This step tends to make the objectives even more incompatible because empirically the optimums are less robust compared to the less good solutions. Thus, this study aims to find the relationship between the objectives and their robustness and to propose the optimums which are less sensitive to perturbations.

The mathematical expression of multi-objective optimization can be expressed as:

– minimize:

$$F\left(\boldsymbol{x}\right)=\left\{f_1\left(\boldsymbol{x}\right),f_2\left(\boldsymbol{x}\right),\ \ldots,\ f_m\left(\boldsymbol{x}\right)\right\}; \qquad (17)$$

– under the constraints:

$$h_j\left(\boldsymbol{x}\right)=0, j=1,\ \ldots,\ q;$$

$$g_k\left(\boldsymbol{x}\right)\le 0, k=1,\ \ldots,\ p; \qquad (18)$$

$$\boldsymbol{x}^{\min}\le\boldsymbol{x}\le\boldsymbol{x}^{\max}, r=1,\ldots n,$$

where $x-n\times 1$ vector of design parameters which forms a design space; $\boldsymbol{x}^{\min}$, and $\boldsymbol{x}^{\max}$ – lower and upper bounds of the design space; $F(\boldsymbol{x})-m\times 1$ vector of objective functions for minimizing; $h_j\left(x\right)$, $g_k\left(x\right)$ – equality or inequality constraints of the system.

Instead of summing all the compositions $f(\boldsymbol{x})$ in $F(\boldsymbol{x})$, the optimization will treat each objective separately. As a result, the optimization plan will propose a set of compromised optimums instead of only one solution, which will form a Pareto front [1, 9, 10]. The definition of one Pareto optimum is one which is not dominated by any other solutions. There may exist one or more solutions which have better performances in some objectives, but they must have worse solutions in other aspects than those of Pareto optimums.

Another characteristic of industrial problems is that the systems are usually black-box models and the mathematical expression of $F(\boldsymbol{x})$ does not exist. Therefore, a Meta-model $F_{Meta}\left(\boldsymbol{x}\right)$ will be constructed before the optimization iterations begin [11, 12]. $F_{Meta}\left(\boldsymbol{x}\right)$ consists of several response surfaces which describe the black-box system with different combination of polynomials. The equation (17) can be replaced by as:

$$F_{Meta}\left(\boldsymbol{x}\right)=\begin{Bmatrix}\left\{f^0_{RS_1}\left(\boldsymbol{x}\right),\ f^1_{RS_1}\left(\boldsymbol{x}\right)\ldots f^{l_1}_{RS_1}\left(\boldsymbol{x}\right)\right\};\\ \left\{f^0_{RS_2}\left(\boldsymbol{x}\right),\ f^1_{RS_2}\left(\boldsymbol{x}\right)\ldots f^{l_2}_{RS_2}\left(\boldsymbol{x}\right)\right\};\\ \left\{f^0_{RS3}\left(\boldsymbol{x}\right),\ f^1_{RS_3}\left(\boldsymbol{x}\right)\ldots f^{l_3}_{RS_3}\left(\boldsymbol{x}\right)\right\},\end{Bmatrix} \qquad (19)$$

where $f^j_{RS_i}\left(\boldsymbol{x}\right)|\left(j=1\ldots l_i\right)$ – j^{th} response surfaces for $f_i\left(\boldsymbol{x}\right)$ constructed from an initial design of experiments (DOE) in the design space; l_i – total

number of response surfaces configurated for $f_i(\boldsymbol{x})$; $f^0_{RS_i}(\boldsymbol{x})$ – new response surfaces for $f_i(\boldsymbol{x})$ who sums all the response surfaces regarding to their quality by cross validation [13].

The meta-model can then replace the black-box model and be used with the genetic optimization algorithm NSGA-II [14, 15].

For the robustness objectives, the calculation of PCE is based on the Meta-model constructed in this step. As the Meta-model has several expressions to represent the system, several estimations of PCE can also be made. The final robustness is a weighted sum of these estimations according to the quality of response surfaces:

$$\sigma\left(f_i(\boldsymbol{x})\right)=\frac{1}{\sum_{i=0}^{l_i}p_j}\sum_{j=0}^{l_i}p_j\sigma\left(f^j_{RS_i}(\boldsymbol{x})\right); \quad (20)$$

$$p_j=\frac{1}{\left(1-R^2_{final}\left(f^j_{RS_i}(\boldsymbol{x})\right)\right)^2}, \quad (21)$$

where $\sigma\left(f^j_{RS_i}(\boldsymbol{x})\right)$ – j^{th} PCE robustness estimation for $f_i(\boldsymbol{x})$ based on the projection of its j^{th} model $f^j_{RS_i}(\boldsymbol{x})$; $R^2_{final}\left(f^j_{RS_i}(\boldsymbol{x})\right)$ – final determination coefficient for $\sigma\left(f^j_{RSi}(\boldsymbol{x})\right)$ when the PCE is converged to ε_1 (see (13)); p_i – weight indicator which judges the quality of i^{th} response surface by comparing it with 1.

The procedure of robust multi-objective optimization is summarized in Fig 4. By iterations, the potential optimums can be proposed by the genetic algorithm based on the objectives' response surfaces. The proposed solutions and their robustness will then be validated by real numerical simulations, of which the results are reused to improve the quality of response surfaces. If the optimization is converged, the solutions proposed will form a Pareto front.

It should be noted that although both the response surfaces and PCEs are in the form of polynomials, the domain of these polynomials are different. For response surface, the variables can cover any values in the design space while for PCE the variables are limited in the neighbourhood of one design value. PCE describes the local behavior of a specific point on the response surface. That's why the global quality of response surface has a great influence on the robustness estimation.

Application of data mining and machine learning

The calculation of PCE by projection method requires much fewer tests compared to purely random sampling methods such as Monte-Carlo, which has been shown by the example in Section IV. However, the integration of robustness into the optimization requires hundreds of PCE calculation which is still expensive even if the number of tests required to compute the robustness at one point has been greatly reduced. Two approaches have been applied at the same time to further reduce the number of samples tested for each point.

The first approach is called inherited design of experiments referenced in [13]. The simulations will stock in a data base and be reused in the local DOE for future calculation of PCE if there already exist test results in a new coming point's neighbourhood. With the enrichment of the data base, the extra number of simulations tends to be reduced.

The second approach is to exploit further the data base with a data-mining algorithm and to learn to construct the PCE without extra samples. In the procedure of PCE calculation by projection method in Section II, the local DOE is used to converge the projected terms and orders in PCE by analyzing the quality of approximation between the PCE response surfaces and the simulation results. Unlike the regression method, where the coefficients of polynomials are calculated directly from the DOE results, the projection method depend mostly on the modelling quality of meta-model. If one can predict the weighting factor in equation (20) of each response surface of meta-model on the point to be studied, there will be no need to run extra simulations for PCE calculations.

The data-mining strategy referenced in [10] which is firstly used for post-processing of Pareto front starts firstly by calculating the normalized correlation distances of different information between each pair of design points *i* and *j*:

$$D^x_{ij}=1-\frac{\left\|\boldsymbol{x}^i-\boldsymbol{x}^j\right\|}{\max\left(\left\|\boldsymbol{x}^t-\boldsymbol{x}^s\right\|,\ t,s=1...N\right)}; \quad (22)$$

$$D_{ij}^{F} = 1 - \frac{\left\| \boldsymbol{F}^{i} - \boldsymbol{F}^{j} \right\|}{\max\left(\left\| \boldsymbol{F}^{t} - \boldsymbol{F}^{s} \right\|,\ t, s = 1...N \right)}; \qquad (23)$$

$$D_{ij}^{P} = 1 - \frac{\left\| \boldsymbol{P}^{i} - \boldsymbol{P}^{j} \right\|}{\max\left(\left\| \boldsymbol{P}^{t} - \boldsymbol{P}^{s} \right\|,\ t, s = 1...N \right)}, \qquad (24)$$

where D_{ij}^{x}, D_{ij}^{F}, D_{ij}^{P} – distance of input variables, objectives and weighting factors of design points i and j; N – number of existing simulations in the data base; $\boldsymbol{x}^{i}$ – i^{th} vector of input parameters; $\boldsymbol{F}^{i}$ – vector of objectives defined in equation (17); $\boldsymbol{P}^{i}$ – vector of weighting factors calculated when combining the estimations from response surfaces in (21).

According to the definition, the correlation between two designs will be good when $D_{ij} \to 1$.

The inter-design matrix D^{x}, inter-objective matrix D^{F} and weighting factor matrix D^{P} are symmetric matrix and can be used to analyze the correlation of each pair of points in the data base (Fig. 7, 8). Another mixed matrix M can be defined to show the correlation of both input and output between two designs:

$$M_{ij} = \left(D_{ij}^{x} \right)^{c_x} \left(D_{ij}^{F} \right)^{c_F}; \qquad (25)$$

$$c_x + c_F = 1,$$

where c_x, c_F – coefficients of mixture defined between 0 and 1.

In order to make the matrix more readable, a bipolarization algorithm cited in [10] will used to arrange the order of design point according to their resemblance level. The algorithm starts with finding the two most different design point in M_{ij} and grouping their neighbors based on a resemblance threshold s. This operation is looped for the rest of non-grouped points until all the points are arranged. The algorithm schema is shown in Fig. 3.

An example of the result after bipolarization is shown in Fig 3. It is a process similar to clustering method in data mining which also regroups the existing solutions according to several features (in this study the parameters and objectives). The typologies of the database can be exploited as a post-processing to find the orientation of multi-objectives in each group. The grouping result will also serve as a base for learning in the next steps.

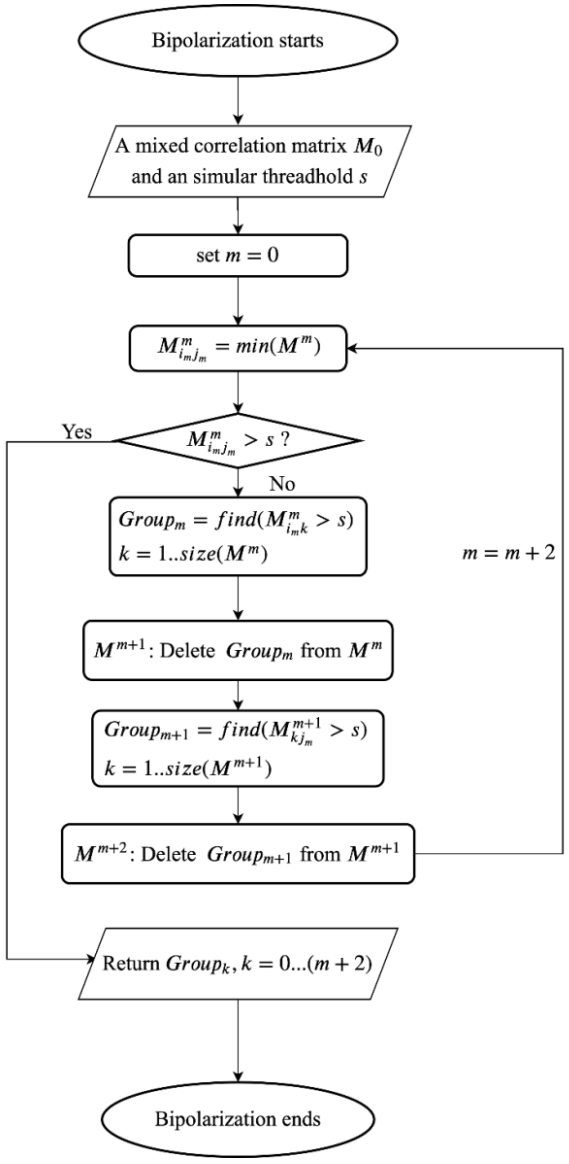

Fig. 3. Algorithm schema for bipolarization method of data mining

Fig. 11 shows D_{ij}^{P} in the groups obtained by mixed design-objective matrix M in Fig. 10. It shows that for the resembling design points, the weighting factors tend also to be alike. It is reasonable because the points in the same group also tend to be neighborhood in the meta-model, where the modelling quality of response surfaces is similar in this area. The neighbourhood has been displaced for a different group thus the modelling quality of each response surface has also changed.

The principle of learning is that if the new design points of which the robustness is to be calculated fall into one existing group, the quality of estimation of each response surfaces can also be learned based on the D_{ij}^{P} information in the group. As a result, the calculation needs no extra simulation.

The algorithm of learning for a new coming design point can be summarized as following:

1) a new line/column is added into the correlation matrix D^{x}, D^{F} to make two $(n+1)(n+1)$ matrix by calculating the correlation distances from the new point to the data base;

2) the minimum correlation distance is to be found between the new point and each existing group. A pre-defined threshold will judge if the new coming point belongs to any group in the data base;

3) if no groups can be referenced. The robustness will be calculated by the local DOE method in Section II. If there exists at least one group that can include the new design point, the vector ***P*** of weighting factors can be learned from those in this group. The combined PCE estimation can be obtained without running simulations.

Example with a quarter car model

A quarter car model has been applied to demonstrate the robust multi-objective optimization strategy proposed in this paper. The model has been shown in Fig. 5: m_1 – unsprung mass which sums the mass of the wheels and a part of half suspension; m_2 – sprung mass of a quarter of the car body; k_1, c_1 – tire stiffness and damping rate; k_2, c_2 – suspension vertical stiffness and damping rate; x_0 – coordinate of the road profile; x_1, x_2 – vertical displacements of the unsprung/sprung masses.

In this example it is assumed that the masses m_1, m_2 and the properties of tire k_1, c_1 are given and the target is to optimize the properties of suspension parameters: k_2 and c_2. The non-linearity of damping ratio c_2 has been considered and thus it consists of four values which define different slopes of force/velocity at high & low velocity and compression & rebound phases $(c_{2i},\ i=1...4)$.

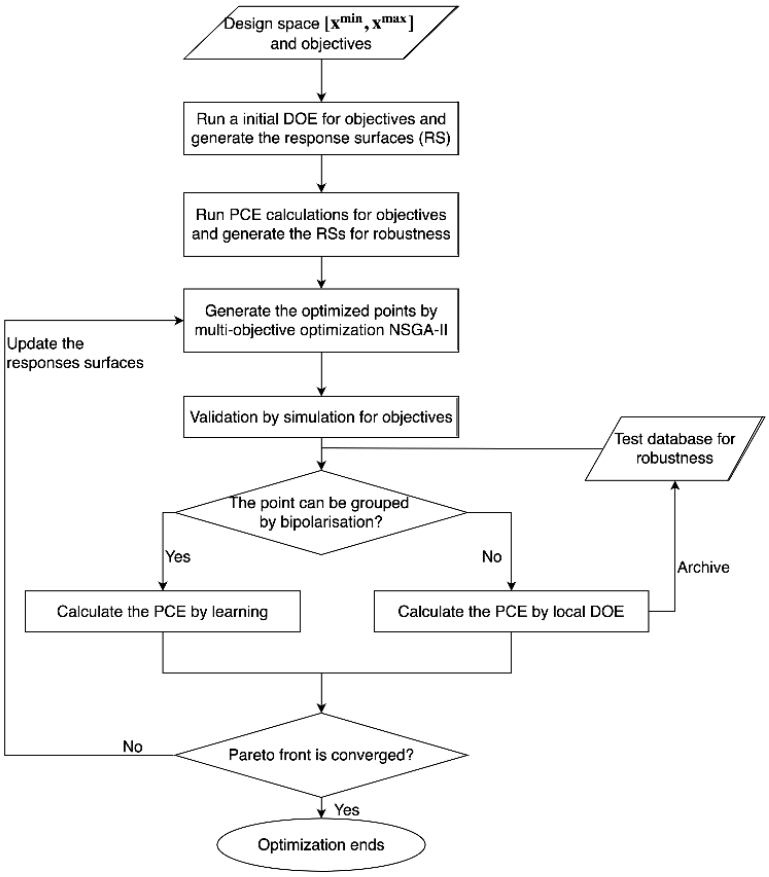

Fig. 4. Summary of the optimization procedure with the integration of PCE calculation and learning algorithm

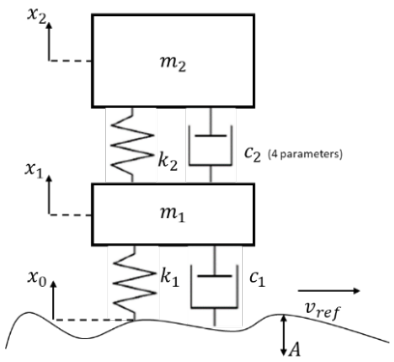

Fig. 5. A quarter car model with its definition of parameters

The objective in optimization is to minimize the equivalent damage force on the m_1 when x_0 is passing a Belgian blocks test track. The definition of equivalent damage force is based on Basquin fatigue low

$$F_{ed} = F_{\max}\left(\frac{\sum d_i n_i}{2N}\right)^{\frac{1}{B}}, \qquad (26)$$

where F_{ed} – equivalent damage force; $F_{\max}$ – maximum force in Basquin model when total damage D = 1; N – number of cycles corresponding to D = 1; d_i, n_i – cumulative damage and its repetitions in the force signal in the simulation which are obtained by rainflow-counting algorithm; B – constant number of the Basquin model.

The second objective is the robustness of F_{ed} due to the uncertainty added in the system: the variation of k_2 and c_{2i}, $i = 1...4$, to represent manufactory tolerances and aging during usage accompanied with passing velocity and road amplitudes as validation process perturbations.

The non-dominated design points between two objectives are shown in Fig. 6 with the PCE method and learning algorithm. The optimum solutions in durability have relatively worse robustness due to perturbations. Tab. 1 shows the comparison between a much larger sampling size (1000 tests) with Latin Hypercubic method, the local DOE with only 8 tests and learning algorithm without tests for 3 design points. The reference point is the design point when the optimization starts. Optimized point 1 is one of the optimums orientated to robustness and optimized point 2 is one oriented to durability. It can be seen that the PCE method succeeded in produce the closed estimations as ones from a larger sampling especially for the first two points. Estimation for the design points oriented to durability is less good but it still shows the tendency of the relationship between the objective and its robustness.

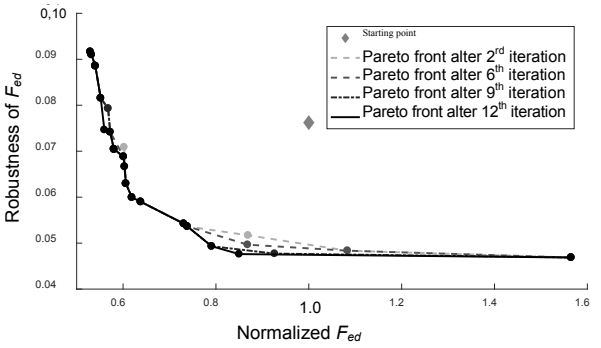

Fig. 6. Evolution of Pareto front between normalized equivalent damage force and its robustness (The damage force of starting point is 1)

Table 1

Comparison of PCE estimations obtained by different methods for 3 points

	Ref. point	Opt. point 1	Opt. point 2
k_2, N/m	20500	10250	10250
c_{21}, Ns/m	250	790	260
c_{21}, Ns/m	2220	4440	1100
c_{21}, Ns/m	2360	4720	1220
c_{21}, Ns/m	2360	4710	1180
F_{ed}, N	2252	2413	1192
PCE by data mining (0 test), %	–	5.34	8.42
Local DOE (8 tests), %	7.45	5.15	7.39
LHS (1000 tests), %	7.73	5.07	6.56

The matrix of D^x, D^F, M regrouped M and D^P in each group are shown in Fig. 7–11 after 12th iteration. It can be seen that the existing design points can be distributed into several small groups where the weighting vectors tends to resemble each other. This offers a good learning basis for new coming design points.

In this optimization totally 113 potential design optimums of robustness have been proposed during meta-model's construction and optimization iterations, which means millions of simulations of durability objectives need to be run if all the robustness is validated by a Monte-Carlo sampling. The size of one local DOE for PCE calculation is set to 8. If a PCE method without either inherited DOE nor learning method has been applied, about 1000 simulations would need to be run theoretically. With the integration of inherited DOE, the total number of simulations can be reduced to 802.

The learning algorithm permits to reduce further 22 % amount of simulations to 628 and the robust estimation keeps the same level. The gain is encouraging when one single simulation takes a long time.

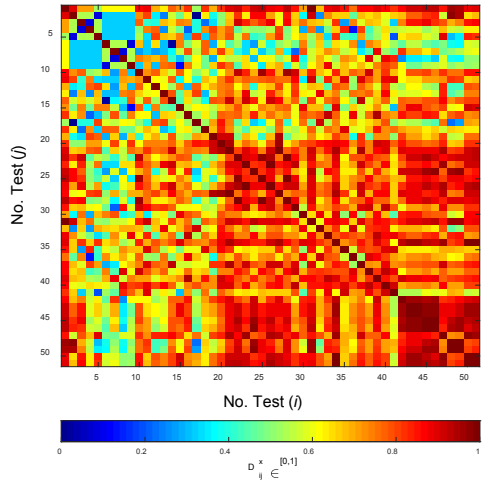

Fig. 7. Inter-design correlation matrix D^x for 91 design vectors

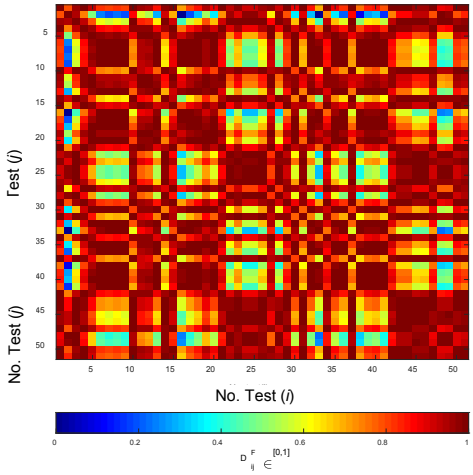

Fig. 8. Inter-objective correlation matrix D^F for 91 objective vectors

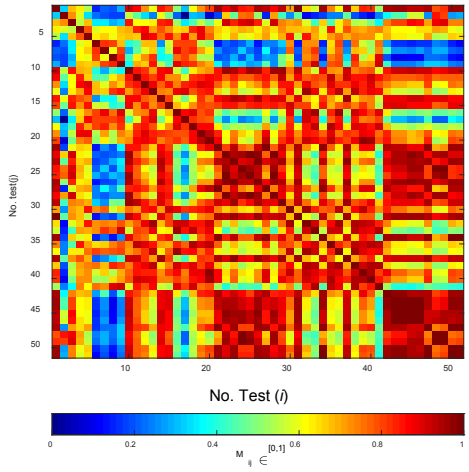

Fig. 9. Mixed design-objective matrix M for Fig. 7, 8 with $c_x = 0.6$, $c_F = 0.4$

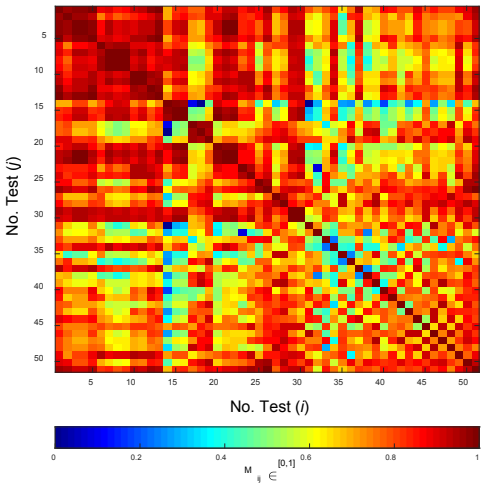

Fig. 10. Group result for the matrix M in Fig. 9. by bipolarization algorithm with $c_s = 0.95$

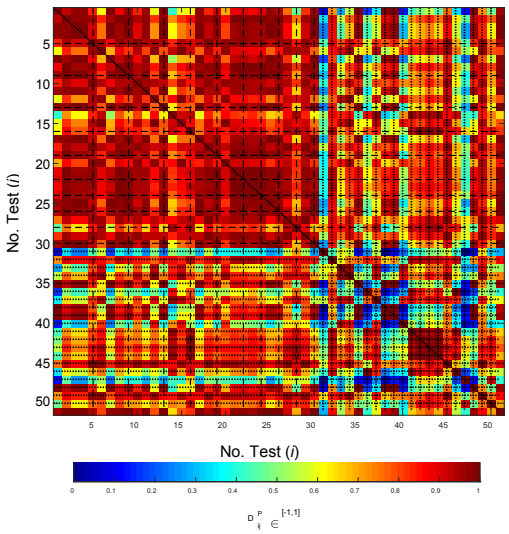

Fig. 11. Weighting matrix D^P in the group of Fig. 10 (black lines mean the groups found in M)

Fig. 12 shows the comparison of the Pareto front between a robust optimization with learning and one without learning. It can be seen that there are some local differences between two strategies, but the tendency of durability objective and its robustness are close. Fig. 13 shows the number of design points suitable for learning algorithm and average additional samples for one PCE calculation according the optimization iterations. The curves have oscillated at the beginning and become stable from 7th iteration. Most of design points are groupable from 7th iteration which means the test data base is complete especially at the region close to the Pareto front.

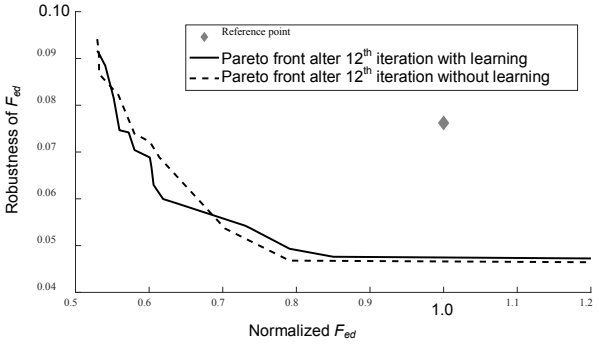

Fig. 12. Comparison of Pareto front between the optimization with or without learning

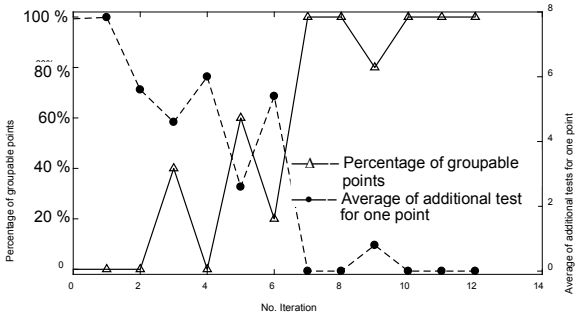

Fig. 13. Evolution of number of groupable numbers (in triangles) and additional tests (in circle) per point with iteration

CONCLUSION

In this paper a robust optimization method has been proposed which aims to reduce the number of tests during the optimization and gives a global view on the relationship between the design objectives and their robustness. The integration of a learning algorithm based on data mining permits to further reduce the necessary simulations. The example shows the data mining plan is suitable for small size data bases and once it is constructed the estimation of robustness needs no more simulations.

REFERENCES

1. Chatillon M. M. (2005) *Méthodologie de Conception Robuste Appliquée Aux Trains de Véhicules de Tourisme*. Doctoral dissertation, Ecully, Ecole Centrale de Lyon.
2. Dessombz O. (2000) *Analyse Dynamique de Structures Comportant des Paramètres Incertains.* Doctoral Dissertation, Ecully, Ecole Centrale de Lyon.
3. Wiener N. (1938) The Homogeneous Chaos. *American Journal of Mathematics*, 60 (4), 897–936. https://doi.org/10.2307/2371268.
4. Xiu D., Karniadakis G. E. (2002) The Wiener-Askey Polynomial Chaos for Stochastic Differential Equations. *SIAM Journal on Scientific Computing*, 24 (2), 619–644. https://doi.org/10.1137/s1064827501387826.
5. Wu J., Luo Z., Zhang Y., Zhang N., Chen L. (2013) Interval Uncertain Method for Multibody Mechanical Systems Using Chebyshev Inclusion Functions. *International Journal for Numerical Methods in Engineering*, 95 (7), 608–630. https://doi.org/10.1002/nme.4525.
6. Kim N. H., Wang H., Queipo N. (2004) Adaptive Reduction of Design Variables Using Global Sensitivity in Reliability-Based Optimization. *10th AIAA/ISSMO Multidisciplinary Analysis and Optimization Conferencep,* 4515. https://doi.org/10.2514/6.2004-4515.
7. Hu C., Youn B. D. (2011) Adaptive-Sparse Polynomial Chaos Expansion for Reliability Analysis and Design of Complex Engineering Systems. *Structural and Multidisciplinary Optimization*, 43 (3), 419–442. https://doi.org/ 10.1007/s00158-010-0568-9.
8. Knio O. M., Najm H. N., Ghanem R. G. (2001) A Stochastic Projection Method for Fluid Flow: I. Basic Formulation. *Journal of Computational Physics*, 173 (2), 481–511. https://doi.org/10.1006/jcph.2001.6889.
9. Eddy J., Lewis K. (2001) Effective Generation of Pareto Sets Using Genetic Programming. *Proceedings of DETC'01 ASME 2001 Design Engineering Technical Conferences and Computers and Information in Engineering Conference*. Pittsburgh, PA, Sept. 9–12, 2001, 132.
10. Loyer B. (2009) *Conception Fonctionnelle Robuste Par Optimisation Multicritère de Systèmes de Suspension Automobile Passifs et Semi-Actifs*. Doctoral Dissertation, Ecully, Ecole Centrale de Lyon.
11. Allen T. T., Bernshteyn M. A., Kabiri-Bamoradian K. (2003) Constructing Meta-Models for Computer Experiments. *Journal of Quality Technology*, 35 (3), 264–274. https://doi.org/10.1080/ 00224065.2003.11980220.
12. Acar E., Rais-Rohani M. (2009) Ensemble of Metamodels with Optimized Weight Factors. *Structural and Multidisciplinary Optimization*, 37 (3), 279–294. https://doi.org/ 10.1007/s00158-008-0230-y.
13. Dumont E., Khaldi M. (2018) *Alternova Layer 1 User Guide for Renault.* Eurodecision, May.
14. Di Pierro F., Khu S. T., Djordjevic S., Savic D. (2004) *A New Genetic Algorithm to Solve Effectively Highly Multiobjective Problems: Poga.* Report Nr 2004/02, Center for WaterSystems, University of Exeter.
15. Wang G. G. (2003) Adaptive Response Surface Method Using Inherited Latin Hypercube Design Points. *Journal of Mechanical Design,* 125 (2), 210–220. https://doi.org/10.1115/1.1561044.

Received: 08.10.2019
Accepted: 10.12.2019
Published online: 31.01.2020

https://doi.org/10.21122/2227-1031-2020-19-1-55-62

UDC 625.7+338.5

Improving the Brake Control Effectiveness of Vehicles Equipped with a Pneumatic Brake Actuator

V. Bogomolov[1)], V. Klimenko[1)], D. Leontiev[1)], L. Ryzhyh[1)], O. Smyrnov[1)], M. Kholodov[1)]

[1)]Kharkiv National Automobile and Highway University (Kharkiv, Ukraine)

Abstract. This paper proposes a way to determine a rational connection between a two-section or three-section brake valve and the main brake system circuits of a wheeled vehicle equipped with simplex or duo-duplex brake gears. The aim is to determine a rational option to connect main brake system circuits with a brake valve to guarantee the maximum effectiveness of an emergency brake system if any device of the brake actuator of a multiaxle wheeled vehicle is out of order, using the methods of combinatorics. The feature of the proposed way, determining the rational connection of a brake valve with the main brake system circuits of a multiaxle wheeled vehicle, is the application of combinatorics methods, taking into account the features of a brake valve design. New mathematical interconnections between the quantities of the connection points of circuits and simplex and duo-duplex brake gears enable us to determine the rational scheme of the application of the brake gear circuits of a multiaxle wheeled vehicle. Mathematical expressions that enable us to compute the number of possible connection points of two-section and three-section brake gears and simplex and duo-duplex brake gears, which are installed on the axles of a multiaxle wheeled vehicle, have been determined. It is proposed to use a universal mathematical dependence to determine the number of rational options to connect the brake actuator circuits of a multiaxle wheeled vehicle. The diagram of the calculated scheme of the connection between circuits and the two-section or three-section brake valve of simplex or duo-duplex brake gears is presented. It simplifies the determination of the number of rational options to connect brake actuator circuits with the brake gears and brake valve of a multiaxle wheeled vehicle. In review the analysis of requirements to be fulfilled in accordance with international standards is provided and the evaluation of the effectiveness of the emergency brake system of some wheeled vehicles is carried out. The general concept to determine the rational layout of the emergency brake system of a multiaxle wheeled vehicle on the basis of the arrangement schemes of the connection between two-section or three-section brake valves and simplex and duo-duplex brake gears is proposed.

Keywords: multiaxle vehicle, pneumatic brake actuator, brake gear, effectiveness factor

For citation: Bogomolov V., Klimenko V., Leontiev D., Ryzhyh L., Smyrnov O., Kholodov M. (2020) Improving the Brake Control Effectiveness of Vehicles Equipped with a Pneumatic Brake Actuator. *Science and Technique*. 19 (1), 55–62. https://doi.org/10.21122/2227-1031-2020-19-1-55-62

К вопросу о повышении эффективности управления тормозами транспортных средств, оснащенных пневматическим тормозным приводом

В. Богомолов[1)], В. Клименко[1)], Д. Леонтьев[1)], Л. Рыжих[1)], О. Смирнов[1)], М. Холодов[1)]

[1)]Харьковский национальный автомобильно-дорожный университет (Харьков, Украина)

Реферат. В статье предлагается способ определения рационального подключения двух- или трехсекционного тормозного крана к контурам рабочей тормозной системы многоосного колесного транспортного средства с тормозными механизмами типа «симплекс» или «дуо-дуплекс». Цель заключается в том, чтобы определить рациональный вариант подключения контуров рабочей тормозной системы к тормозному крану для обеспечения наивысшей эффективности действия запасной тормозной системы при выходе из строя какого-либо устройства, входящего в состав тормозного

Адрес для переписки
Леонтьев Дмитрий
Харьковский национальный
автомобильно-дорожный университет
ул. Ярослава Мудрого, 25,
61002, г. Харьков, Украина
Тел.: +380 97 943-78-85
dima.a3alij@gmail.com

Address for correspondence
Leontiev Dmytro
Kharkiv National
Automobile and Highway University
25 Yaroslav Mudry str.,
61002, Kharkiv, Ukraine
Tel.: +380 97 943-78-85
dima.a3alij@gmail.com

привода многоосного колесного транспортного средства. Особенностью рассматриваемого способа является применение метода комбинаторики с учетом особенностей конструкции тормозного крана. Наличие математических взаимосвязей между количеством точек подключения контуров к тормозным механизмам типа «симплекс» или «дуо-дуплекс» позволяет найти рациональную схему использования контуров тормозного привода многоосного колесного транспортного средства. Определены математические выражения, с помощью которых можно рассчитать число возможных точек подсоединения двух- и трехсекционных тормозных кранов к тормозным механизмам «симплекс» или «дуо-дуплекс», установленным на осях многоосного колесного транспортного средства. Для определения количества рациональных вариантов подключения контуров тормозного привода многоосного колесного транспортного средства предложено использовать универсальную математическую зависимость. В графическом виде представлена расчетная схема подключения контуров к двух- или трехсекционному тормозному крану тормозных механизмов «симплекс» или «дуо-дуплекс», что упрощает задачу определения количества рациональных вариантов подключения. Приведен анализ требований, которые необходимо выполнить в соответствии с международными стандартами. Произведена оценка эффективности действия запасной тормозной системы некоторых типов колесных транспортных средств. Предложена общая концепция определения рациональной схемы организации запасной тормозной системы многоосного колесного транспортного средства на основе компоновочных схем подключения двух- или трехсекционных тормозных кранов к тормозным механизмам типа «симплекс» или «дуо-дуплекс», установленным на транспортном средстве.

Ключевые слова: многоосное транспортное средство, пневматический тормозной привод, тормозной механизм, коэффициент эффективности

Для цитирования: К вопросу о повышении эффективности управления тормозами транспортных средств, оснащенных пневматическим тормозным приводом / В. Богомолов [и др.] // *Наука и техника*. 2020. Т. 19, № 1. С. 55–62. https://doi.org/10.21122/2227-1031-2020-19-1-55-62

Introduction

International standards require that the brake control of a wheeled vehicle should include a main brake system and a parking brake system as well as an emergency brake system. According to international standards, the system is effective if it provides a minimum deceleration rate of 2.2 m/s^2 for vehicles of categories N2 and N3 and 2.5 m/s^2 for vehicles of categories M2 and M3. The standards also emphasise that in case the pneumatic circuit of a brake actuator has any failure, the remaining effectiveness of a main brake system must have a minimal braking deceleration as follows:

– for loaded vehicles of categories M2 and M3 – 1.5 m/s^2;

– for loaded vehicles of categories N2 and N3 – 1.3 m/s^2;

– for unladen vehicles of categories M2 and N3 – 1.3 m/s^2;

– for unladen vehicles of category M3 – 1.5 m/s^2;

– for unladen vehicles of category N2 – 1.1 m/s^2.

A percentage of the total effectiveness of a main brake system is as follows:

– for loaded vehicles of categories M2 and M3 – 30 %;

– for loaded vehicles of categories N2 and N3 – 26 %;

– for unladen vehicles of categories M2 and N3 – 26 %;

– for unladen vehicles of category M3 – 30 %;

– for unladen vehicles of category N2 – 22 %.

A main operational brake system must provide a minimal deceleration rate of 5 m/s^2 for a vehicle of categories N2, N3, M2 or M3. In percentage terms of the total effectiveness of a main brake system, the effectiveness of an emergency brake system must be minimum:

– for vehicles of categories N2 and N3 – 44 %;

– for vehicles of categories M2 and M3 – 50 %.

So, if the effectiveness of an emergency brake system is 50 % minimum of the total effectiveness of a main brake system for vehicles of categories N2, N3, M2 and M3, we will meet all international standards in terms of the effectiveness of the braking of a wheeled vehicle for both an emergency brake system and a main brake system in case any device of a brake actuator is out of order.

Literature review

One of the main requirements for a wheeled vehicle is stable braking without skidding. Therefore, this paper does not deal with a so called "diagonal" scheme of the separation of the circuits of main and emergency brake systems. Close attention is paid to the distribution of a brake system circuits along a wheeled vehicle axles to organise

an emergency brake system on the basis of a main brake system. International standards allow such a layout of circuits. The layout is frequently used in the brake control of a vehicle of categories N2, N3, M2 and M3.

We will consider an emergency brake system of a two-axle vehicle. The emergency brake system is designed on the basis of a two-circuit main brake system (Fig. 1).

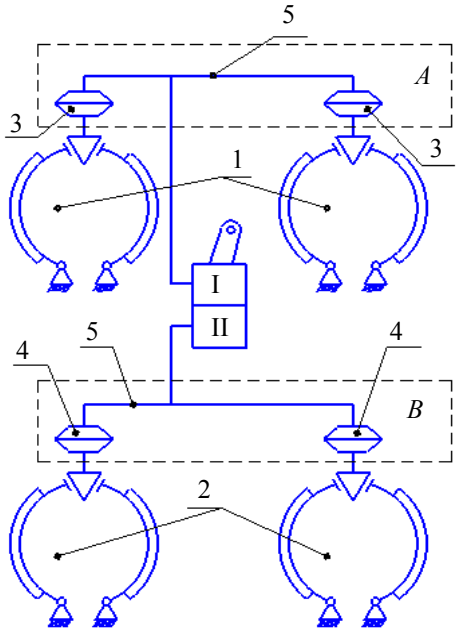

Fig. 1. Scheme of a two-circuit main brake system of a wheeled two-axle vehicle equipped with a pneumatic actuator with simplex brake gears: 1, 2 – front and rear simplex brake gears; 3, 4 – brake chambers of the front and rear axles of vehicle; 5 – pipelines; I – section of a brake valve that is connected with point *A* where a brake circuit is connected with the corresponding brake chambers of axle; II – section of a brake valve that is connected with point *B* where a brake circuit is connected with the corresponding brake chambers of axle; *A*, *B* – sequence places where a corresponding circuit is connected with brake chambers 3 and 4 of a front and rear axles

In general, the effectiveness of a main brake system of a vehicle has to meet the condition

$$j_e = \frac{R_{x1} + R_{x2}}{m_a} \geq [j], \qquad (1)$$

where R_{x1}, R_{x2} – total braking forces of the corresponding front and rear axles of a wheeled vehicle, H; m_a – mass of a wheeled vehicle, kg; $[j] = 5$ m/s^2 – permissible minimum deceleration of a braking wheeled vehicle when applying a main brake system.

In order to guarantee 50 % effectiveness of an emergency brake system, if any device in the circuits of the front or rear axles of a wheeled vehicle is out of order, we will meet conditions:

$$j_{e1} = \frac{R_{x1}}{m_a} \geq 2.5 \text{ m/s}^2; \qquad (2)$$

$$j_{e2} = \frac{R_{x2}}{m_a} \geq 2.5 \text{ m/s}^2. \qquad (3)$$

Expressions (2) and (3) show that generally the decelerations that are available when a wheeled vehicle is braking can be unequal

$$j_{e1} \neq j_{e2} \qquad (4)$$

that's, if we take into account expression (1), it looks as follows:

$$j_{ei} = n_i j_e \geq 2.5 \text{ m/s}^2, \qquad (5)$$

where n_i – so-called effectiveness factor of the i^{th} circuit that is involved in the braking of a vehicle.

Like expression (4), (5) means that, for example, for a wheeled two-axle vehicle the values of the effectiveness factors of the i^{th} circuit are not equal in general case, that's, there is inequality

$$n_1 \neq n_2 \qquad (6)$$

then, in a particular case if $j_e = 5$ m/s^2, expressions (1)–(3) clearly indicate that we will meet the condition

$$n_1 \geq 0.5 \leq n_2 \qquad (7)$$

therefore, the effectiveness of an emergency brake system is the minimum value of effectiveness factors n_i and a corresponding deceleration j_{ei}.

The practice of the brake control design for the vehicles of categories N2, N3, M2 and M3, for example, of special purpose or specialised ones, indicates that it is difficult to meet the condition (7). As a rule, it is due to controversial requirements that are stated in Annexes 4 and 10 of the international rules No 13 [1].

For example, computation shows that the agricultural vehicle KAZ-4540 [2] has the following ratio of the effectiveness factors of a front and rear axles:

$$n_1 = 0.6;\ n_2 = 0.4. \qquad (8)$$

It is obvious that condition (7) is not valid for such a vehicle.

According to the analysis of the research that is conducted at the Department of Vehicles named after A. B. Gredeskul in Kharkov National Automobile and Highway University, in case of (8), in order to meet requirement (5), it is necessary to guarantee the main brake system minimum effectiveness of 6.25 m/s^2 at the expense of constructive decisions that often complicate and raise the price of brake systems. For example, it is possible to improve the main brake system effectiveness due to the replacement of the simplex brake with the duo-duplex brake (Fig. 2) [3] as it is done in the design of the main brake system of the LiAZ-5256 [4] (Fig. 3).

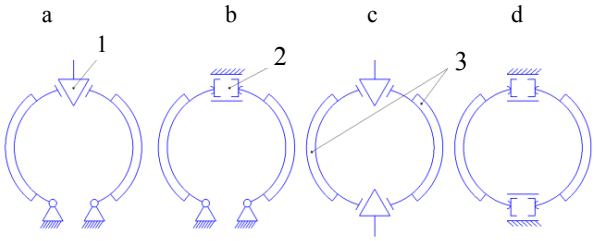

Fig. 2. Schemes of drum brake gears: a – simplex scheme with a pneumatic actuator and a wedge; b – simplex scheme with a hydraulic actuator; c – duo-duplex scheme with a pneumatic actuator and a wedge; d – duo-duplex scheme with a hydraulic actuator; 1 – wedge; 2 – main brake cylinder; 3 – brake shoe

According to Fig. 3, if one of the two circuits of the main brake system fails, the brake gears of a wheeled vehicle start operating as a simplex scheme instead of a duo-duplex scheme; it guarantees a wheeled vehicle braking effectiveness at the level of 68 % minimum of the total effectiveness of a main brake system.

Condition (5) exceeds the minimum value as the effectiveness factors are $n_1 = n_2 \cong 0.68$.

One more way to improve the effectiveness of a main brake system is to increase the number of brake actuator circuits, for example, from two (Fig. 4) to three (Fig. 5). The implementation of a three-circuit main brake system is expedient for vehicles that have three axles minimum and three places minimum to connect corresponding circuits with brake chambers (Fig. 5).

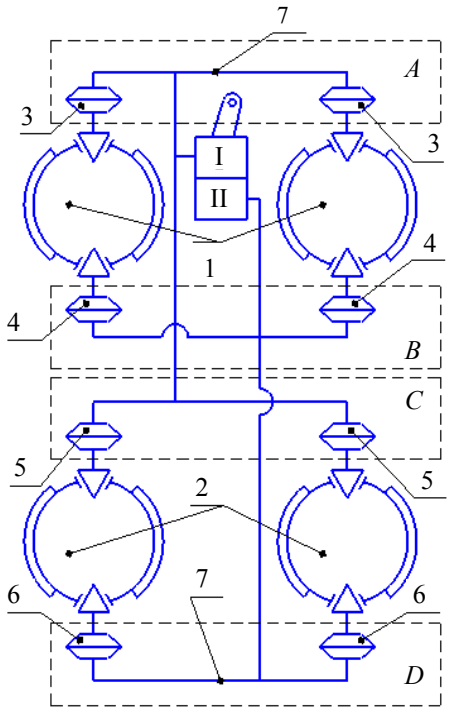

Fig. 3. Scheme of a dual circuit main brake system with a pneumatic actuator for a two-axle wheeled vehicle with duo-duplex brake gears; 1, 2 – duo-duplex front and rear brake gears correspondingly; 3, 4, 5, 6 – brake chambers of the front and rear axles of a vehicle; 7 – pipelines; I – brake valve section that is connected with places *A* and *C* where a brake circuit is connected with the brake chambers of front and rear axles; II – brake valve section that is connected with places *B* and *D* where a brake circuit is connected with the brake chambers of front and rear axles; *A*, *B*, *C*, *D* – sequence places to connect a corresponding circuit with the corresponding brake chambers 3, 4, 5, 6 of front and rear axles

The analysis of scientific and technical literature [2, 3, 5] shows that a three-circuit brake system becomes possible to use after the Public Joint-Stock Company Volchansk Aggregate Plant (the town of Volchansk, Kharkiv region, Ukraine) has put into serial production a three-section brake valve (Fig. 6) that was designed by the Research and Production Enterprise Avtoagregat (the city of Kharkiv, Ukraine).

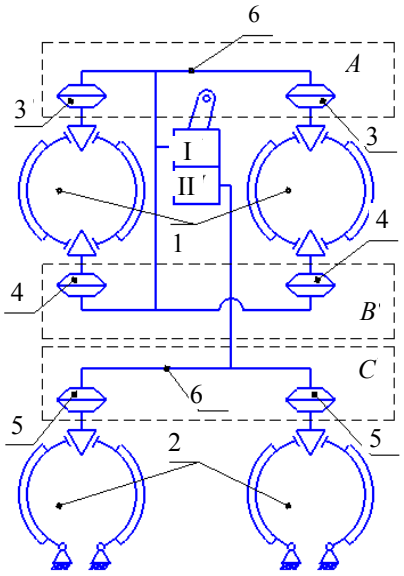

Fig. 4. Scheme of a dual circuit main brake system with a pneumatic actuator of a two-axle wheeled vehicle: 1 – duo-duplex front brake gear; 2 – simplex rear brake gear; 3, 4, 5 – brake chambers of vehicle front and rear axles; 6 – pipelines; I – brake valve section that is connected with places *A* and *B* where a brake circuit is connected with the brake chambers of a front axle; II – brake valve section that is connected with place *C* where a brake circuit is connected with corresponding brake chambers of a rear axle; *A*, *B*, *C* – sequence places to connect a corresponding circuit to the brake chambers 3, 4, 5 of front and rear axles

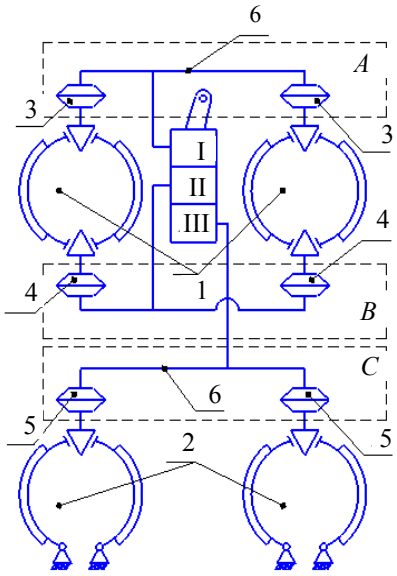

Fig. 5. Scheme of a three-circuit main brake system with a pneumatic actuator for a two-axle vehicle: 1 – duo-duplex front brake gear; 2 – simplex rear brake gear; 3, 4, 5 – brake chambers of the front and rear axles of a vehicle; 6 – pipelines; I – brake valve section that is connected with place *A* where a brake circuit is connected with the brake chambers of a front axle; II – brake valve section that is connected with place *B* where a brake circuit is connected with the brake chambers of a front axle; III – brake valve section that is connected with place *C* where a brake circuit is connected with the brake chambers of a rear axle; *A*, *B*, *C* – sequence places to connect a corresponding circuit with the brake chambers 3, 4, 5 of front and rear axles

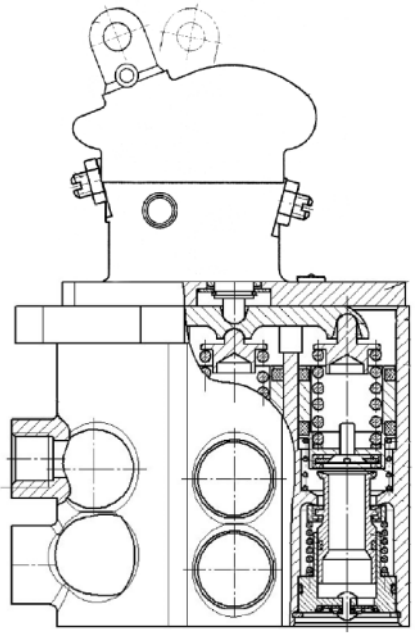

Fig. 6. Cross-section of a three-section brake valve that is manufactured at the Public Joint-Stock Company Volchansk Aggregate Plant

The use of several circuits enables us to improve the effectiveness of an emergency brake system due to the simultaneous use of two circuits of three ones available if one of the main brake system circuits is out of order.

Calculations show that for the scheme in Fig. 5 the effectiveness factor of the first and second circuits, which take part in the braking of a wheeled vehicle, is 0.41; the effectiveness factor of the third circuit is 0.4, according to (8).

Therefore, supposing that the first circuit is out of order, the two others left (2nd and 3rd circuits) guarantee 81 % of a minimum vehicle braking effectiveness. The same is true if the second circuit is out of order.

If the third circuit is out of order, the first and second circuits are operational and the effectiveness of an emergency brake system is 82 % minimum. It reliably guarantees the minimum deceleration of a wheeled vehicle due to an emergency brake system and it meets the requirements in terms of the effectiveness of an emergency brake system.

Aim and problem statement

Taking into consideration the above-mentioned, the aim of the paper is to determine the regularities of the emergency brake system effectiveness change of the wheeled vehicles of categories N2, N3, M2 and M3 when we vary the following parameters:

– the number of circuits (two or three) that compose a main brake system;

– the number of wheeled vehicle axles (k_m) [6];

– types of brake gears: simplex and duo-duplex.

Analysis of emergency brake system effectiveness change

To determine the number of the most rational options of the component arrangement of emergency brake system circuits, the experiment planning theory can be used [7, 8]. The total number of the rational options of the component arrangement of circuits can be calculated using this equation

$$N_r = k^{m-k}, \quad (9)$$

where k – number of the circuits of a main brake system (numbered by Arabic numerals in Fig. 2, 3); m – number of possible points to connect circuits (lettered in Latin in Fig. 1, 3–5).

The number of possible combinations to connect circuits and brake gears can be determined, taking into account a type of a brake valve, on the basis of these expressions:

– for a two-section brake valve

$$N = 2^m - 2; \quad (10)$$

– for a three-section brake valve

$$N = 3^m - 3 \cdot 2^m + 3. \quad (11)$$

For further analysis of possible variants to connect circuits and corresponding brake chambers, the following designation will be applied:

– for a dual circuit brake system

$$\text{I} - \text{II}; \quad (12)$$

– for a three-circuit brake system

$$\text{I} - \text{II} - \text{III}. \quad (13)$$

In expressions (12) and (13) Roman numerals designate a brake valve section number, which corresponds to a circuit number.

Each section of a brake valve can be connected with several points of brake chambers *A*, *B*, *C*, *D* etc. So within one section of a brake valve (I, II or III) they will be designated as a fraction, for example, in accordance with Fig. 4, the designation of section I will be as follows:

$$\text{I} \rightarrow A/B,$$

and designation of II correspondingly

$$\text{II} \rightarrow C.$$

Taking into consideration the above-mentioned, we will consider the rational options of circuit component arrangements under possible combinations of the points of connection with a brake valve.

For example, for dual circuit main brake systems that have two points to join circuits (Fig. 1) expressions (9) and (10) give the following results:

$$N_r = 2^{2-2} = 1;$$

$$N = 2^2 - 2 = 2.$$

So one possible rational option of a circuit component arrangement has two possible combinations of connection, namely, according to (12), we will write *A–B* or *B–A* having the effectiveness factor $n_1 = n_2 = 0.5$.

Under connection shown in Fig. 4, we will get:

$$N_r = 2^{3-2} = 2;$$

$$N = 2^3 - 2 = 6.$$

So there can be two options for a rational circuit component arrangement and six combinations of connection, namely:

1) *A–B*/*C* or *B*/*C–A*, or option (*A–C*/*B* or *C*/*B–A*);

2) *A*/*B–C* or *C–A*/*B*.

Options *B*/*A–C* or *C–B*/*A* have no sense as the points of connection *A* and *B* belong to the same duo-duplex brake gear, in accordance with the scheme in Fig. 4.

In case the connection is made as in Fig. 3, we will get:

$$N_r = 2^{4-2} = 4;$$

$$N = 2^4 - 2 = 14.$$

There are only four options of a rational circuit component arrangement and fourteen combinations of connection, according to the scheme in Fig. 3:

1) *A*/*B–C*/*D* or *C*/*D–A*/*B*;

2) *A*/*B*/*C–D* or *D–A*/*B*/*C*, or option (*A*/*B*/*D–C* or *C–A*/*B*/*D*);

3) *A*/*C*/*D–B* or *B–A*/*C*/*D*, or option (*B*/*C*/*D–A* or *A–B*/*C*/*D*);

4) *A*/*C–B*/*D* or *B*/*D–A*/*C*, or option (*A*/*D–B*/*C* or *B*/*C–A*/*D*).

The other options for the scheme in Fig. 3 have no sense as the points of connection *A*/*B* and *C*/*D* belong to corresponding duo-duplex brake gears.

When connecting a three-axle vehicle equipped with simplex brake gears and a two-section brake valve, we will have a scheme of a rational circuit component arrangement as for the brake actuator scheme in Fig. 4:

$$N_r = 2^{3-2} = 2;$$

$$N = 2^3 - 2 = 6.$$

So there can be two options of a rational circuit component arrangement and six connection combinations:

1) *A–B*/*C* or *B*/*C–A*, or option (*B–A*/*C* or *A*/*C–B*);

2) *A*/*B–C* or *C–A*/*B*.

Other options have no sense as the rearrangement of axles that are united in one circuit does not change their effectiveness.

Changing from dual circuit systems to three-circuit ones, according to (9) and (11), a three-axle vehicle has the results:

$$N_r = 3^{3-3} = 1;$$

$$N = 3^3 - 3 \cdot 2^3 + 3 = 6.$$

So there is only one option of a rational circuit component arrangement and six schemes to connect axles and a brake valve, namely: *A–B–C* or *A–C–B*, or *B–A–C*, or *B–C–A*, or *C–B–A*, or *C–A–B*.

When a three-axle vehicle having a three-section brake gear has four points of connection, the number of rational circuit component arrangement and the connections between axles and a brake valve are as follows:

$$N_r = 3^{4-3} = 3;$$

$$N = 3^4 - 3 \cdot 2^4 + 3 = 36.$$

So there are three options of a rational circuit component arrangement and 36 schemes to connect the points of corresponding axles with a brake valve.

When there are five points to connect a three-axle vehicle with a three-section brake valve, according to (9) and (11), the results are as follows:

$$N_r = 3^{5-3} = 9;$$

$$N = 3^5 - 3 \cdot 2^5 + 3 = 150.$$

The calculation shows that there are nine options of a rational circuit arrangement and 150 options to connect axles and a brake valve.

As we can see, the increase of the number of circuits and vehicle axles has the regularities of combinatorics. Therefore, the increase of combinations results in the increase of computation efforts.

As of the brake system effectiveness factor, according to international requirements [1], for three-axle wheeled vehicles, we will have the following results:

$$n_1 = 0.4;\ n_2 = n_3 = 0.3. \qquad (14)$$

For vehicles that have more than three axles or more than three points to connect circuits with the brake chambers of corresponding axles, according to scientific and technical literature [6, 9–12], the brake system effectiveness factor can be calculated as follows:

$$n_j = \frac{1}{k_m}, \qquad (15)$$

where n – share of the j^{th} axle effectiveness in the total effectiveness of a main brake system; k_m – number of wheeled vehicle axles.

On the basis of the j^{th} axle effectiveness share in the main brake system total effectiveness, it is easy to determine the effectiveness factor of the i^{th} circuit that is applied to brake a wheeled vehicle if we add the effectiveness shares of the axles that are connected with corresponding circuits of a vehicle.

The analysis of scientific and technical literature [6] has shown that further computations can involve axles 2, 3, 4, 6, 8, 9, 12 only.

Thus, if we model a failure of a brake actuator circuit, the proposed approach can easily determine a wheeled vehicle braking effectiveness.

For example, let's compute the scheme in Fig. 4 and the results of the computation are provided in Tab. 1 to make the analysis easy. Tab. 1 shows that the most acceptable arrangement option is the connection scheme *A*/*B–C* that corresponds to the circuit connection (1–1–2) as this scheme meets the condition (7) if any circuit is out or order.

Table 1

Possible variants of the rational circuit component arrangement effectiveness factors for a wheeled vehicle emergency brake system

No connection point			Failure of 1st circuit	Failure of 2nd circuit	Effectiveness factor of an emergency brake system
A	*B*	*C*			
1	2	1	0.34	0.84	0.34
1	1	2	0.50	0.50	0.50
1	2	2	0.84	0.34	0.34

Similarly, we can compute possible variants of the effectiveness factors of the rational emergency brake system circuit component arrangements for vehicles with more axles. For example, the effectiveness factors of the accepted axles are in Tab. 2.

Table 2

Possible variants of the effectiveness factors of the rational circuit component arrangements of an emergency brake system on the basis of a dual circuit and three-circuit main brake system

Wheeled vehicle axles	Emergency brake system effectiveness factors					
	Dual circuit main brake system			Three-circuit main brake system		
	All simplex brake gears	Combination of simplex brake gears and duo-duplex brake gears	All duo-duplex brake gears	All simplex brake gears	Combination of simplex brake gears and duo-duplex brake gears	All duo-duplex brake gears
Two	0.5	0.50	0.68	–*	0.50	0.680
Three	0.4	0.57	0.68	0.600	0.60	0.770
Four	0.5	0.59	0.68	0.500	0.67	0.760
Six	0.5	–**	0.68	0.667	–**	0.787
Eight	0.5	–**	0.68	–**	–**	–**
Nine	–**	–**	–**	0.667	–**	0.786
Twelve	0.5	–**	0.68	0.667	–**	0.787

* Impossible variants.
** Options are not computed.

CONCLUSIONS

1. Emergency brake system effectiveness depends on the distribution of brake forces along the axles of a wheeled vehicle and does not depend on the quantity of axles.

2. Emergency brake system effectiveness increases as the quantity of main brake system circuits increases by 23 % on average if simplex brake gears are used.

3. Emergency brake system effectiveness increases if the quantity of main brake system circuits increases by 27 % on average when using duo-duplex brake gears instead of simplex brake gears.

REFERENCES

1. United Nations Economic Commission for Europe (2016) *Regulation No 13 of the Economic Commission for Europe of the United Nations (UN/ECE). Uniform Provisions Concerning the Approval of Vehicles of Categories M, N and O with Regard to Braking.* Available at: https://op.europa.eu/en/publication-detail/-/publication/0a43f880-d612-11e5-a4b5-01aa75ed71a1/language-en.
2. Frumkina K. A. (1984) *KAZ-4540 "Colchis" Agricultural Dump Truck: Technical Description and Instruction Manual.* Moscow, Mashinostroenie Publ. 280 (in Russian).
3. Turenko A. N., Bogomolov V. A., Klimenko V. I., Kirchatyi V. I., Khodyrev S. Ya. (2002) *Improving Methods for Regulating the Output Parameters of the Brake System of Vehicles*. Kharkiv, Kharkiv National Automobile and Highway University, 400 (in Russian).
4. Demkin V. V., Dremin A. P., Zatsepilov K. I., Stepnenko V. V. (2001) *Bus LiAZ-5256 and its Modifications. Manual.* Moscow, Atlasy Avtomobilei Publ. 512 (in Russian).
5. Turenko A. M., Bohomolov V. O., Klymenko V. I. and et. (2003) Functional Calculation of the Brake System of the Car with Drum Brakes and Regulator of Braking Forces. Kharkiv, Kharkiv National Automobile and Highway University, 120 (in Ukrainian).
6. Aksenov P. V. (1989) *Multi-Axle Cars*. Moscow, Mashinostroenie Publ. 280 (in Russian).
7. Barabashchuk V. I., Kredentser B. P., Miroshnichenko V. I. (1984) *Engineering Experiment Planning*. Kiev, Tekhnika Publ. 200 (in Russian).
8. Kononiuk A. E. (2011) *Fundamentals of Scientific Research (General Theory of Experiment). Book 2*. Kiev, KTN Publ. 452 (in Russian).
9. Leontev D. N., Ryizhih L. A., Lomaka S. I., Klimenko V. I. (2011) On the Methodology of Analysis and Selection of the Distribution of Braking Forces between the Axles of a Biaxial Vehicle. *Izvestiya MGTU "MAMI"*, 1 (11), 31–35 (in Russian).
10. Turenko A. N., Leontev D. N., Klimenko V. I., Ryizhih L. A., Lomaka S. I. (2011) On the Methodology of Analysis and Selection of the Distribution of Braking Forces between the Axles of the Car, Taking into Account the Requirements of UN/ECE Regulation No 13. *Avtomobil'nyi Transport. Sbornik Nauchnykh Trudov* [Automobile Transport. Scientific Collection]. Kharkiv, Kharkiv National Automobile and Highway University, 29, 29–36. (in Russian).
11. Turenko A. N., Bogomolov V. A., Leontev D. N. (2016) A Method for Determining the Deceleration of a Multiaxial Car Based on the Realized Clutches of its Wheels and the Location of the Center of Mass Coordinate. *Visnik Kharkivs'kogo Natsional'nogo Avtomobil'no-Dorozhnogo Universitetu = Bulletin of Kharkiv State Automobile and Highway Technical University*, 75, 13–17 (in Russian).
12. Mikhalevich N. G., Turenko A. N., Bogomolov V. A., Klimenko V. I., Ryzhikh L. A., Leont'ev D. N., Krasyuk A. N. (2015) *The Implementation of Intelligent Functions in the Electronic-Pneumatic Brake Control of a Vehicle.* Kharkiv, Kharkiv National Automobile and Highway University, 450 (in Russian).

Received: 08.10.2019
Accepted: 10.12.2019
Published online: 31.01.2020

https://doi.org/10.21122/2227-1031-2020-19-1-63-75

UDC 629

Engineering of Light Electric Commercial Vehicle

R. Dorofeev[1)], A. Tumasov[1)], A. Sizov[1)], A. Kocherov[1)], A. Meshkov[1)], D. Porubov[1)]

[1)]Nizhny Novgorod State Technical University named after R. E. Alekseev (Nizhny Novgorod, Russian Federation)

Abstract. The paper describes the process and results of the development of the light commercial electric vehicle. In order to ensure maximum energy efficiency of the developed vehicle the key parameters of the original electric motor. The article also presents the results of power electronic thermal calculation. For the mathematical model of the vehicle, the driving cycle parameters of the electric platform were determined in accordance with UNECE Regulations No 83, 84. The driving cycle was characterized by four successive urban and suburban cycles. The mathematical model also takes into account the time phases of the cycle, which include idling, vehicle idling, acceleration, constant speed movement, deceleration, etc. The model of the electric part of the vehicle was developed using MatLab-Simulink (SimPowerSystems library) in addition to the mechanical part of the electric car. The electric part included the asynchronous electric motor, the motor control system and the inverter. This model at the output allows to obtain such characteristics of the electric motor as currents, flows and voltages of the stator and rotor in a fixed and rotating coordinate systems, electromagnetic moment, angular speed of rotation of the motor shaft. The developed model allowed to calculate and evaluate the performance parameters of the electric vehicle. Technical solutions of the electric vehicle design were verified by conducting strength calculations. In conclusion, the results of field tests of a commercial electric vehicle are presented.

Keywords: electric vehicle, thermal analysis, electric drive, mathematical simulation, strength calculation

For citation: Dorofeev R., Tumasov A., Sizov A., Kocherov A., Meshkov A., Porubov D. (2020) Engineering of Light Electric Commercial Vehicle. *Science and Technique*. 19 (1), 63–75. https://doi.org/10.21122/2227-1031-2020-19-1-63-75

Разработка легкого коммерческого электромобиля

Р. Дорофеев[1)], А. Тумасов[1)], А. Сизов[1)], А. Кочеров[1)], А. Мешков[1)], Д. Порубов[1)]

[1)]Нижегородский государственный технический университет имени Р. Е. Алексеева (Нижний Новгород, Российская Федерация)

Реферат. В статье описаны процесс и результаты создания легкого коммерческого электромобиля. С целью обеспечения максимальной энергоэффективности разрабатываемого транспортного средства определены основные параметры оригинального электродвигателя. Представлены результаты теплового расчета силовой электроники. Для математической модели транспортного средства определены параметры ездового цикла электрической платформы в соответствии с Правилами № 83, 84 ЕЭК ООН. Цикл движения характеризовался четырьмя последовательными циклами городского и пригородного режимов движения. Математическая модель также учитывает временные фазы цикла, которые включают холостой ход транспортного средства, ускорение, движение с постоянной скоростью, замедление и т. д. Модель электрической части транспортного средства разработана с использованием MatLab-Simulink (библиотека SimPowerSystems) в дополнение к механической части электромобиля. Электрическая часть включала асинхронный электродвигатель, систему управления двигателем и инвертор. Данная модель на выходе позволяет получить такие характеристики электродвигателя, как токи, поведение магнитного поля, напряжения статора и ротора в неподвижной и вращающейся системах координат, электромагнитный момент, угловая скорость вращения вала

Адрес для переписки
Дорофеев Роман
Нижегородский государственный технический университет
имени Р. Е. Алексеева
ул. Минина, 24,
603950, г. Нижний Новгород, Российская Федерация
Tel.: +7 9040 62-36-75
roman.dorofeev@nntu.ru

Address for correspondence
Dorofeev Roman
Nizhny Novgorod State Technical University
named after R. E. Alekseev
24 Minin str.,
603950, Nizhny Novgorod, Russian Federation
Tel.: +7 9040 62-36-75
roman.dorofeev@nntu.ru

двигателя. Разработанная модель позволила рассчитать и оценить параметры производительности электромобиля. Технические решения конструкции электромобиля были проверены на прочность путем расчетов. Представлены результаты полевых испытаний коммерческого электромобиля.

Ключевые слова: электрический автомобиль, температурный анализ, электрический привод, математическое моделирование, расчет прочности

Для цитирования: Разработка легкого коммерческого электромобиля / Р. Дорофеев [и др.] // *Наука и техника.* 2020. Т. 19, № 1. С. 63–75. https://doi.org/10.21122/2227-1031-2020-19-1-63-75

Introduction

Road transport electrification is currently one of the main trends in the development of the global automotive industry (Along with the trends of increasing autonomy, shared use and inclusion in the information environment) [1]. Despite the fact that in 2015 the share of electric vehicles in the global fleet was insignificant – about 0.1 %, according to forecasts, this share will grow rapidly and will be about 10 % by 2030 and about 40 % by 2050 (in the estimates of the International Energy Agency only such types of electric vehicles as PHEV and BEV were taken into account) [2].

The main motivation for the spread of electric vehicles is associated with improved environmental performance and with a number of consumer characteristics: no noise motor, dynamic characteristics, etc. It is worth noting that the commercial transport has a significant impact on the environment because of constant operation with minimal downtime.

The key barriers to the spread of electric vehicles are:

– high cost of batteries/fuel cells;

– relatively low power reserve on a single charge;

– underdevelopment of infrastructure, first of all – charging stations.

Because of the barriers listed above, electric vehicle developers face an important and time-consuming task. It is to develop an energy-efficient electric drive system. This problem can be solved by an integrated approach to modeling the key components of the electric drive, the development of an adequate mathematical model of the electric car.

The object of the research

The GAZ Group is the leader on Russian market of commercial vehicles and holds about 70 % in the LCV category and 65 % in the LDT category [3]. The electrification was considered as the priority method to improve the environmental safety of this manufacturer products.

To implement the mentioned technologies, employees of the NNSTU, with the support of engineers from the Joint Engineering Center of the GAZ Group and specialists from PJSC GAZ, are working to create an electric platform for a light commercial vehicle (LCV) (Fig. 1). The chassis of the light commercial vehicle GAZelle NEXT was chosen as the object of research.

Fig. 1. The object of the research

Brief technical characteristics of the vehicle are presented in Tab. 1.

Table 1

Brief technical specifications of LCV GAZelle NEXT

Wheel arrangement	4×2
Drive type	Rear
Gross weight, kg	3500
Curb weight, kg * * *	2520
Load distribution of the vehicle total weight on the road through the tires, front wheels rear wheels, kg	1960 3745
Base, mm	3145/3745
Ground clearance (under the crankcase of the rear axle at full weight), mm	170
Minimum turning radius along the track of the outer front wheel, m	5.7/6.5
The maximum car speed on a horizontal section of a flat highway, km/h	130

Motor

The fundamental component of any electric drive is an electric motor. Thus, the energy efficiency of the electric vehicle as a whole will depend on how optimally the electric motor was selected. For this purpose, it was decided to develop an original electric motor for the developed electric platform.

As it is known, the mechanical characteristic of the motor has two distinct zones: a constant torque zone and a constant power zone. The ratio between the sizes of these zones significantly affects the choice of transmission ratio and dynamic characteristics of the vehicle [4]. The developed electric motor is designed to operate in two modes with different values of mechanical torque and duration. By preliminary traction calculation target mechanical characteristics of the electric motor were determined (Tab. 2, Fig. 2).

Table 2

Motor characteristics

Characteristic	Value
Motor type	Asynchronous
Number of phases	3
Rated voltage, V	400
Maximum revolutions, rpm	10000
Maximum power, kW	47
Cooling system	Liquid type
The type of construction in accordance with IEC 600034-7	IM B5
Maximum height of use above sea level according to IEC 600034-1, m	Not more than 2500 without power reduction
Insulation temperature class according to IEC 600034-1	H
Protection degree in accordance with IEC 600034-5	IP65
Radial shaft run-out class according to DIN 42955	N
Noise level according to DIN EN ISO 1680	75dB+3dB
The level of vibration according to IEC 600034-14	Level A
Ambient temperature	From –40 °C to +70 °C

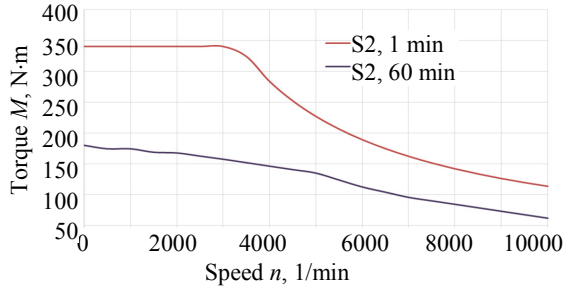

Fig. 2. Mechanical characteristics of the electric motor

At the initial stage of the motor design the optimal configuration of the rotor and stator slots were determined (Fig. 3).

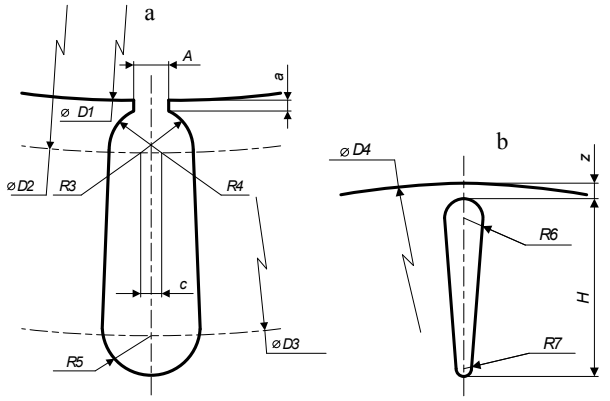

Fig. 3. Shape of stator (a) and rotor (b) slots

The stator has semi-open for laying the winding. The stator is made of electrotechnical steel plates with a thickness of 0.27 mm. Rotor is made of electrical steel plates the same as the stator. The rotor has closed oblong shape slots for the placement of short-circuited winding roads. The short-circuited winding is performed by pouring the rotor set with aluminum under pressure. Structurally, the winding is made of soft multi-strand Litz wire and placed in the stator slots. A winding is a group of coils connected in a star pattern, herewith such a winding cannot be considered as containing two parallel coils in each phase, since the middle points of the coil groups are not combined.

During the design of the electric motor, several prototypes were created to test the assumptions inherent in the calculation models [5, 6].

In the process of the electric motor model preparing the boundary conditions were given. The outer contour of the magnetic system is specified as a first class boundary condition, magnetic potential $\varnothing = 0$. The rest of the boundary conditions were determined automatically by the numerical simulation system in accordance with the materials and current-carrying areas. After setting the boundary conditions, a finite elements grid was constructed. Triangles were used as grid elements (Fig. 4).

During the calculation process, the solver automatically rebuilt the grid to achieve the specified accuracy of the solution. In the process of solving, 6 grid rearrangements were made. As a result, the number of grid elements was increased from 14.734 to 56.574. The error in determining the magnetic field energy at the last iteration

of the solution was 0.009 %. In the process of solving the distribution of the magnetic field in the motor parts material was obtained. Fig. 5 shows the distribution of magnetic induction in the motor parts. The maximum value of the magnetic field induction was 1.7105 T.

As a result of modeling, the greatest electromagnetic losses in absolute value caused by an alternating electromagnetic field were determined. Losses in absolute value are the sum of losses that are different in nature:

– losses in the winding wires determined by the Joule – Lenz law;

– hysteresis losses;

– eddy current losses.

Maximum losses were 6391 W at speeds from 2100 rpm to 3900 rpm.

Despite the total loss of almost 6.4 kW, the motor has an efficiency of 95 % in this range (Fig. 6). The efficiency is reduced in the zone of lowest speed and in the constant power end zone after 4000 rpm. In the high revs from 6000 rpm the motor torque and its efficiency are significantly reduced. Operation in this speed range is not recommended. The current distribution has a maximum of 219 A at the end of the constant torque zone. The maximum power of the electric motor was 81 kW (Fig. 6).

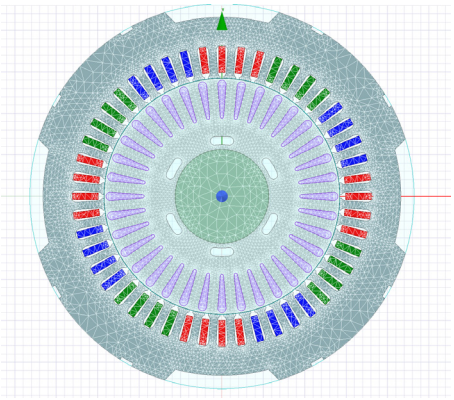

Fig. 4. Finite elements grid

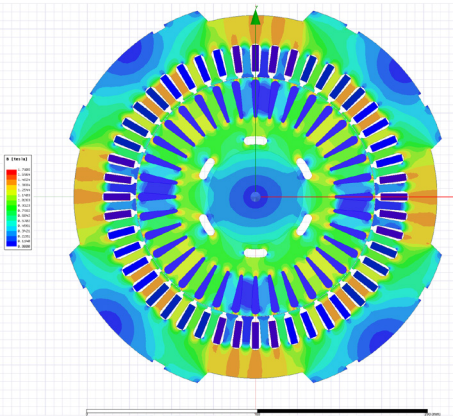

Fig. 5. Magnetic induction distribution in motor parts

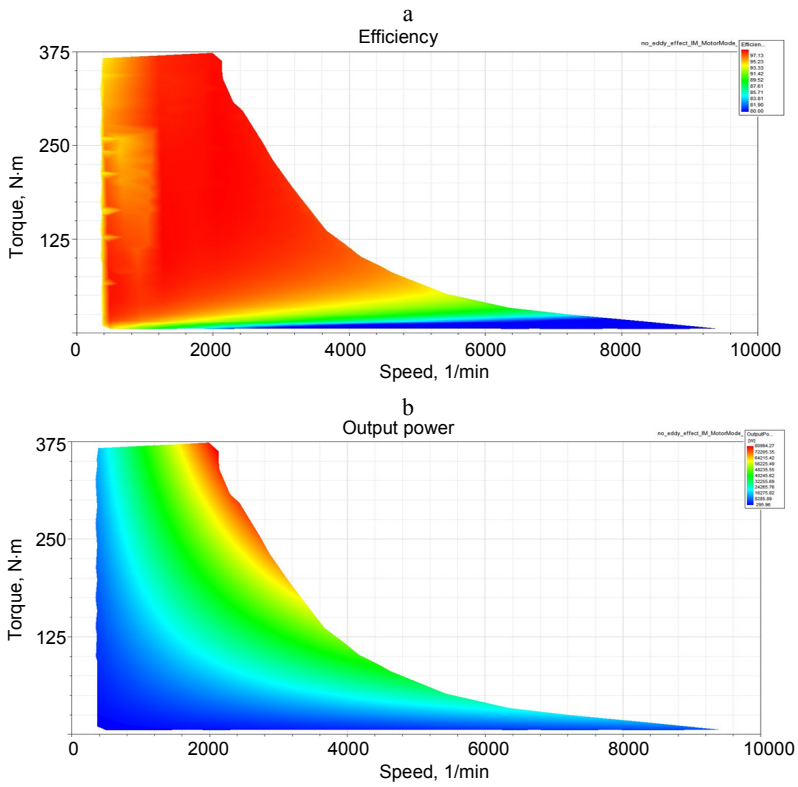

Fig. 6. Efficiency (a) and power (b) distribution

Thermal modeling

The objects of thermal modeling were the electric motor and the battery subpack.

The information about the heat release in the motor parts was transmitted from the results of the electromagnetic calculation obtained earlier. The boundary conditions for the thermal calculation of the electric motor were adopted as follows: the ambient temperature of 55 °C and the heat transfer coefficient of 5 W/(m^2·deg). The assumed value of the heat transfer coefficient corresponds to natural convection in cramped conditions in the absence of external airflow. These conditions are obviously worse than the operating (maximum operating temperature of the motor is 40 °C). The geometric model of the electric motor liquid circuit and the results of thermal calculation are presented in Fig. 7.

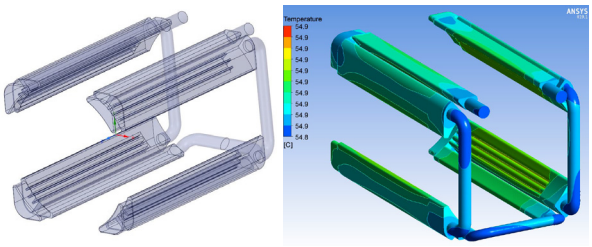

Fig. 7. Geometric model of the motor liquid circuit and the results of thermal calculation

Table 3

Calculated thermal-hydraulic parameters

Parameter	Unit
Maximum stator temperature, °C	55
Maximum temperature of stator windings, °C	55
Maximum rotor temperature, °C	55
The maximum temperature of the rotor closed-loop winding, °C	55
Maximum coolant temperature, °C	55
Coolant temperature at the outlet of the cooling channels, °C	55
Pressure drop between inlet and outlet of cooling channels, °C	10000

To calculate the thermal state of the battery subpack elements, it is necessary to specify the heat sources and heat transfer conditions between the subpack structural elements. The main sources of heat are battery cells, with the heat release of 38830 W/m^3. On the outer surfaces of the battery subpack elements, the convective heat exchange condition similar to that of an electric motor was set. The geometric model of the battery subpack and the thermal calculation results are presented in Fig. 8.

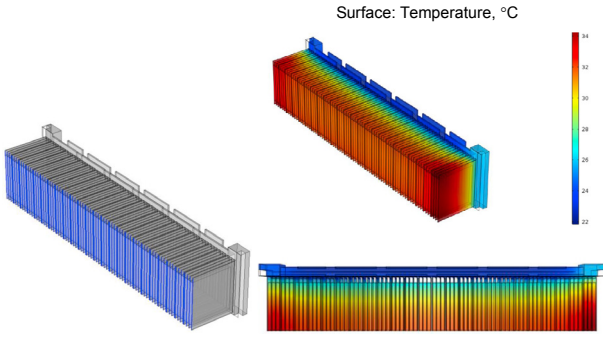

Fig. 8. Geometric model of the battery subpack and thermal calculation results

In calculation process the temperature distribution in the battery subpack elements (Tab. 4), the coolant temperature at the outlet of the cooling system channel, the coolant pressure drop between the inlet and outlet of the cooling system channels, as well as general information about the nature of the coolant flow in the cooling channels were obtained.

Table 4

Calculated thermo-hydraulic parameters

Parameter	Unit
Pressure drop between inlet and outlet of cooling channels, Pa	11125
Coolant temperature at the outlet of the cooling channels, °C	23.9
Maximum battery cell temperature, °C	33.2
Average battery cell temperature, °C	28.4

The maximum temperature of the cell was 33.2 °C. This value was higher than the upper value of the battery cell operating temperature equal to 30 °C. These temperature values are in an area that is poorly cooled by the radiator coolant since the radiator channel does not cover the entire heat exchange surface with L-shaped radiators. It is recommended to either reduce the number of cells in the radiator, or extend the flow of the radiator in such a way as to provide a more uniform cooling of the battery cells.

Mathematical modeling

The process of mathematical modeling of the electric platform was divided into three technical

parts: mechanical, electrical and motor control parts. For the mechanical part, a model has been developed to calculate the necessary amount of power required to drive at a given speed, in which the resulting power is due to the sum of all the resistance forces to the electrical platform movement, the same approach will be applied to the evaluation of the recovery energy returned to the battery by braking the vehicle.

In the electrical part, the general circuitry of the electric vehicle including its main parts is considered: an asynchronous motor, an inverter and a battery. It will make it possible to estimate the total run-out of the vehicle in a given driving mode. This unit has a direct connection with the mechanical part. Each part will be assembled separately according to the automobile mathematical equations theory and the theory of electric machines. All created subsystems interacted with each other in the process of modeling the car movement-braking. The calculation was performed in one-dimensional design environment by means of Matlab Simulink block package.

To assess the possibility of the car movement, it is necessary to analyze the scheme shown in Fig. 9, which shows the main forces involved in the car movement. These forces include the driving force realized on the driving wheels in the form of traction torque and forces that create resistance to movement [7].

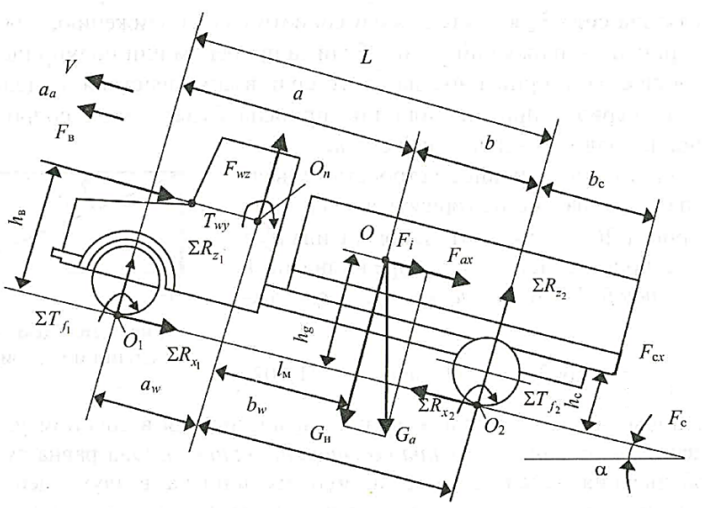

Fig. 9. Forces and torques acting on the car in the general case of motion

A general equation characterizing the rectilinear motion of the car with a trailer in general was written down

$$F_{to} - F_\psi - F_b - F_a = 0,$$

where F_{to} – traction force on the driving wheel; F_ψ – road resistance force: the wheel rolling resistance force and of resistance force to rise; F_b – resistance force of the incoming air flow during the car movement; F_a – inertial force or resistance force to translational motion.

Traction force on the car driving wheels

$$F_{to} = \frac{T_e u_{tr} \eta_{tr}}{r_d} - \frac{(\gamma_e T_e + J_e)\varepsilon_e u_{tr} \eta_{tr}}{r_d},$$

where T_e – engine crankshaft torque, N·m; u_{tr} – transmission ratio; η_{tr} – vehicle transmission efficiency; r_d – wheel free radius, m.

Road resistance force

$$F_\psi = f_{aw} G_a \cos\alpha \pm G_a \sin\alpha,$$

where f_{aw} – road resistance coefficient; G_a – vehicle force weight, N; a – lifting gradient angle, deg.

Air resistance force

$$F_b = 0.5 c_x \rho_b A_b v_w^2,$$

where c_x – vehicle drag coefficient; ρ_b – air density; A_b – midsection area, m^2; v_w – vehicle speed, m/s.

Inertial force

$$F_a = \delta m_a a_a,$$

where m_a – vehicle weight, kg; a_a – vehicle acceleration, m/s^2; δ – rotating masses coefficient

$$\delta = 1 + \sigma_1 u_k^2 u_d^2 + \sigma_2;$$

u_k – transmission ratio; u_d – gear ratio of the additional gearbox;

$$\sigma_1 = \frac{(\gamma_e T_e + J_e) u_0^2 \eta_{tr}}{m_a r_d r_k};$$

$$\sigma_2 = \frac{\sum J_k}{m_a r_d r_k}.$$

For most vehicles, values are taken in the following ranges $\sigma_1 = 0.03–0.05$; $\sigma_2 = 0.04–0.06$ [7].

To obtain an adequate mathematical model of the electric platform, it is necessary to choose the

most typical picture of the speed changing process and acceleration of the vehicle in question, taking into account the movement regional specifics in different conditions. This process must contain both the urban movement cycle and the suburban driving cycle. Such an evaluation regime can be a test cycle according to GOST R EN 1986-1–2011 [8] (analogue of the European driving cycle – NEDC (New European Driving Cycle) used to assess the toxicity of vehicles [9]).

At the same time, the urban cycle itself is characterized by the duration of 195 s and includes the following time phases (Fig. 10):

– idling for 60 s;
– vehicle idling for 9 s;
– gear change time, lasting 9 s;
– acceleration, lasting 36 s;
– driving time at a constant speed of 57 s;
– deceleration, lasting 25 s.

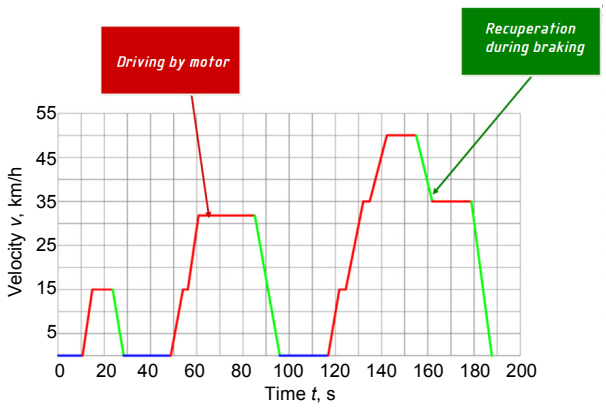

Fig. 10. Diagram of a simple urban cycle

In this cycle, the vehicle must travel with four main speed limits: 15 km/h (4.17 m/s), 32 km/h (8.9 m/s), 35 km/h (9.72 m/s) and 50 km/h (13.9 m/s); five main positive acceleration limits: 1.04 m/s^2, 0.69 m/s^2, 0.79 m/s^2, 0.51 m/s^2, 0.46 m/s^2; and the following main negative acceleration limits: –0.83 m/s^2, –0.81 m/s^2, –0.52 m/s^2, –0.97 m/s^2.

Fig. 11 shows the speed dependence of the suburban cycle. For this cycle, the average speed is within 62.60 km/h and the distance covered is 6956 m.

The country cycle is characterized by duration of 400 s and includes the following time phases:

– stop for 40 s;
– acceleration, lasting 109 s;
– constant speed driving time 209 s;
– deceleration, lasting 42 s.

In this cycle, the vehicle must travel with four main speed limits: 50 km/h (13.9 m/s), 70 km/h (19.4 m/s), 100 km/h (27.8 m/s) and 120 km/h (33.3 m/s); six main positive acceleration limits: 0.69 m/s^2, 0.51 m/s^2, 0.42 m/s^2, 0.43 m/s^2, 0.24 m/s^2, 0.28 m/s^2; and the following main negative acceleration limits: –0.69 m/s^2, –1.04 m/s^2, –1.39 m/s^2.

Fig. 12 shows the assembled circuit of the electric platform mechanical part calculating the consumed-renewable power for the selected driving cycle. In this case, the model takes into account all the technical features of the designed electric platform: transmission ratios and its efficiency. Also, the calculation model includes parameters such as the gross mass involved in the calculation of the resistance forces to movement and the Mid-section coefficient, which characterizes the car cross-sectional area.

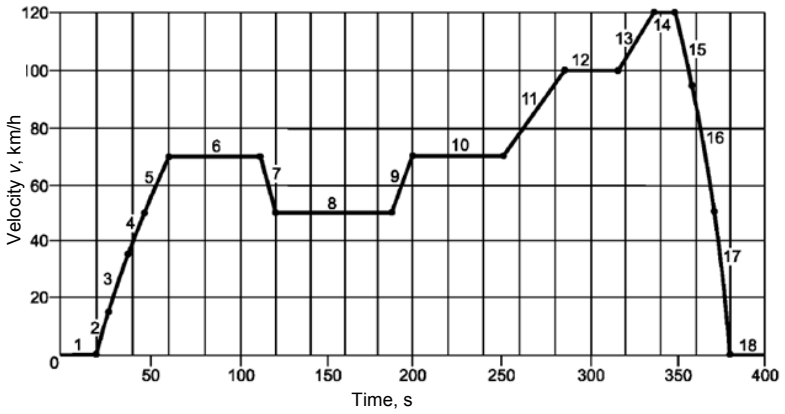

Fig. 11. Suburban cycle diagram

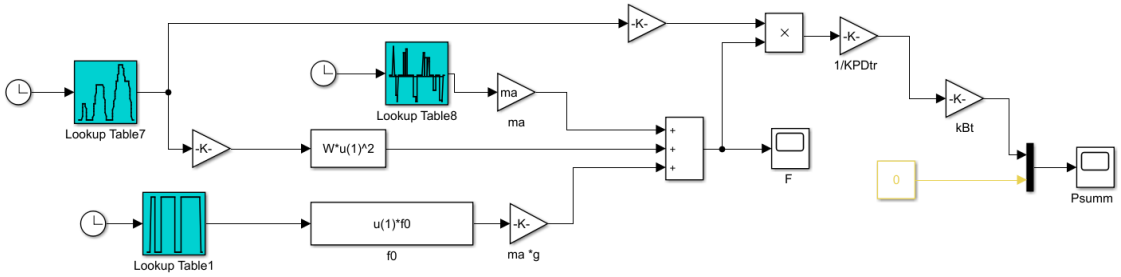

Fig. 12. Mixed cycle diagram for a vehicle with a gross weight of up to 3.5 t

For the convenience and simplicity of modeling the electrical part of the electric platform, blocks of the SimPowerSystems library containing all the necessary electrical part components of the designed electrically powered vehicle were used. This approach can reduce the design time of complex electrical parts, increase the computational model performance, simplifying the calculation and reducing the calculation time. Thus at the design stage and the effectiveness evaluation of the developed electrical platform it can significantly reduce the time to run test models.

To model an asynchronous machine with a squirrel-cage rotor, the standard asynchronous machine unit is used. It can be applied in two modes: as an electric motor and a generator [10].

To create a model of an inverter that converts DC to AC, a "universal bridge" block from the standard library SimPowerSystems Simulink application is used. This unit allows to create a number of semiconductor devices (diodes, thyristors, ideal keys, as well as fully controlled thyristors, IGBT and MOSFET transistors shunted by reverse diodes) [10].

The battery was simulated using a standard battery pack, which can also be found among SimPowerSystems applications in a Simulink environment. This model contains the main types of self-discharging batteries that are currently the most common in technical equipment. This unit contains four types of batteries with different physical and chemical properties, taking into account different parameters, from the initial charge of the battery to the temperature modes of charge and self-discharges. This device is suitable for quick efficiency evaluation of the power supply and allows evaluating the various advantages of each of the presented battery types.

Fig. 13 shows the equivalent scheme of the battery pack under consideration.

Fig. 14 shows the assembled electrical part circuit of the electrical platform. This scheme consists of a standard asynchronous motor unit, which is fed to the design torque obtained in the mechanical part of the mathematical model. The induction motor is powered by a three-phase voltage generated in the inverter. The signal for the inverter is a control unit that regulates the angular velocity calculated in the model mechanical part.

There is a battery in the circuit diagram of the electric part unit. In this case, a Nickel-metal hydride battery with a voltage of 400 V and a capacity of 140 Ah is shown.

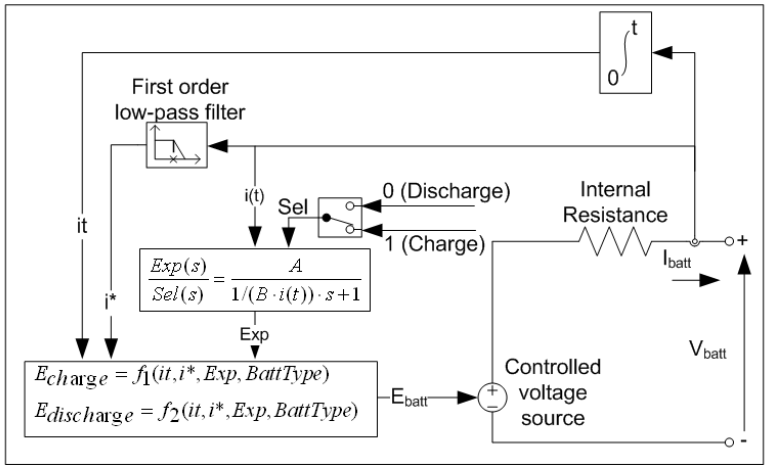

Fig. 13. Battery equivalent circuit

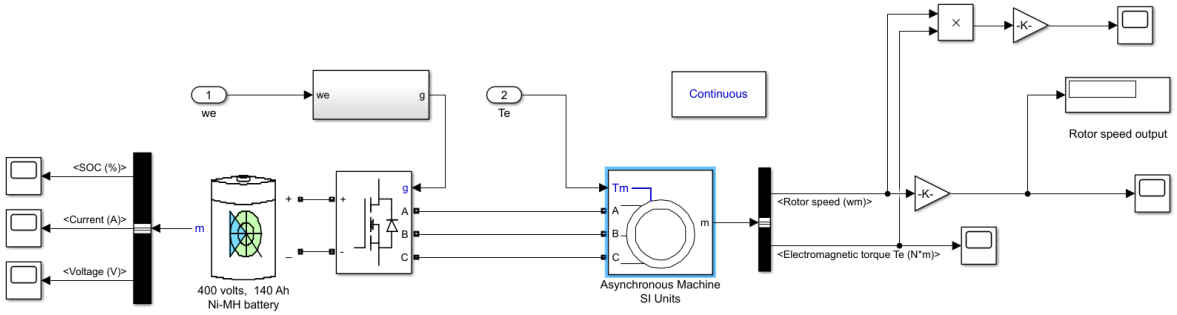

Fig. 14. Electrical part of electric platform with engine speed control unit

By connecting the mechanical and electrical parts of the electrical platform a general mathematical model of the developed vehicle, shown in Fig. 15, is obtained.

The developed model will allow calculating and evaluating the efficiency parameters of the traction electric drive of electric platforms.

To assess the effectiveness of the electric platform, a review of batteries in the modern market was conducted, since, as previously noted, it is the power sources that are one of the main elements of the electric vehicle traction system. This element directly determines both the car traction and speed characteristics, and its full power reserve.

Based on the given technical parameters of the cells, several possible power sources of the electric platform for the calculating case are formed. The most common voltage in electric commercial vehicles is 400 V. Blocks consisting of the basic power sources (cells) connected in series to each other and batteries are formed and summarized in Tab. 5.

To analyze the energy efficiency, 4 models of the battery are formed. For each of the considered battery the desired amount of energy required to move a given speed, according to the selected mode of the elementary urban cycle with duration of 195 s is calculated according to GOST R EN 1986–2011. The calculation determined the values of the required energy for movement in the elementary cycle. On the basis of the designed electrical platform where was a mathematical model of the battery discharge the following predicted values of the reserve shown in Tab. 5 were obtained. It is worth noting that in these calculation models were not taken into account additional power sources, such as air conditioning, external and internal lighting, etc., which can reduce the total mileage.

Table 5

Expected power reserve of the electric platform

Battery	Battery specifications	Quantity on the prototype	Expected cruising range, km
1	$V = 400$ V $C = 36$ Ah $m = 207$ kg	2	108
2	$V = 400$ V $C = 40$ Ah $m = 200$ kg	2	120
3	$V = 400$ V $C = 35$ Ah $m = 150$ kg	2	105
4	$V = 400$ V $C = 40$ Ah $m = 200$ kg	2	120

Based on the above, it is recommended to use battery No 2 as a power source for the electric platform as an effective option among the considered batteries.

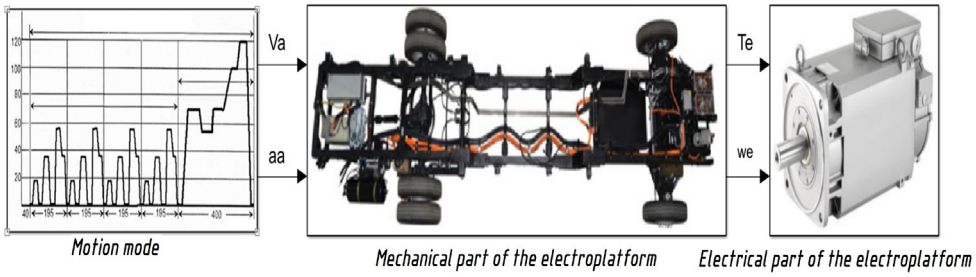

Fig. 15. Electric platform model

Strength calculation

At the design stage of the electroplaters light commercial vehicle it was required to analyze the comparative stiffness of the middle suspension battery for basic configuration and for the variant with the welded corners reinforcement inside and out.

Fig. 16 shows the design diagram for the two variants of the electric vehicle battery suspension.

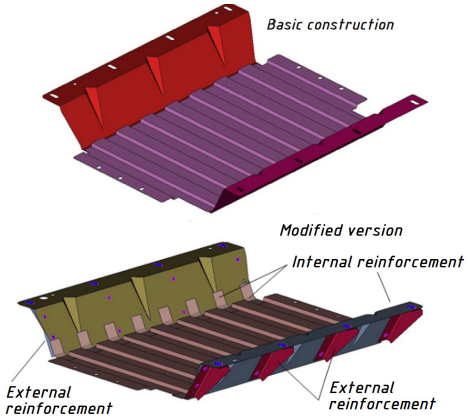

Fig. 16. Structural diagrams of battery suspension options

Four design options were considered:

– basic configuration;

– option where interior and exterior corners are added on both sides;

– the same, but the outer corners of the "flat" side are missing;

– option only with outer corners on both sides.

To determine the stiffness in the transverse direction to the structure forces were applied (Fig. 17):

1000 N at the lower midpoint (point *A*);

300 N at the upper midpoint (point *B*).

In addition, the structure was loaded with its own weight.

The calculation results are summarized in Tab. 6.

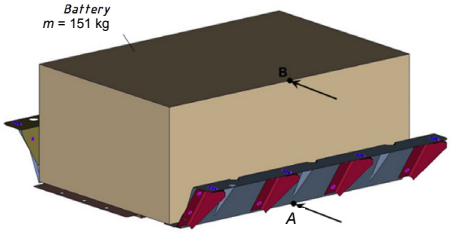

Fig. 17. Force application diagram

According to the results of the calculations, with the use of full reinforcement (inside and outside on both sides), the transverse rigidity of the battery suspension structure of the electric vehicle increases by about 8 times. At the same time the eigen frequency of the structure increases in the transverse direction.

Table 6

Calculation results

	1st eigen frequency, Hz	Movement with 1 kN force applied at the bottom point, mm	Movement with 300 N force applied at the upper point, mm
Basic version	6.47	1.42	1.56
The option with the outer corners of one side + internal corners	17.4	0.29 (490 %)*	0.34 (459 %)*
The option with the outer corners on both sides + inner corners	22.9	0.16 (888 %)*	0.20 (780 %)*
Option with outer corners on both sides, but without inner corners	20.1	0.23 (617 %)*	0.29 (538 %)*

* In parentheses there is percentage increase in stiffness compared to the base case.

Additionally, the strength calculation of the electric vehicle frame was carried out.

Fig. 18 shows a structural diagram for the calculation of the light commercial electroplater frame.

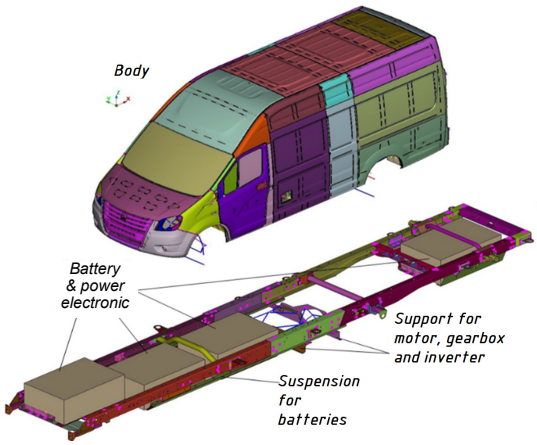

Fig. 18. Structural diagram of the frame calculation

The nominal weight of the loaded electric platform was assumed to be equal to 3.5 t. The cargo weight (1.2 t) was evenly distributed over 3 euro pallets 1200×800 mm, fixed to the body floor.

In the context of work 2 design cases were discussed: triple vertical overload and front wheel hanging.

In the case of a triple vertical overload, a triple gravitational load was applied to the model in the

vertical direction with acceleration equal to 3g = = 3 · 9810 = 29430 mm/s^2.

In the case of the front wheel hanging the torque was applied to the front axle midpoint

$$M_x = \frac{Gbc}{2(a+b)},$$

where $G = mg$ – gross vehicle weight; m – total weight, t; c = 1750.2 mm – front chassis base (distance between the wheels); a, b – see the diagram in Fig. 19.

Thus a = 2220.06 mm; b = 1418.64 mm; m = 4,05 t; $M_x = 1.354 \cdot 10^7$ N·mm.

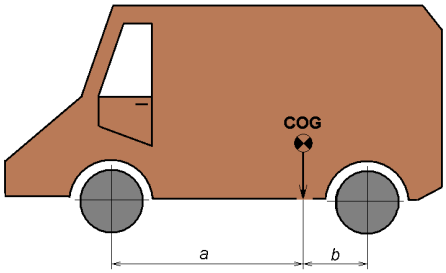

Fig. 19. Mass center position of the model relative to the axes

Calculation results

1. Case of triple vertical overload

The calculation results are shown in Fig. 20. The maximum equivalent voltages (564 MPa) will be in the rear pallet corrugation zone.

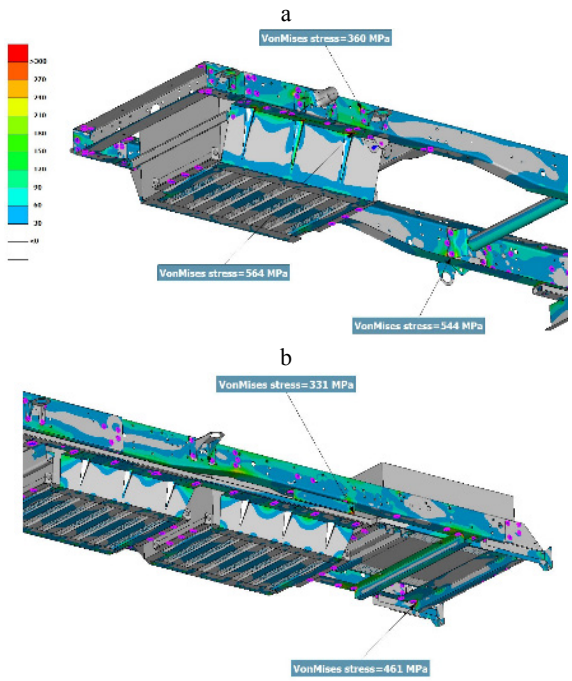

Fig. 20. Equivalent stresses according to Mises, MPa, triple vertical acceleration: a – rear part; b – front part

2. Front wheel hanging case

The calculation results are shown in Fig. 21. The maximum equivalent stresses (450 MPa) will be in the area of the junction of the front crossbar under the battery with the spar.

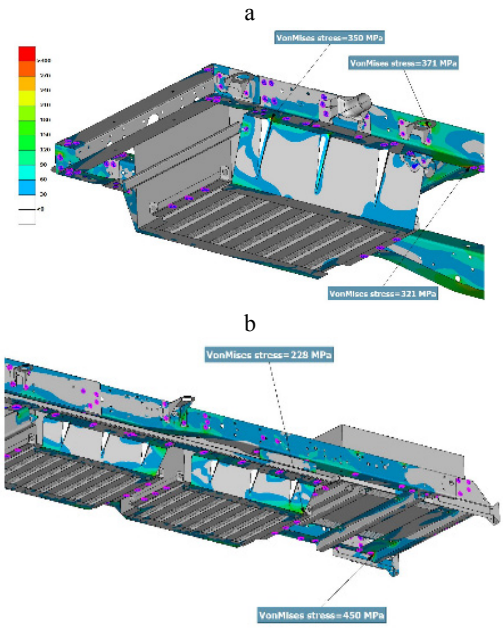

Fig. 21. Equivalent stresses according to Mises, MPa, front wheel hanging case: a – rear part; b – front part

Running tests

The purpose of the tests was: to set the power reserve for the developed electric light comercial vehicle, to fix the mileage of the vehicle as the charge level of the traction battery decreases.

The GAZ Group's motor range in the Berezovaya Poima settlement was used as the test site. The test conditions correspond to the normal climatic conditions specified in paragraph 5.2 [11] (T5-temperate climate). The actual ambient temperature was 27 °C.

The vehicle was weighed in running order, then the vehicle was loaded to the full weight of 3.5 (Fig. 22).

The vehicle was installed on a flat horizontal surface. The CAN adapter PCAN-USB X6 CAN-FD (hereinafter referred to as the CAN Adapter) was connected to the vehicle's on-board network, the Racelogic VBOX 3i RTK multifunction speed meter kit was installed and connected.

The following parameters were recorded during the test:

– the coordinates of the vehicle location (speed);

– battery charge level;

– fixing the maximum and average speed on the track;

– vehicle mileage until the battery is fully discharged;

– the voltage level in the traction battery;

– current consumption and current recovery;

– time.

Fig. 22. Vehicle weighing in running order

The first type of the test is traffic simulation in the city.

The tests were carried out at the vehicle test site (50 % of the time) and on straightforward sections of the asphalt road (Fig. 23). Maximum speed 50 km/h (±5), the average speed for the entire run was at least 22 km/h.

In the process and according to the test results, the following values were recorded:

– average and maximum speed on the track;

– mileage at battery discharge from 90 to 60 %;

– mileage reach time 50 km.

At the beginning of the tests, the charge level of the traction battery was 92 %, and the voltage on the battery was 379 V.

To determine the indicators, the test driver was driving at a speed of not less than 22 km/h and not exceeding 50 km/h. According to the test results, the average speed on the track was 24 km/h, the maximum – 55 km/h. Results are presented in Tab. 7.

The second type of test-driving cycle.

The vehicle was tested in cycles. One cycle includes: acceleration to 10 km/h, movement at a speed of 10 km/h for 1 min, stop. Repetition of acceleration and movement with speeds multiple of 10 up to 60 km/h. According to the test results, the following parameters were determined:

– the total number of cycles during the test before the battery is fully discharged;

– maximum speed during tests;

– vehicle mileage before full battery discharge (10 %);

– vehicle mileage at a charge level of 90 to 10 %, in increments of 10 %.

Fig. 23. Test location

Table 7

Vehicle movement parameters. The first type of test

Battery charge, %	Voltage on battery, V	Mileage, m
90	394	2495
80	385	16417
70	371	32894
60	371	48722

At the beginning of the tests, the charge level of the traction battery was 98 %, the voltage on the battery was 397 V.

To determine the total number of cycles during the test, the test driver accelerated the vehicle to a speed of 10 km/h and moved at this speed for 1 min. Then it stopped completely. The acceleration and the movement were repeated at speeds that are multiples of 10 to 60 km/h. The total number of cycles during the test until the battery discharge to 10 % was 22 cycle. This test was carried out 1 time. The vehicle was accelerated to a maximum speed. The maximum speed of the vehicle during the tests was 102 km/h.

According to the data presented in Tab. 8, the vehicle mileage was 112.9 km at battery discharge from 98 % to 10 %.

Table 8

Vehicle movement parameters. The second type of test

Battery charge, %	Voltage on battery, V	Mileage, m
90	385	11539
80	371	25921
70	368	40673
60	353	55270
50	349	67862
40	334	78705
30	331	93314
20	323	102090
10	331	112977

CONCLUSION

According to the results of the tests, it can be concluded that the battery charge of the developed electric vehicle, with a total weight of 3500 kg, is enough to overcome the distance of more than 100 km, at a temperature of 20 degrees and above. The discrepancy between the values of the mileage obtained experimentally and theoretically was less than 6 %. Thus, we can talk about the adequacy of the developed mathematical model of the electric vehicle. The results of this work will be a good starting point for the development of energy-efficient electric commercial vehicles.

ACKNOWLEDGMENT

This work was carried out at the NNSTU named after R. E. Alekseev, with financial support from the government in the face of the Russian Ministry of Education under the Federal Program “Research and development on priority directions of the scientific-technological complex of Russia for 2014–2020”, the unique identifier of the project: RFMEFI57717X0268. The experimental research conducted with the use of measurement equipment of the NNSTU Centre of collective using “Transport Systems”.

REFERENCES

1. Knupfer S. M., Hensley R., Hertzke P., Schaufuss P. (2017) *Electrifying Insights: How Automakers Can Drive Electrified Vehicle Sales and Profitability*. Available at: https://www.mckinsey.com/industries/automotive-and-assembly/our-insights/electrifying-insights-how-automakers-can-drive-electrified-vehicle-sales-and-profitability.
2. International Energy Agency (2016) *Global EV Outlook 2016 Beyond One Million Electric Cars*. https://doi.org/10.1787/9789264279469-en.
3. *Commercial Vehicles*. Available at: https://rim3.ru/comauto/news/perspektivy-gruppy-gaz/ (Accessed 30 May 2018) (in Russian).
4. Vol'dek A. I., Popov V. V. (2010) *Electrical Machines. AC Machines*. St. Petersburg, Piter Publ. 356 (in Russian).
5. Hameyer K., Belmans R. (1999) *Numerical Modeling and Design of Electrical Machines and Devices.* Boston, WITpress, 340.
6. Bianchi N. (2005) *Machine Analysis Using Finite Elements.* Boca Raton CRCpress, 290. https://doi.org/10.1201/9781315219295.
7. Kravets V. N., Selifonov V. V. (2011) *The Theory of a Car*. Moscow, OOO “Greenlight +”, 884 (in Russian).
8. GOST 1986-1–2011 *Electrically Propelled Road Vehicles. Measurement of Energy Performances. Part 1. Pure Electric Vehicles.* Moscow, Standartinform Publ. 2012, 19 (in Russian).
9. UNECE No 83, 84 *Uniform Provisions Concerning the Approval of Vehicles with Regard to the Emission of Pollutants According to Engine Fuel Requirements*. Available at: https://www.unece.org/fileadmin/DAM/trans/main/wp29/wp29regs/R083r5e.pdf.
10. Chernyh I. V. (2008) *Modeling of Electrical Devices in MatLab, SimPowerSystems i Simulink.* Moscow, DMK Press Publ. 288 (in Russian).
11. GOST R 15150–69 *Machines, Instruments and Other Industrial Products. Modifications for Different Climatic Regions. Categories, Operating, Storage and Transportation Conditions as to Environment Climatic Aspects Influence.* Moscow, Standartinform Publ. 2006, 59 (in Russian).

Received: 08.10.2019
Accepted: 10.12.2019
Published online: 31.01.2020

https://doi.org/10.21122/2227-1031-2020-19-1-76-84

UDC 349

How to Make the Charging Simple, Convenient and Efficient

W. Cheng[1)], Y. Wang[1)]

[1)]Beijing Matrix Mobility Technology Co., Ltd (Beijing, People's Republic of China)

Abstract. With the large-scale application of electric vehicles (EV) in the world and also in China, the contradiction between the EV and charging stations has become more and more prominent. People always cannot easily find the charging stations or when they find them finally found they do not work. To connect the vehicle, charging station/pile and end-users for making the charging simple, convenient, efficient and visible is becoming very important. People need a platform to tell them where, when and how to charge for their EV. Matrix Mobility is focusing on realizing this comprehensive charging solution together with OEM, charging point operator (CPO), electric power company and parking lots by using big data analysis. Matrix Mobility installs the charging solution into the car unit before cars go off production line and meanwhile integrates the same function into OEM's own APP with opening API to help end-users increase their charging experience.

Keywords: e-mobility, charging solution, connected charging system, electric vehicle, CPO, big data

For citation: Cheng W., Wang Y. (2020) How to Make the Charging Simple, Convenient and Efficient. *Science and Technique.* 19 (1), 76–84. https://doi.org/10.21122/2227-1031-2020-19-1-76-84

Как сделать зарядку электромобиля простой, удобной и эффективной

У. Ченг[1)], И. Ван[1)]

[1)]Пекинская матрикс мобилити технолоджи компания, Лимитид (Пекин, Китайская Народная Республика)

Реферат. По причине широкого использования электромобилей во всем мире, а также в Китае все более актуальной становится решение проблемы электромобилей и зарядных станций. В настоящее время не всегда легко найти зарядные станции, а когда, наконец, находишь их, то обнаруживаешь, что они не работают. Поэтому для того, чтобы сделать процесс зарядки простым, удобным, эффективным и заметным, необходимо обеспечить взаимодействие между транспортным средством, зарядной станцией и потребителем. Потребитель нуждается в информационной платформе, которая предоставит ему ответы на следующие вопросы: где, когда и сколько будет стоить зарядка электромобиля? Используя результаты анализа огромного количества данных, компания «Матрикс мобилити» прилагает усилия для решения вопросов зарядки транспортных средств с помощью использования соответствующего программного обеспечения, а также четкого взаимодействия с оператором пункта зарядки, энергетической компанией и администрацией паркингов. «Матрикс мобилити» предлагает выполнять зарядку транспортного средства до того, как оно сойдет с производственной линии. В то же время решение этой задачи интегрируется в приложение программного обеспечения с действующим прикладным программным интерфейсом, чтобы повысить качество процесса зарядки для потребителя.

Ключевые слова: использование электромобиля, решение зарядного процесса, подключенная зарядная система, электромобиль, оператор пункта зарядки, большие объемы данных

Для цитирования: Ченг, У. Как сделать зарядку электромобиля простой, удобной и эффективной / У. Ченг, И. Ван // *Наука и техника*. 2020. Т. 19, № 1. С. 76–84. https://doi.org/10.21122/2227-1031-2020-19-1-76-84

Адрес для переписки
Ченг Уильям
Пекинская матрикс мобилити технолоджи компания, Лимитид
Навинфо Плаза, Пекин роуд, район Хайдьян,
г. Пекин, Китайская Народная Республика
Тел.: +86 185 15-27-88-08
william.cheng@navinfo.com

Address for correspondence
Cheng William
Beijing Matrix Mobility Technology Co., Ltd
Navinfo Plaza, Beijing Road, Haidian District,
Beijing, People's Republic of China
Tel.: +86 185 15-27-88-08
william.cheng@navinfo.com

Introduction

Environmental pollution is becoming a headache for the entire world. Global temperature increasing, greenhouse gases, air pollution and acid raining are only part of those negative phenomenons. And between all different contributors to the pollution, the vehicle emission is the primary cause. Switch from traditional engines to electric vehicles is the main effective way to reduce the pollution. This demand leads to the growing application of electric vehicle (EV) and plug-in hybrid electric vehicle (PHEV) technologies because of their reduced fuel usage and greenhouse emissions, and this is also accepted worldwide. While current charging experience for end-users are still not good, for example:

a) bad charging time – it takes 1–3 hours to fully charge the vehicle comparing to 1–3 minutes for fuel adding;

b) bad charging infrastructure – it's not easy to find a charging station when you need it, the distribution density is too low to charge;

c) bad charging system – it takes long time for end-users to start charging successfully and have to install too many APPs due to every CPO has their own system. And even worse is that those systems are not good;

d) bad payment system – not convenient for end-user to pay via credit card or back account, it takes too many fussy processes to successfully finish payment;

e) bad information – nor accurate information about charging points, it happens when end-user find a charging point after long time looking for and finally see a charging point, while when he goes for charging found out it was not usable due to damage or not under operation;

f) bad surrounding – charging points are not aligned with parking lots, the charging area can not park which will increase the complaint from end-users.

To stimulate the usage of EV and PHEV, the most important way is to let the end-users feel comfortable with the electric vehicles, which means those vehicles should get charged as simple and convenient as traditional vehicles. The best way to realize it is to work out a comprehensive charging solution together with OEM, charging point operator (CPO), fleets, electric power company and parking lots by using big data analysis to improve the quality of charging experience. Take China as example, there are around 3 million EV and PHEV running on the road, but charging is still the most painful point for end users who's using new energy vehicles (NEV including EV and PHEV).

From the following figure (Fig. 1), you can see there are hug amount of demand for electricity – 300 billion kW·h by 2030, this requires a very simple and efficient charging solution for the EVs.

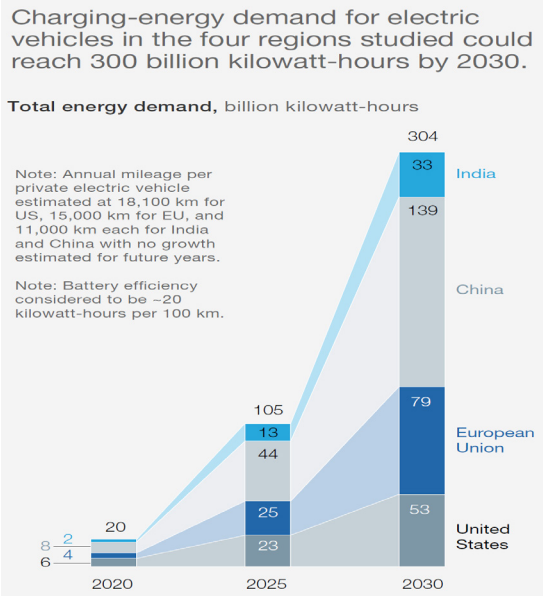

Fig. 1. Electricity demand till 2030

From Fig. 2 you can see the demand of public charging occupies a high portion of overall charging scenarios.

This paper analyzed the high qualified big data of EV running (including battery data from BMS), charging behavior, charging stations, power grid localization, battery usage to work out a charging solution which works better for OEM, CPO (charging point operator), fleets and end users.

Comprehensive charging solution study

Regarding the EV charging eco-system, we can see there are OEMs, Telematics suppliers, Internet suppliers, Big Data analyzers, Public Charging Station, Wall-box charging, Mobile Charging and the EMSP (e-mobility service provider). The EMSP is the bridge and liaison between the downstream end users and the upstream OEM and CPO. It collects all the data from different parties and analyze, optimize and integrate them to be fit for the parties inside the ecosystem (Fig. 3).

To build the charging platform need to integrate the big data capabilities of Cloud Data Platform, incorporate the data and services of CPOs,

connect the navigation, charging and peripheral services, and refine operation and management capabilities through Big Data analysis (Fig. 4). Take Matrix Mobility as an example, they have connected more than 97 % of the public charging points with the overall number is about 430 K charging points together with cloud provider, OEMs like BMW and Daimler and also fleets.

To realize the overall charging solution, we can divide it as 5 phases.

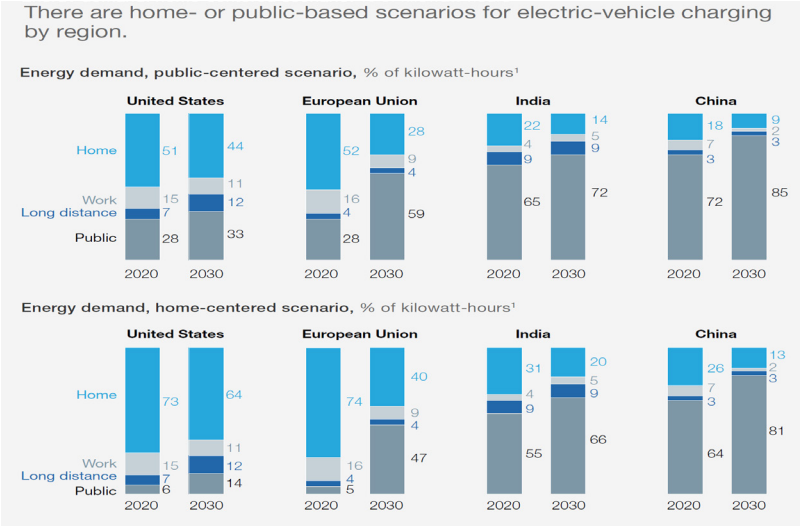

Fig. 2. Charging scenarios by region

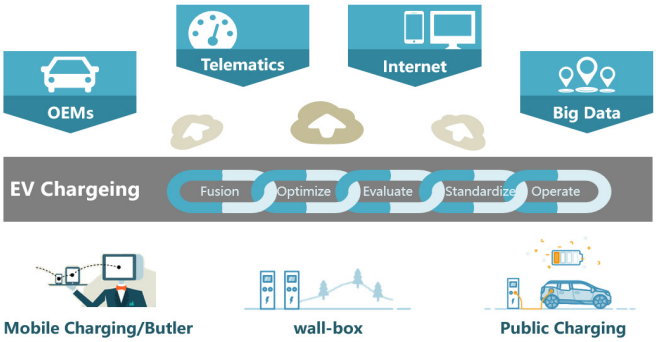

Fig. 3. EV charging ecosystem

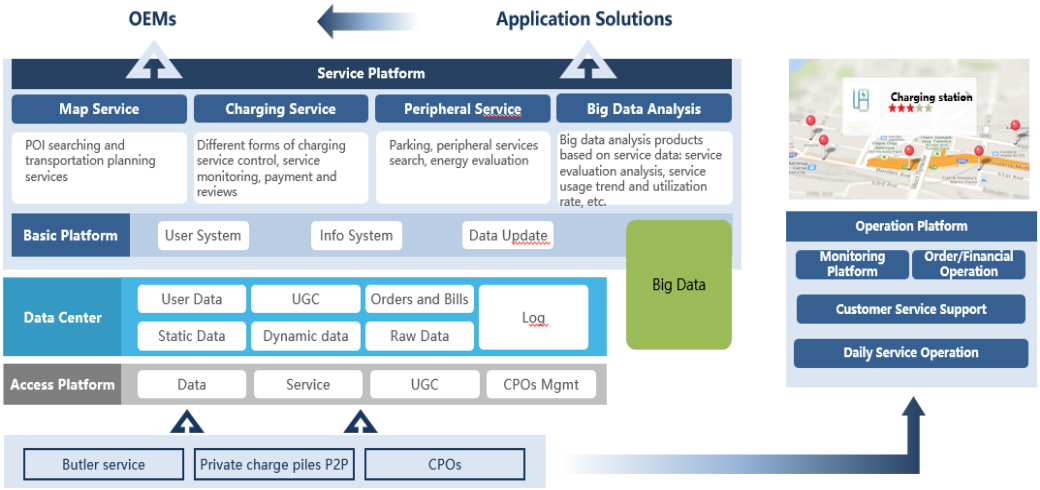

Fig. 4. EV charging platform

Phase 1. Integrate the charging service into vehicle units that is synchronized to the mobile APP (Fig. 5).

Fig. 5. Vehicle head unit integrated

Phase 2. Integrate the public charging services of 3rd party CPOs, combine with map, navigation and route planning, to provide public charging standard solutions. Since each CPO only has their own network and service, which limits the service number of CPOs for end-users who only use the service from one of those CPOs. It will cause inconvenience and reduce the satisfaction of end-users. To create one platform, which integrated all of the CPOs, is very necessary from of the point of serving end-users better (Fig. 6).

Fig. 6. Combined public CPOs

Phase 3. Aggregate individual charging point resources and build P2P sharing economy through the 3rd party sharing service and charging operation platform (Fig. 7). Upgrade the unconnected individual charging points with 4G-model to connect the static and dynamic data to the data center, then share the individual points to public who need to charge. From the statistics we can see that the number of individual charging points are much higher than public CPOs, which means if we can share them, the end-users will have much more choice for charging.

Fig. 7. Individual charging point

Phase 4. Integrate the 3rd party services of the butler, providing high-level butler charging services covering the core cities of the whole country. E.g. parking and charging for customers (Fig. 8), customer can stop and go for their own arrangement, when he/she comes back the vehicle has been charged.

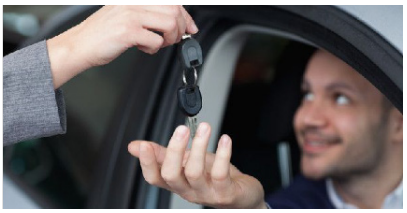

Fig. 8. Parking and charging for cusotmer

Phase 5. Integrate the resources of mobile charging service operators to achieve services such as mobile charging or charging rescue when emergency happens (Fig. 9). This is also one of the main way for reusing the vehicle battery after several years usage in the vehicle. It is called 'cascade utilization' of battery.

Fig. 9. Movable charging station

Phase 6. Provide charging point operation management platform for exclusive charging station, small charging pile operators, personal charging piles as operation trusteeship support (Fig. 10). Those charging methods need an efficient connected platform to manage all charging points for operators to reduce the cost of management and maintanence.

Fig. 10. Exclusive charging station

Supporting above phases, we need to collect and fuse data from map provider (Fig. 11), CPOs and OEMs, store them at cloud platform, do analysis and send them to customers with different applications including static and dynamic data of CPOs.

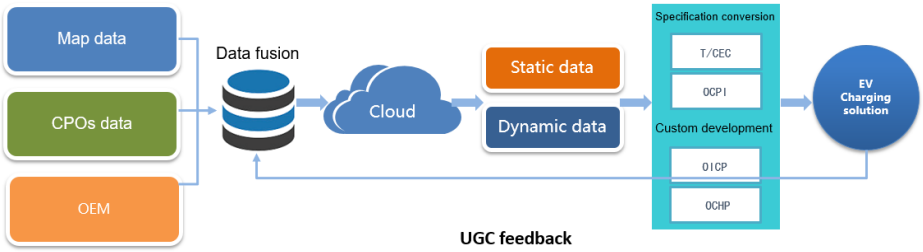

Fig. 11. Framework of data

Among all the different data, CPO data is the base and foundation for an EMSP to provide qualified service to end-users (Fig. 12). In order to ensure the data you provide is qualified, EMSP need to do field check after they get data from CPOs due to the data from CPOs sometimes are not so accurate, for both static and dynamic information. In addition, those data check job should be updated real time to make sure it is the freshest data.

With the integration of many CPOs' charging service, EMSP can provide many convenient services to end users (Fig. 13). Such as:

– financial convenience – help OEM do financial settlement with CPO including payment, prepayment and the invoice process;

– risk management – set the security and risk control of the payment process, and also predict the cost of charging;

– flexible payment – support pre-pay and post-pay mode and provide marketing promotion platform to support packages, coupons, etc.;

– multi-brand support – integrate CPOs in the platform for the end users have the right to choose different service from different CPOs.

To ensure the charging process be efficient, we need to do following jobs (Fig. 14):

– CPO Identification: encoding information transfers to the platform through scanning QR code, according to the rules of encoding information, the platform automatically matches the different CPOs and establishes the connection;

– charging point data check. After establishing the connection, the platform will acquire the information of the corresponding charging point, automatically detect whether the device can be controlled or not. If the control can be realized, the dynamic and static information of the device will be acquired to feedback the user to verify the equipment information;

– charging Start/Stop: after the user sends the start/stop instruction, the EMSP transmits the instruction to the CPO platform, receives the feedback of the execution of the instruction, CPO platform will remote the charging point and synchronously starts/stops the state to the user;

– charging process monitoring: in the charging process, continuous docking between EMSP and CPO platform, receiving or actively grabbing dynamic charging information feedback from CPO platform and synchronizing it to user.

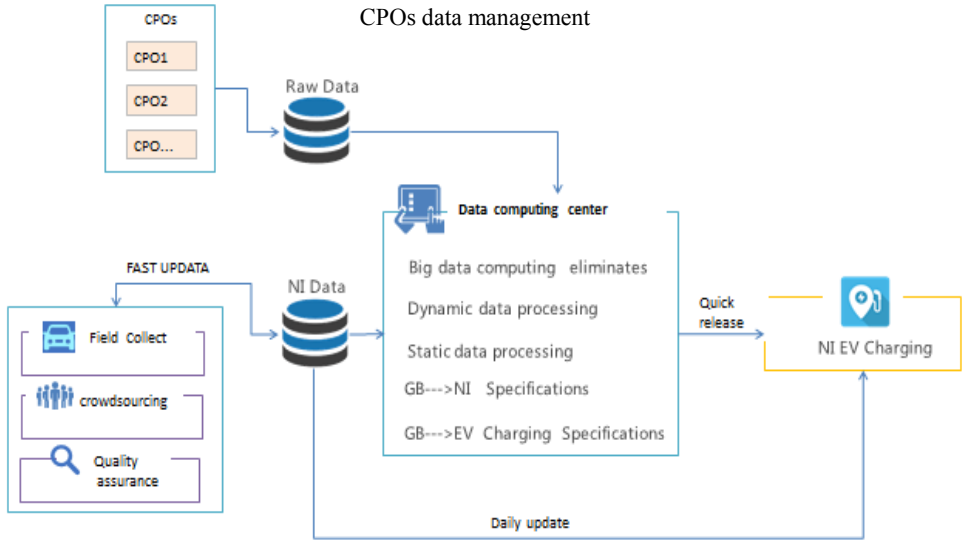

Fig. 12. CPO data management

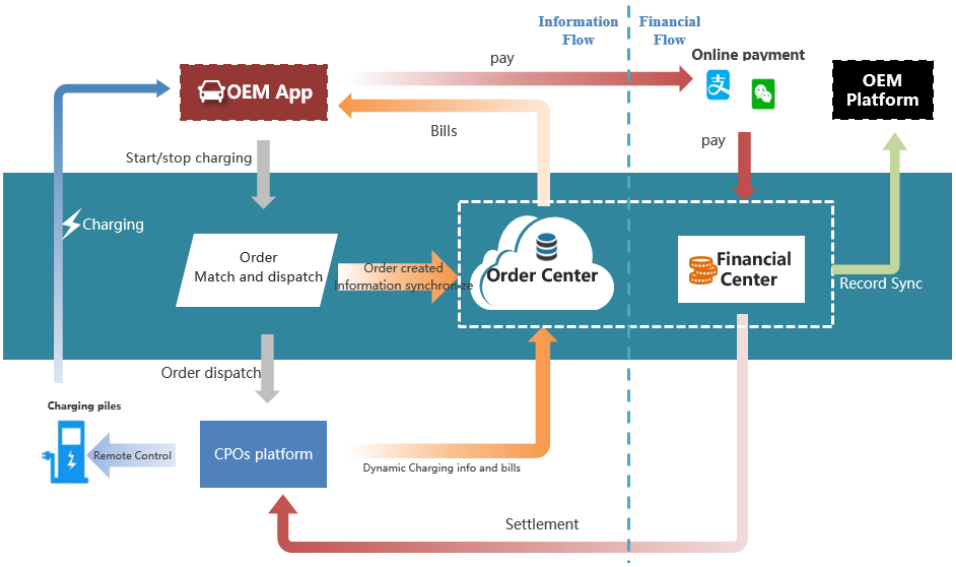

Fig. 13. EMSP order process

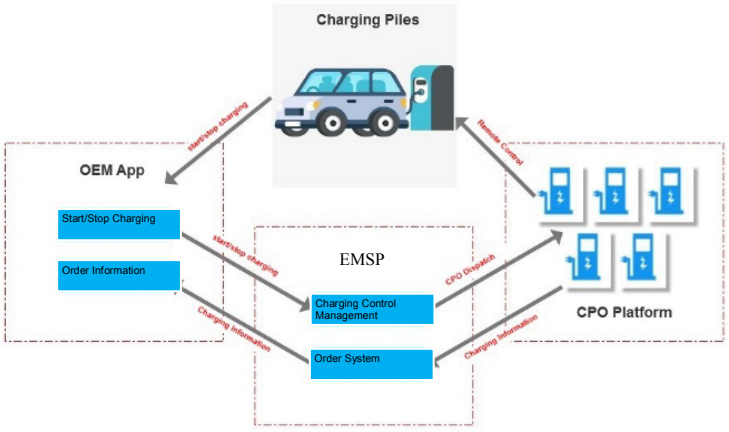

Fig. 14. Charging synchronizing process

Regarding the charging payment process (Fig. 15), users without unpaid orders could send charging control command through the front-end of OEM to start charging process.

After the user sends the charging stop order, the bills generated by CPO platform are first pushed to the backend of EMSP, and then pushed to the frontend of OEM.

Users can choose the appropriate payment method (Wallet/ WeChat/ Alipay/ Credit card, etc.) to pay their charging bills with different tariffs may include time-based fees, energy-based fees which should not exceed the CPO public prices or flat rates. The financial center will record the payment details of all the bills and generate the reconciliation statement.

Online payment service platform supports a variety of flexible transaction payment methods, including Pre-pay, Post-pay, Package, Coupons, etc. (Fig. 16).

Pre-pay and Post-pay are the supporting functions of standard charging service platform. The realization of Storage card, Packages and Coupons can be realized by building a marketing promotion platform parallel to charging service platform.

We recommend standard payment schemes including Pre-pay and Post-pay.

In case there is bad debt happens, the system will limit the service to users. Once the direct-pay mode failed or pre-payment is not enough, users have to finish all payments before opening a new charging order. To avoid or reduce the lost due to above situation, a 3rd party financial monitoring platform can be introduced into the process such as Alipay or Paypal.

In order to provide more support for OEM's marketing activities after SOP, EMSP need to

provide a marketing platform independent from the basic charging service platform (Fig. 17). These two platforms act different responsibilities and provide many support to each other.

The purpose of the marketing promotion platform is to encourage the users to like using EVs and charging for EVs, to do from providing free charging to route planning and usage reports, users will love to travel with EVs (Fig. 18).

In order to make the process and status more visible, the charging platform can provide customers with behavior analysis, service status, financial reports, call center, charging points status, demand prediction, etc. (Fig. 19).

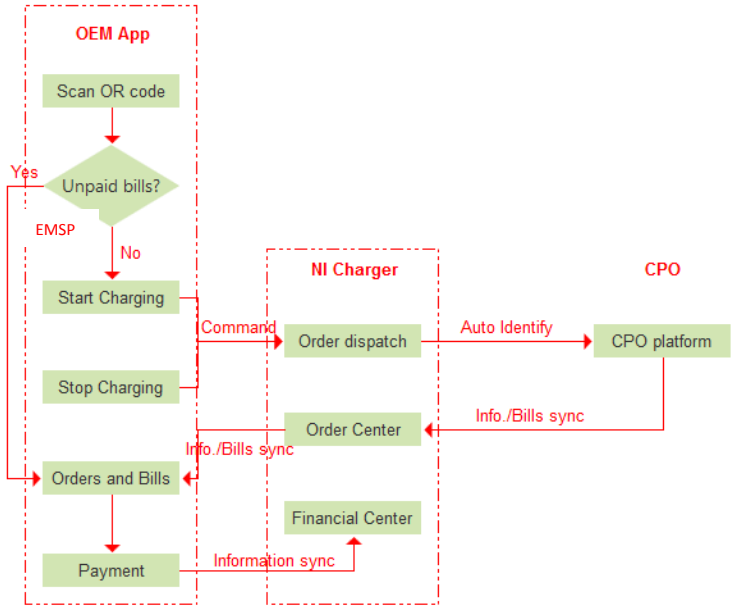

Fig. 15. Payment process

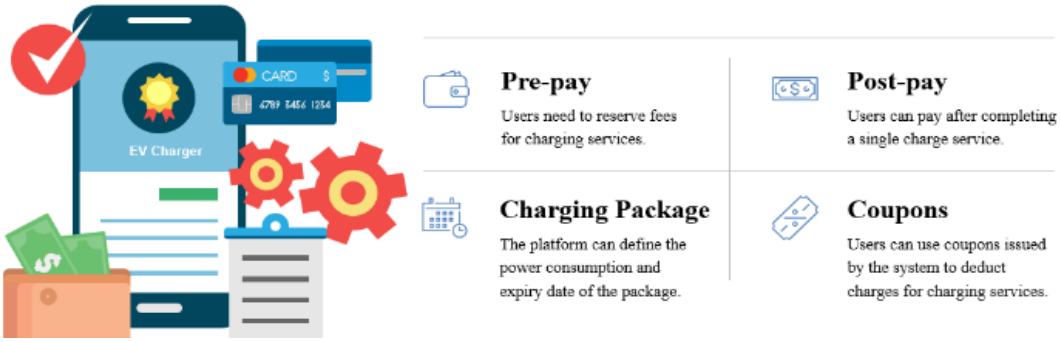

Fig. 16. Payment modes

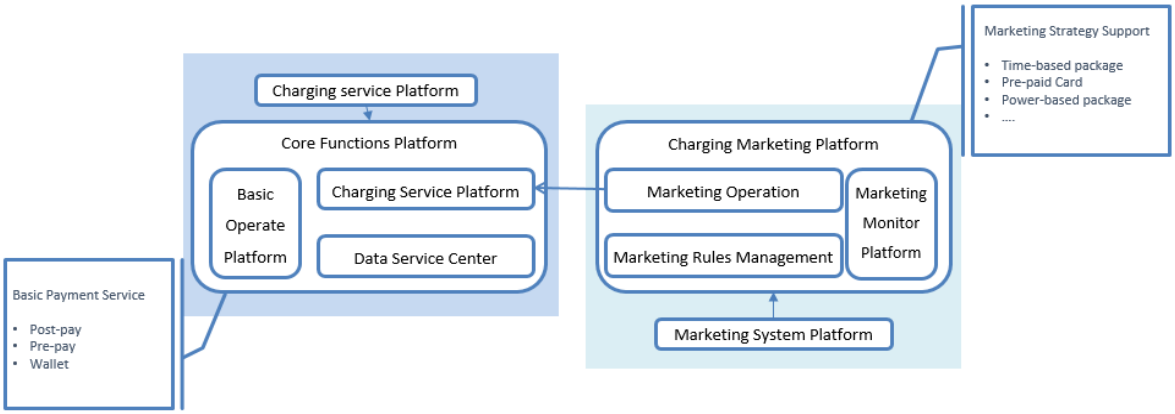

Fig. 17. Interaction of service and marketing platform

Fig. 18. Charging marketing promotion

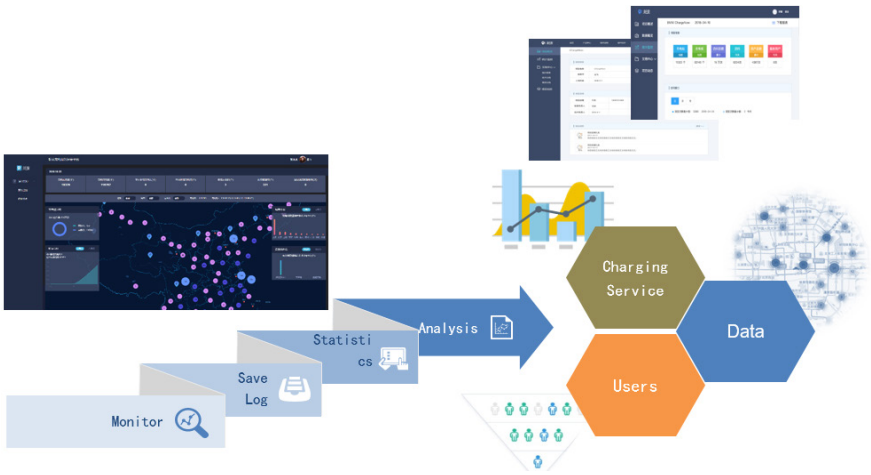

Fig. 19. Visible charging platform

CONCLUSIONS

1. This paper studied from the overall environmental situation, EV market status, demand, current EV and charging solutions, did analysis based on those data, combined the real demand from end-users, we suggested a comprehensive charging solution which integrates OEMs, CPOs, Power Grids and also users. This charging solution we call it EMSP, it can not only provide service to OEMs, CPOs, Power Grids, but also can serve to end-users from indicating where is the charging point, how to charge to the payment of charging – one stop charging solution. It can also keep the solution as a visible platform for all different users with providing them various reports including charging history, behaviors, demand prediction, cost analysis and prediction, etc.

2. We believe this charging solution will bring a big benefit to the whole EV industry, to accelerate the development of industry, to make people love to drive EVs, to reduce the emission of vehicles and to make our world much cleaner and more beautiful.

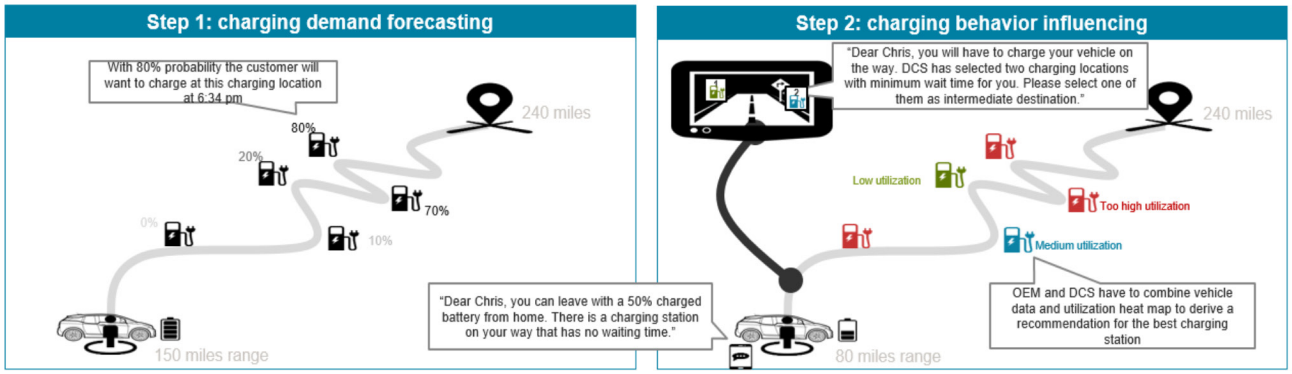

Fig. 20. Make EV running on the way

REFERENCES

1. Ying Wang, William Cheng (2018) *Introduction of Beijing Matrix Mobility Comprehensive Charging Solution*. Beijing, Matrix Mobility.
2. Emadi A., Ehsani M., Miller J. M. (2003) *Vehicular Electric Power Systems: Land, Sea, Air, and Space Vehicles*. New York, Marcel Dekker. https://doi.org/10.1201/9780203913468.
3. Larminieand J., Lowry J. (2003) *Electric Vehicle Technology Explained*. New York, Wiley.
4. Saber A. Y., Venayagamoorthy G. K. (2015) One Million Plug-in Electric Vehicles on the Road by 2015. *12th International IEEE Conference on Intelligent Transportation Systems*, 141–147. https://doi.org/10.1109/itsc.2009.5309691.
5. Massachusetts Division Energy Resources, MA (Sep. 2000) *Installation Guide for Electric Vehicle Charging Equipment.*
6. CHAdeMO Association (2011). *Desirable Characteristics of Public Quick Charger.* Tokyo Electric Power Company, Tokyo, Japan.
7. Haghbin S., Khan K., Lundmark S., Alak¨ula M., Carlson O., Leksell M., Wallmark O. (2010) Integrated Chargers for EV's and PHEV's: Examples and New Solutions. *The XIX International Conference on Electrical Machines – ICEM 2010*, 1–6. https://doi.org/10.1109/icelmach.2010.5608152.
8. Musavi F., Edington M., Eberle W., Dunford W. G. (2012) Evaluation and Efficiency Comparison of Front end AC–DC Plug-in Hybrid Charger Topologies. IEEE Trans. Smart Grid, 3 (1), 413–421. https://doi.org/10.1109/tsg.2011. 2166413.
9. SAE International (2011, Sep. 8) *SAE's J1772 "Combo Connector" for AC and DC Charging Advances with IEEE's Help*. Available at: http://www.sae.org/mags/aei/10128.
10. Mathoy A. (2008) *Definition and Implementation of a Global EV Charging Infrastructure.* Final Rep. Brusa Elektronik, Sennwald, Switzerland, 2008. Available at: https://www.yumpu.com/en/document/view/39489467/definition-and-implementation-of-a-global-ev-park-charge.
11. Su W., Zeng W., Chow M. Y. (2012) A Digital Testbed for a PHEV/PEV Enabled Parking Lot in a Smart Grid Environment. *2012 IEEE PES Innovative Smart Grid Technologies (ISGT)*, 1–7. https://doi.org/10.1109/isgt.2012.6175581.
12. Fasugba M. A., Krein P. T. (2011) Cost Benefits and Vehicle-to-Grid Regulation Services of Unidirectional Charging of Electric Vehicles. *IEEE Energy Conversion Congress and Exposition,* 827–834. https://doi.org/10.1109/ecce.2011.6063856.
13. Sortomme E., El-Sharkawi M. (2011) Optimal Charging Strategies for Unidirectional Vehicle-to-Grid. *IEEE Trans. Smart Grid*, 2 (1), 131–138. https://doi.org/10.1109/tsg.2010.2090910.
14. De-Sousa L., Bouchez B. (2010) *Combined Electric Device for Powering and Charging.* Int. Patent WO 2010/057892A1.
15. Mi C. *Safely Charging EV and PHEV from the Electricity Grid*. Dept. Elect. and Comput. Eng., Univ. of Michigan-Dearborn, Dearborn.
16. Qian K., Zhou C., Allan M., Yuan Y. (2011) Modeling of Load Demand due to EV battery Charging in Distribution Systems. *IEEE Transactions on Power Systems*, 26 (2), 802–810. https://doi.org/10.1109/tpwrs.2010.2057456.
17. Yang Y., Lin Z., Qin D., Hu M., Yang Y. (2007) Control Strategy and Simulation Study on NiMH Battery Quick Charging for Regenerative Braking of HEV. *Journal of Chongqing University (Natural Science Edition)*, 30 (3), 1–5.
18. Li Z., Sahinoglu Z., Tao Z., Teo K. (2010) Electric Vehicles Network with Nomadic Portable Charging Stations, in Proc. *2010 IEEE 72nd Vehicular Technology Conference – Fall.,* 1–5. https://doi.org/10.1109/vetecf.2010.5594437.
19. Chen Q., Sun F., Zhu J. (2004) *Modern Electric Vehicle Technology*. Beijing, China: Beijing Institute of Technology Press.

Received: 08.10.2019
Accepted: 10.12.2019
Published online: 31.01.2020

https://doi.org/10.21122/2227-1031-2020-19-1-85-88

UDC 349

Imitating a Safe Human Driver Behaviour in Roundabouts Through Deep Learning

Á. S. J. Cervera[1)], F. J. Alonso[2)], F. S. García[1)], Á. D. Alvarez[1)]

[1)]Universidad Politécnica de Madrid, ETSI de Sistemas Informáticos (Madrid, Kingdom of Spain),
[2)]Universidad Politécnica de Madrid, Escuela Técnica Superior de Ingenieros Industriales (Madrid, Kingdom of Spain)

Abstract. Roundabouts provide safe and fast circulation as well as many environmental advantages, but drivers adopting unsafe behaviours while circulating through them may cause safety issues, provoking accidents. In this paper we propose a way of training an autonomous vehicle in order to behave in a human and safe way when entering a roundabout. By placing a number of cameras in our vehicle and processing their video feeds through a series of algorithms, including Machine Learning, we can build a representation of the state of the surrounding environment. Then, we use another set of Deep Learning algorithms to analyze the data and determine the safest way of circulating through a roundabout given the current state of the environment, including nearby vehicles with their estimated positions, speeds and accelerations. By watching multiple attempts of a human entering a roundabout with both safe and unsafe behaviours, our second set of algorithms can learn to mimic the human's good attempts and act in the same way as him, which is key to a safe implementation of autonomous vehicles. This work details the series of steps that we took, from building the representation of our environment to acting according to it in order to attain safe entry into single lane roundabouts.

Keywords: deep learning, Neural Networks, driver behaviour, roundabouts, imitation learning

For citation: Cervera Á. S. J., Alonso F. J., García F. S., Alvarez Á. D. (2020) Imitating a Safe Human Driver Behaviour in Roundabouts Through Deep Learning. *Science and Technique*. 19 (1), 85–88. https://doi.org/10.21122/2227-1031-2020-19-1-85-88

Моделирование безопасного поведения водителя на перекрестках с помощью глубинного обучения

А. С. Х. Сервера[1)], Ф. Х. Алонсо[2)], Ф. С. Гарсиа[1)], А. Д. Альварес[1)]

[1)]Мадридский политехнический университет, Высшая техническая школа компьютерных систем инженерии (Мадрид, Королевство Испания),
[2)]Мадридский политехнический университет, Высшая техническая школа промышленной инженерии (Мадрид, Королевство Испания)

Реферат. Кольцевые транспортные развязки обеспечивают безопасное и быстрое движение, а также ряд экологических преимуществ. Но водители, придерживающиеся ненормативных правил поведения при вождении по ним, могут вызвать проблемы с безопасностью, что приводит к несчастным случаям. В статье предлагается способ обучения водителя автономного транспортного средства с целью обеспечения правильного и безопасного поведения при въезде в кольцевую транспортную развязку. Поместив несколько камер в транспортное средство и обработав видеозапись

Адрес для переписки
Альваро Сан Хуан Сервера
Мадридский политехнический университет,
Высшая техническая школа компьютерных систем инженерии
Карретера де Валенсия (А3) 7-й км,
28040, г. Мадрид, Королевство Испания
Тел.: 0034 91 336-53-00
alvaro.sanjuan@upm.es

Address for correspondence
Alvaro San Juan Cervera
Universidad Politécnica de Madrid,
ETSI de Sistemas Informáticos
Carretera de Valencia (A3) km. 7,
28040, Madrid, Kingdom of Spain
Tel.: 0034 91 336-53-00
alvaro.sanjuan@upm.es

видеопотоков с помощью ряда алгоритмов, включая и машинное обучение, можно получить представление о состоянии окружающей среды. Затем используется другой набор алгоритмов глубокого обучения для анализа данных и определения наиболее безопасного пути кругового движения с учетом текущего состояния окружающей среды, включая ближайшие транспортные средства с их предполагаемым местоположением, скоростью и ускорением. Анализируя многочисленные примеры безопасного и опасного поведения водителя во время движения по кольцевой транспортной развязке, предлагается второй набор алгоритмов, который позволяет моделировать правильное поведение водителя, что и является главным условием безопасного применения автономных транспортных средств. В статье подробно описываются все этапы работы, начиная от построения рассматриваемой окружающей среды и заканчивая соответствующим поведением в зависимости от ситуации, что позволяет обеспечить безопасное движение в кольцевой развязке с одной полосой движения.

Ключевые слова: глубинное обучение, нейронные сети, поведение водителя, кольцевая транспортная развязка, имитационное обучение

Для цитирования: Моделирование безопасного поведения водителя на перекрестках с помощью глубинного обучения / А. С. Х. Сервера [и др.] // *Наука и техника*. 2020. Т. 19, № 1. С. 85–88. https://doi.org/10.21122/2227-1031-2020-19-1-85-88

Introduction

Computer Vision is a field that is undergoing a tremendous evolution. Over the last few years Artificial Neural Networks (from now on will be referred also as ANN or NN) are being used to process images due to their high accuracy and fast performance, easily outperforming more traditional approaches in benchmarks, while being relatively easy to implement and reusable.

The goal of this investigation is delivering a system capable of determining whether or not is it safe to enter a roundabout given the current traffic conditions. In order to achieve that, we use the footage from a single camera installed in our vehicle instead of relying on LIDAR (Light Detection and Ranging) data, which would be a more traditional approach.

LIDAR is a surveying method that used a series of laser beams to measure the distance to a target by tracking the time the light takes to bounce back to the sensor. Having one of these sensors on top of our vehicle spinning multiple times per second (normally at a rate of 20 spins per second), creates a 3*D*-scan of the environment in real time. The downside to this approach is that this kind of sensors are expensive and not as common as a regular camera (although prices are coming down in recent years).

Traditional cameras are very common type of sensor, so being able to rely on its data and leaving aside the expensive LIDAR, will enable future investigation and implantation in autonomous vehicles to become much more approachable. Doing this task should be feasible as a human subject is capable of performing the same task using just one eye, relying on years of experience perceiving environments.

From the images recorded by this monocular camera (which we will call "red-green-blue images, or rgb"), we use multiple Artificial Neural Networks to perform various operations, including vehicle detection, distance estimation, environment recreation and motion tracking to obtain their relative speeds and accelerations. All this work has been done using Carla Simulator [1] for the testing environment and Keras as the Deep Learning Framework.

Environment perception with Neural Networks

Artificial Neural Networks are systems that resemble the biological neural networks in our brains (although they're not identical). These systems can "learn" how to perform a task given a correct design (called architecture) and a learning process (commonly referred to as training). When these systems complete their learning process, they build a model that we can use to perform the task that they were created for.

Their usage in image recognition is becoming popular in the last ten years. They can be used for trivial tasks like, for example, analyzing a series of images and detecting which ones contains dogs. They are widely used in ways out of the scope of this investigation, such as spam detection, shopping recommendations, voice recognition, photo enhancement and creating complex virtual assistants.

In this project, we are using various Neural Networks working together to attain our goal. First, we feed each of the frames captured by the camera through an object detection network. Instead of designing a network architecture from scratch, we've decided to choose YOLO (version 3 [2]) as our object detection system. The reasons for this are: YOLO [3] usage is very extended throughout numerous projects and it has been proved to provide a good ratio between accuracy and performance. Keep in mind that this system is going to be used in real time on a reduced hardware environment, so high performance is absolutely necessary. In our test, using images of size 416×416, we can do the object detection task at 28 frames per second, which is well above our target 20 frames per second.

There are plenty of datasets available to use with YOLO, even pre-trained models freely available to use. In order to maximize its performance and minimize the error of the predictions, we have crafted a custom dataset using images extracted from Carla, some examples can be seen in Fig. 1.

Fig. 1. Sample car images taken from our dataset

The dataset contains just four classes (types of objects that we want to identify): vehicles (including cars, buses, trucks, bikes and motorbikes), traffic lights, traffic signs and pedestrians, which is much less than the twenty general-purpose classes used in the default dataset. Fine tuning the dataset and model to our needs creates a smaller, lighter model which results in faster and more precise predictions. Keep in mind that the only class relevant to this project is the "vehicle" class, the rest of the classes are included in the dataset just for future use.

This is the first and most important NN in our system. The raw data from the camera is passed through it and the process begins. The network detects the objects in the current frame and returns the list of the detected bounding boxes. A bounding box has the following attributes: the coordinates of the object's upper left and lower right corners in the image, the object's class (vehicle, traffic light, traffic sign or pedestrian) and the confidence level of the prediction. We set a minimum confidence level threshold to validate the predictions and store all the detected bounding boxes above that threshold to further analyze them.

Our next step is motion tracking. There are two possible scenarios for each object in the frame: being a new object or being an object previously detected on another frame. We check for consistency between the new bounding boxes and the bounding boxes we had already detected. A process of trying to pair each new object with an object from the previous frame begins here: we check every bounding box of the current frame against the ones we had from the previous frame and try to pair the ones that offer the best overlap. For each object, if the best overlap ratio is lower than a threshold, we consider that the new bounding box was not on the scene before this frame, which means that the object is new, so we add this object to the scene. Conversely, if the overlap meets our threshold, the object might be one that we are already tracking. The next step to decide if it's a new object or not is to check color consistency between the two objects, the new one and the candidate from the previous frame. Only if the colours are similar we consider them to be the same object.

Here's when a second Neural Network starts to work. As we saw earlier, one important step of the process is to estimate the distance between our vehicle and the rest of the vehicles. Doing this with LIDAR would have been much easier, as it gives you the distance to all surrounding objects with a high precision and low error rate. Getting that measurements with a stereo camera setup is also feasible, as that is the way the human brain can estimate the depth of the different points of the surrounding environment. The challenge is getting this data with just one camera image as we lack a lot of the information that makes the estimation possible.

A lot of the work done on this step is based on the work done in this project [4], but we are using another network architecture to try to speed up the process while losing the minimum possible precision.

We built a dataset consisting on standard pictures captured with a camera and their corresponding depth maps. In the real world, you would need a LIDAR to get the actual measurements, but Carla provides us with tools to get this data. After getting more than two thousand pairs of standard and depth images, we train a new network to construct a depth map from any given image. Using a mean squared error metric, we get an error of 0.0058 on the training set and 0.0087 which means that our predictions should be, by average, within a 9.73 % margin of the real value.

Fig. 2 shows an example of an image, its real depth map and the predicted depth map created by our network.

Having this second network creating the necessary depth map makes possible the next step: estimating the distance between our vehicle and each one of the detected bounding boxes. This is a straightforward process: first, we get the bounding box of each object (the bounding box contains the pixel coordinates of the top-left and bottom-right corners of the object in the rgb image), we then get the average colour for that region in the depth map, (discarding atypical values in order to reduce error). Then using linear regression, we map that pixel's rgb value to a numeric value corresponding to the distance. Every object in the scene contains the history of the object's estimated distances as well as their associated timestamps.

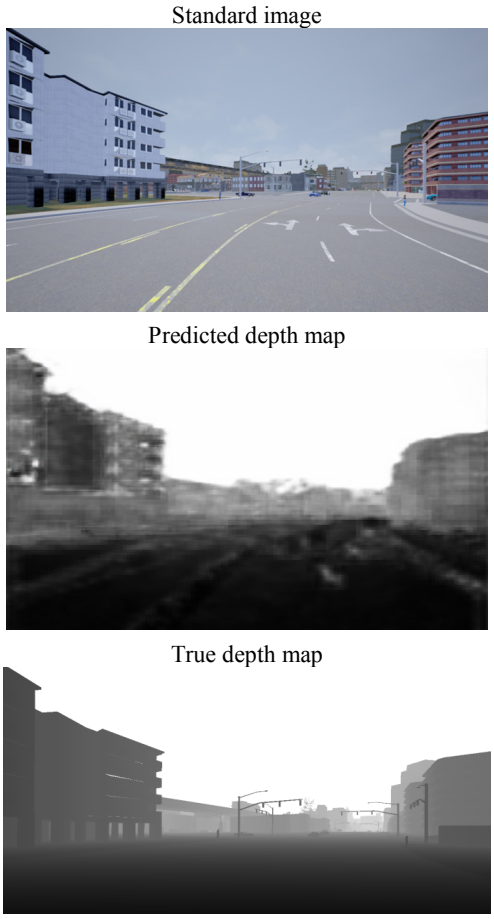

Fig. 2. Real and predicted depth maps comparison

If this is not a new object, we should have an old distance estimate accompanied by the timestamp of that measurement. Having this, we can calculate the delta distance and the elapsed time between the two instants and estimate the current relative velocity of the object (related to our vehicle). In the same way, we can estimate the current relative acceleration if we have multiple velocities recorded for the object.

Decision making with a Neural Network

Once our system is able to generate all the data we need, we can put it together into our practical case: determining whether is it safe or not to perform the incorporation into the roundabout. As we approach the roundabout, we are gathering information about the rest of the vehicles. This is where the last NN begins doing its job, but first we have to train it.

The training process is as follows: a human driver watches the environment through the camera feed and, he inputs to the training data if a incorporation would be safe given the conditions in that instant. This time, the output of the network would be a simple "yes" or "no". The user's elections are recorded with their time stamps, as well as the video feed from the camera. Then we use this data as training data, feeding it into our NN. Given enough data and time to compute it, out network can associate scene features to one of the output labels (yes/no) and learn how to make the predictions.

CONCLUSIONS

1. We have created a reusable framework that sets the foundation for future projects. As this system requires no specialized hardware aside from a regular camera and a computer, we can easily replicate the job done in the simulator in the real world, without the need of spending money on expensive sensors or performing irreversible modifications in a vehicle.

2. We have achieved depth estimation and 3*D*-point reconstruction with a mono camera with sufficient precision, but further refinements to the system will be done. Right now, it doesn't take into account important factors such as camera FOV, and camera height. Taking these factors into account will improve our estimations and allow us to put the system to work on different configurations, which is impossible right now without losing accuracy.

3. Object recognition will continue to improve. Future versions of current architectures or newly developed architectures from now on will benefit this project, as its modular nature allows us to easily swap and integrate components into our system.

4. Motion tracking should be improved in the future, as it is key to speed and acceleration estimations. Using stereo cameras doesn't add much cost to the required hardware and will give us a boost in accuracy, which will improve the data gathered by the system, although, in its current state, we can replicate the desired behavior safely.

REFERENCES

1. Dosovitskiy A., Ros G., Codevilla F., Lopez A., Koltun V. (2017) *CARLA: an Open Urban Driving Simulator*. Available at: https://arxiv.org/abs/1711.03938.
2. Redmon J., Farhadi A. (2018) *YOLOv3: an Incremental Improvement*. https://arxiv.org/pdf/1804.02767.pdf.
3. Redmon J., Divvala S., Girshick R., Farhadi A. (2015) You Only Look Once: Unified, Real-Time Object Detection. *2016 IEEE Conference on Computer Vision and Pattern Recognition (CVPR)*. https://doi.org/10.1109/cvpr.2016.91.
4. Casser V., Pirk S., Mahjourian R., Angelova A. (2019) Depth Prediction without the Sensors: Leveraging Structure for Unsupervised Learning from Monocular Videos. *Proceedings of the AAAI Conference on Artificial Intelligence*, 33, 8001–8008. https://doi.org/10.1609/aaai.v33i01.33018001.

Received: 08.10.2019
Accepted: 10.12.2019
Published online: 31.01.2020